CAVITIES AND WAVES FROM EXPLOSIONS IN SHALLOW WATER

A. R. Kriebel

URS Research Company
Burlingame, California

October 1969

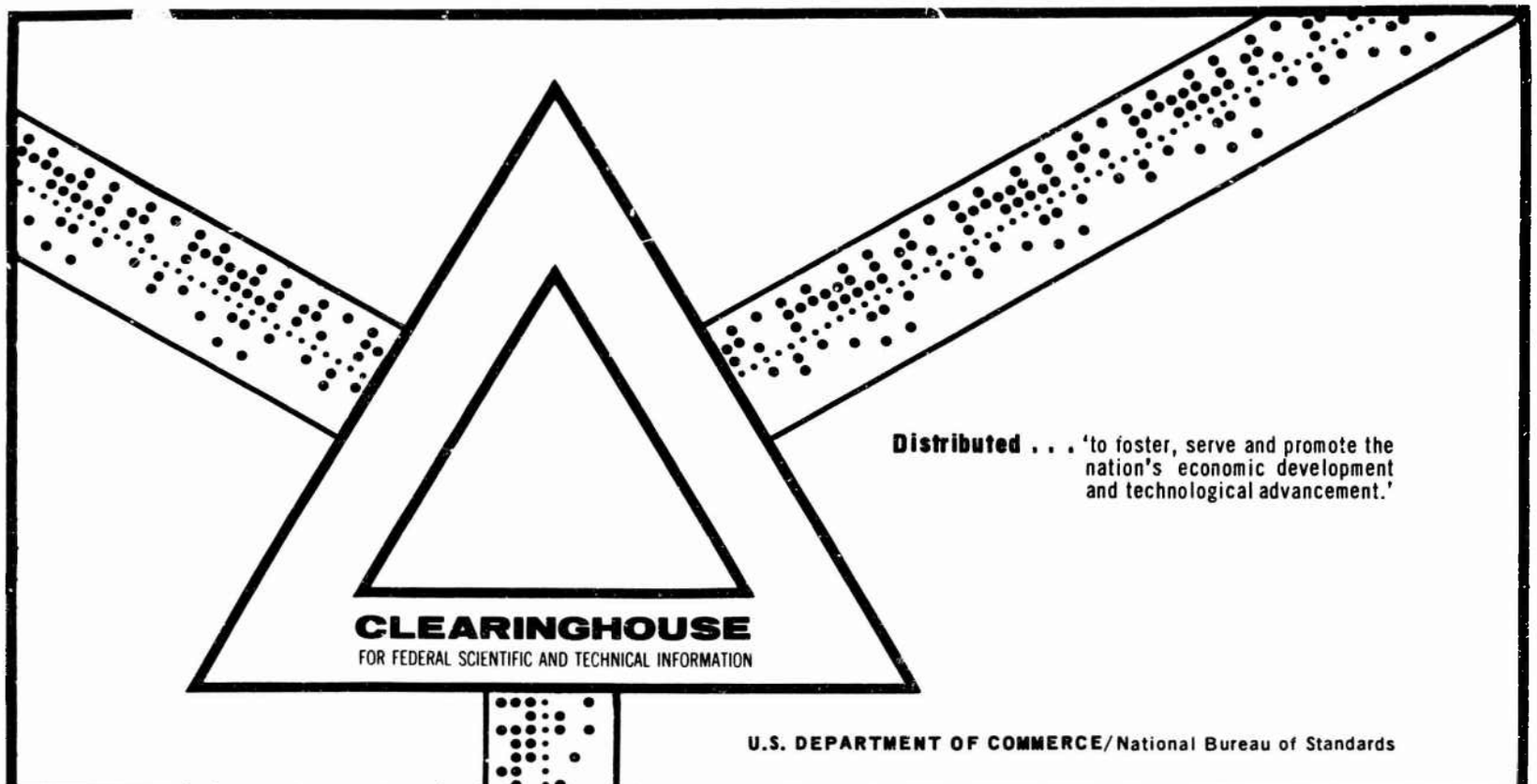

URS 679-5

CAVITIES AND WAVES FROM EXPLOSIONS IN SHALLOW WATER

Final Report

October 1969

Contract No. N00014-67-C-0451
(NR 089-053/12/20-66)

URS RESEARCH COMPANY

A URS Systems Affiliate

URS 679-5

CAVITIES AND WAVES FROM EXPLOSIONS IN SHALLOW WATER

Final Report

October 1969

by

A. R. Kriebel

URS RESEARCH COMPANY
1811 Trousdale Drive
Burlingame, California 94010

Prepared for
OFFICE OF NAVAL RESEARCH
Department of the Navy
Washington, D.C. 20360

Sponsored by
DEFENSE ATOMIC SUPPORT AGENCY
and
OFFICE OF NAVAL RESEARCH
Washington, D.C. 20360

Contract No. N0014-67-C-0451
(NR 089-053/12/20-66)

ACKNOWLEDGMENTS

The author gratefully acknowledges the assistance of several URS staff members in performing the work described herein, particularly Chuck Wilton and Austin Dickinson for the experimental work and Scott Bechtel for the computations. The author is also grateful for the cooperation of Mr. Jacob Warner, the ONR Scientific Officer for the project, and for the sponsorship of the Defense Atomic Support Agency.

CONTENTS

NOTATION

C,D	Functions of σ, Eqs. (10), (11)
D_c	Maximum cavity depth below waterline, ft
d	Depth of burst, ft
d_w	Water depth, ft
F,G,H	Functions defined by Eqs. (1), (2), (3)
g	Acceleration of gravity, 32.2 ft/sec^2
$J_{0,1,2}$	Bessel functions
K	Ratio of measured to calculated peak wave height
R	Horizontal range from charge, ft
R_c	Cavity Radius at waterline, when cavity depth is maximum (ft) (Fig. 66)
R_o	Radius of charge, approximately 1.5 in. except for shots 12 – 15
$R_a R_b$	Cavity radii, ft (Fig. 66)
T	Time shift for matching calculated and measured peak wave, sec
t	Time from release of cavity, sec, Eq. (4)
t_c	Time from detonation to formation maximum cavity depth, sec
t_m	Time from detonation to arrival of peak wave, sec
W	Weight of equivalent sphere of TNT, lb
Y	Charge yield in kt, $2 \times 10^6 W$
η_I	Height of water surface above mean waterline, ft or in. (Fig. 67)
η_m	Peak wave height above waterline, ft (Fig. 66)
η_w	Absolute value of wave height from waterline, ft (Fig. 67)
τ	Wave period, sec, Eq. (6)
λ	Wave length, ft, Eq. (5)
θ	A function defined by Eq. (4)
$\sigma, \sigma_{a,b,k}$	Functions defined by Eqs. (5), (20), and (12)
ϕ	A function of σ defined by Eq. (7)

Subscripts 0,1,2 refer to values at the charge, the first wave gage, and the second wave gage respectively.

Section 1
INTRODUCTION

This report is the fifth of a series describing a study undertaken by URS Research Company of water surface waves generated by (1) explosive charges partially submerged in water near their "upper critical depth," where they are most effective in generating waves, and (2) in gradually decreased depths of water such that the bottom begins to interfere with the motion of the water cavity and the radially expanding wave train generated by this motion.

The first report (Ref. 1) presented an analysis of the upper critical depth effect which indicated that anomalous reflection of the water shock wave from the water surface near the charge might cause the effect. No experimental evidence has been obtained to prove or disprove this hypothesis, except possibly from photography of the fireballs emerging from some of the charges fired at Mono Lake (Fig. A-1b, Ref. 1). These suggest that the outgassing of the expanding cavities was retarded as the depth of burst was increased from zero, as suggested by the analysis.

The second report (Ref. 2) described the movable bottom which was added to the wedge tank to make subsequent tests in shallow and shoaling water possible. Plots of available data for wave generation both in very shallow and in deep water were presented to illustrate the lack of data for intermediate water depths where the bottom begins to interfere with wave generation.

The third report (Ref. 3) described the basic wedge tank facility and some initial data for cavities and waves generated in deep water. The fundamental advantage of the wedge tank over field tests is that both the cavity and the wave train generated by an explosive charge (equivalent to a 1-lb sphere of TNT) can be viewed directly through windows in the tank sidewall (Fig. A-3, Ref. 3). Thus a measured wave train can be related directly to the size and shape of the cavity which generated it and comparison made with the theoretically predicted relationship.

The fourth report (Ref. 4) summarized the experimental results obtained in the wedge tank through 1968 and compared them with Mono Lake data.

In this report all of the data obtained in the wedge tank will be presented and compared with NRDL data for cavity shapes generated in deep water with a 1-lb HBX charge (Ref. 4) and recently reported WES data for wave trains generated in deep water with TNT charges weighing between 1/2 and 385 lb (Ref. 5). The wave trains and cavities generated in the wedge tank will also be compared with analytical predictions based on the theory developed by Whalin (Ref. 6). Finally, a prediction technique based on the wedge tank data will be presented.

Section 2
TEST FACILITY AND INSTRUMENTATION

Basically the URS wedge tank consists of a wedge of water 12 deg wide by 8 ft deep by 60 ft long as shown in Fig. 1. The back side of the tank is one wall of an underground tunnel which is surrounded by massive reinforced concrete walls. Most of the water surface is visible through windows in the front side, which extend to within 1 ft of the charge. A wave absorber is mounted at the far end of the tank. A movable bottom, consisting of four hinged sections, can be raised or lowered on support cables. Each floor section can be expanded laterally against the sidewalls to seal off the volume of water below the floor. The charge for nearly all of the tests consisted of 13.5 grams of C-4 explosive molded around a detonator (0.3 gm of PETN) and inserted into a removable lead charge holder at the apex of the tank. The charge shape was nearly a 12-deg wedge of a 3-in.-diameter sphere and was nearly equivalent to a 1-lb TNT sphere (in open water). For four shots 6.25 grams of C-4 were used to construct a charge equivalent to about a 1/2-lb sphere of TNT.

The instrumentation of the wedge tank consisted of three movie cameras viewing the cavity formation and two vertical scales placed on the sidewall windows across the waterline at distances of 20 and 40 ft from the wedge apex. The framing rates of the cameras were approximately 60 frames per second for the camera near the apex and 32 frames per second for the two "wave gage" cameras. Initial tests with capacitive and resistive types of electric wave gages indicated nonlinear calibrations; hence the photographic gages were employed since they give the water height directly and also clearly show the formation and characteristics of breaking waves. Some tests with electronic pressure transducer types of wave gages were also made, but these gages were abandoned because of difficulty in achieving adequate frequency response without shock wave noise and because the variation of static pressure at a point beneath waves traveling over shallow water does not correspond directly the variation of water level above the point.

Section 3
MEASURED DATA

TABULATED RESULTS

The test results from the wedge tank are listed in Table 1 (p. 98). The first eleven shots were fired in water 8 ft deep with five different charge depths. A second series of sixteen shots was fired with four water depths and four charge depths. Three shots (28, 29, and 30) were fired with a sloping bottom contour. Shots 31 through 63 were fired in 1969 in shallow water, over contoured bottoms, and over a sand bottom. The charges for all of these shots were nearly equivalent to a 1-lb TNT sphere except for Shots 12 through 15, which were fired with a 1/2-lb equivalent charge. Two wave gages were located at ranges of 20 and 40 ft through Shot 30, after which the gages were located at ranges of 23.5 and 47 ft. The bottom was flat except for the shots listed in Table 2, where the bottom contours are given. The contours consisted of four flat slopes between hinges located 9, 23, and 46 ft from the apex as shown in Fig. 2. For Shots 28, 29, and 30 the water depths at the wave gages were as follows:

Gage	Range, R (ft)	Water Depth (in.)
1	20	10.1
2	40	5.0

For Shots 42 through 55, the wave gage ranges were 23.5 and 47 ft, so that the water depth is essentially the same as at the hinge locations in Table 2.

The maximum depth of the cavity, D_c, along with the corresponding time from detonation, t_c, and the cavity radius at the waterline, R_c, are given in Table 1. The peak wave height from the waterline, η_m, the corresponding arrival time, t_m, are also tabulated for the two wave gages.

Data to supplement these tabulated results will be given next. For the first five shots, the cavity shapes and wave trains have already been reported in Ref. 3.

CAVITY SHPAES

Two typical cavity shapes with the water 8 ft deep are shown in Fig. 3, where the indicated dimensions of the expanded cavity were obtained using the window frames as a grid (2 ft center-to-center). About 15 frames (or 1/4 sec) were required to form the "fully expanded" cavity, which is defined to occur when the observed depth D_c is maximum. At this time, D_c was consistently somewhat smaller than R_c, the corresponding cavity radius at the waterline, as shown by Fig. 3 and Table 1. The collapse of the cavity is indicated in Figs. 4 and 5, which are typical for all of the shots in which the cavity did not touch bottom. As shown by Fig. 6, the shape of the expanded cavity is not noticeably distorted by the bottom even when the cavity nearly contacts it. For shallower water, the expanded cavity and its collapse are shown in Figs. 7 and 8. The fully expanded cavity (i.e., when the expansion over the bottom is maximum) occurs at about the same time and has the same radius as for deep water.

WAVE ENVELOPES

The measured wave trains are given in Figs. 9 through 63, for Shots 6 through 63. The exceptions are Shots 34, 38, and 41, for which no wave data were obtained. Comparable wave envelope curves predicted by theory from the measured cavities are shown in several of these figures.

For deep water the first measurable wave at 20 ft is the trough following the collapsed lip of water, since the lip becomes indistinguishable as it spreads away from the cavity, as indicated in Fig. 4. The trough is followed by a turbulent breaker, which is the peak wave within about four cavity radii, as shown in Fig. B-2, Ref. 3. For water shallower than 4 ft, the first measurable wave is the crest generated by the mound of water, as shown by Frame 40 in Fig. 7.

Section 4
DISCUSSION OF DATA

In Fig. 1 of Ref. 1, the peak wave heights for the first 27 shots in Table 2 have been reduced, plotted, and compared with WES data (from Ref. 6). This comparison showed that the peak wave heights generated by explosions at shallow depths of burst in the wedge tank are roughly comparable with those from equivalent 1-lb charges exploded in open water. However, the variation of peak wave height with charge depth was distinctly different, and no upper critical depth effect was obtained in the wedge tank. The effect of depth of burst and water depth on the waves generated in the wedge tank has also been shown in Figs. 2 and 4 of Ref. 4. There was almost no effect of depth of burst, although the peak wave height increased slightly with depth to the largest value tested ($d = 4R_o = 6$ in.). The peak wave height did not begin to decrease with reduced water depth until the expanded cavity began to contact the bottom. The product of range times peak wave height is constant ideally for an expanding wave train, as shown by the Kranzer-Keller theory. This product is actually usually somewhat lower at the closer (20 ft) gage station than at the farther station, as shown in Table 3. This experimental result agrees with Fig. 2.1 of Ref. 6, which shows that closer than about 23 ft from a 1-lb charge, the wave train has not become stabilized. Thus the wave data measured at 40 ft are preferable for comparison with free-field data and theory. It can be seen from Figs. 9 through 63 that the wave envelopes at the greater range are more clearly defined, since there are more waves and the envelope is a smoother curve.

REPEATABILITY

The reliability of the wedge tank data is indicated by the repeated shots (from 1 to 11 in Table 1). For the three shots at zero charge depth, the cavity radius varied between 3.3 and 3.8 ft and the peak wave height at Station 2 varied between 1.6 and 1.8 in. Similarly when the charge was

submerged half a radius, four repeated shots gave cavity radii between 3.4 and 3.8 ft and peak wave heights between 1.7 and 2.0. All of these variations are within a range of 15 percent.

The greatest uncertainty in the data is the detonation time (or zero time) for the farthest wave gage during the first series of eleven shots. The detonation was indicated on the "wave gage" movies as a vibration of the tank wall, water surface, and camera mounts, and for the later shots by a flashing light in the ignition circuit. However, it can be seen that t_m in Table 1 varies widely for the repeated shots and is unreasonably short in some cases. Since the peak of the wave envelope propagates at about 4.5 ft/sec over deep water (from Fig. 2.287 of Ref. 6), it should arrive at the second gage about 4.5 sec after the first, or $t_{m_2} - t_{m_1} \simeq 4.5$ sec. Although nearly all of the tabulated values of t_{m_2} for the first eleven shots appear to be too small, the corresponding time scales for the wave envelopes are accurate except for the location of zero time.

A series of six tests were fired in an open pool of water with 1-lb charges of C-4 explosive to investigate repeatability. The charges were fired at three depths of burst, with each shot repeated twice. The charge depths were zero, one-half, and one charge radius. The plumes from these shots were photographed to determine whether the plume diameter was larger at the intermediate depth (corresponding with an upper critical depth effect), and whether the plume diameter was more repeatable than the water wave data from small TNT charges fired near the water surface (Ref. 6) and from wedge tank tests in Table 1. It was thought that the detonation of these charges might be more repeatable because C-4 is more easily detonated than TNT and because the charge weight was about 30 times larger than the wedge tank charges. However, the data were very erratic, and the plume diameters derived from the movies ranged between 5.5 and 9.7 ft. There was a slight increase in the plume diameter at the intermediate charge depth, but the increase was much smaller than the variation etween repeated shots. Hence the data will not be reported further.

COMPARISON OF CAVITY DATA WITH NRDL DATA

The cavities and plumes measured by Hendricks et al. in deep water with 1-lb spherical charges are shown in Fig. 64 for two depths of burst corresponding to the two largest values in Table 1. It can be seen that the downward impingement of a central jet of gas and water (originating from the water column) onto the bottom of the cavity caused a deep penetration, as described by Hendricks. This effect was not observed in the wedge tank, perhaps because the windows extend only to within 1 ft of the wedge apex. However, the formation of the jet may also have been retarded by the presence of the ceiling 6 ft above the water level in the wedge tank and by friction along the tank walls and a splash plate. This plate extended the transparent wall to the ceiling near the apex of the wedge tank to prevent spillage of the mound of water indicated in Fig. 7. Except for the jet penetration, however, the expanded cavities observed in the wedge tank are only slightly smaller than those shown for the full 1-lb charge in Fig. 64. The horizontal lines in Fig. 64 indicate the relative locations of the ceiling and floor for the wedge tank without the movable bottom (i.e., for the water 8 ft deep). It can be seen that the detonation products emerge through the top of the water column before it becomes as high as the ceiling for the shallower shot in Fig. 64. For the deeper shot, however, water is projected higher than the ceiling. Thus, the detonation products are probably enclosed by a column of water extending to the ceiling in Fig. 5. The cavity appears to form more slowly but to collapse more rapidly in Fig. 5 than for the comparable cavity at the bottom of Fig. 64. This may have been caused by the interference of the ceiling and the absence of jet impingement on the bottom of the expanding cavity in the wedge tank.

It seems unlikely that the downward jet will exist for very large uncontained charges since the ratio of the water cavity size to the charge size becomes smaller, and the detonation gasses do not overexpand to such a low pressure that the water column collapses inward. This is indicated by the inward taper of the water columns in Fig. 64 as compared with the vertical columns for large charges shown in Refs. 5 and 8.

SCALING

In deep water the quantity $(R_c D_c)^2$ (for an expanded cavity with a given shape) is proportional to the charge weight if the potential energy of the cavity is a fixed fraction of the charge yield, (for example, see Table 3 of Ref. 1). Hence, the product $R_c D_c$ for the 1/2-lb charges (Shots 12 to 15) should be 72 percent as large as for the 1-lb charges (Shots 6 through 11), and should vary from 7.0 to 9.5 ft^2. The measured values in Table 3 vary from 7.4 to 11.1 ft^2, which indicates that the smaller charge was more efficient in generating cavities, particularly when both charges were most deeply submerged. Similarly, the energy in an expanding wave train is proportional to $\eta_m^2 R^2$ ideally; and Fig. 2 of Ref. 4 shows that the 1/2-lb charge was more efficient than the 1-lb charge in generating waves when both charges were both submerged in deep water (d_w = 6 ft and 8 ft). No definite reason can be given for these apparent differences in efficiences or departures from ideal scaling. However, neither the shock wave losses to the wedge tank walls nor the interference of the ceiling with the water plume are held to scale in the wedge tank when the charge size varies. There also appear to be anomalies in the scaling of the wave generation process by uncontained charges near the surface of open water, as shown by Fig. 1 of Ref. 4.

It seems apparent that because of the sidewall and ceiling effects previously mentioned, the wedge tank cannot be used to simulate accurately the effects of depth of burst or charge weight. However, these anomalous effects occur early during the expansion of the cavity and plume. It appears that after the cavity has expanded, the subsequent water motion and wave generation in the wedge tank are reliably representative of those processes for a cavity in open water of any depth, provided that scaling is based on the cavity size rather than the charge weight. This is indicated by the last column in Table 3, which shows that the ratio $\eta_m R/R_c D_c$ is nearly constant for all the shots in which the cavity did not touch bottom. Furthermore, the measured values of the ratio are nearly equal to the theoretical value (0.51 from Table 3 of Ref. 1) for the wave train generated by the release of a parabolic cavity with depth D_c and radius R_c in deep water. Nearly the same theoretical value

was obtained for a lipped cavity described by a fourth-order polynomial (i.e., 0.49 from p. 395 of Ref. 6). However, values as high as 0.77 and 0.89 are obtained respectively for the lipped cavity shape used in previous computations by National Marine Consultants (Table 3 of Ref. 1) and for the lipped parabolic cavity from Section 5. It can be seen from Fig. 65 that very nearly all of the URS wedge tank data, even with shallow water, where the cavity touches bottom, fall within the range of these theoretical predictions for deep water.

The foregoing agreement of measured and predicted values of the ratio $\eta_m R/R_c D_c$ indicates that most of the potential energy stored in the expanded cavity is propagated away by the surface waves with little dissipation. It is probably more accurate to say that the dissipated energy apparently nearly equals the kinetic energy of the expanded cavity, since it is never perfectly motionless.

EFFECT OF BOTTOM CONTOURS

Shots 42 through 55 were fired at zero depth over the bottom slopes and contours shown in Fig. 2 and Table 2. The data for these shots (in Table 1) can be compared with those for shots over flat bottoms and with the same water depth under the charge as shown in Table 4, where the comparable values are given for the radius and depth of the cavity and for the peak wave height and water depth at two gage stations. It can be seen that there was no appreciable effect on the cavity radius as the water depth was reduced and that the bottom of the expanded cavity was simply truncated when the water depth was made somewhat shallower than the depth of the cavity in deep water.

At the closer wave gage, the water depth was always at least four times greater than the peak wave height, except for the shots over the contoured bottoms, where the water depth was betweeen two and four times greater than the peak wave heights. There is no consistent pattern for the shoaling effect on the peak wave height at the closer wave gage. Comparison of the peak wave heights (η_{m_1}) for the sloped and flat-bottom shots indicates that the sloped bottom decreased η_{m_1} for the deeper water shots and increased η_{m_1} for the shallower water shots. For the contoured bottoms, the peak wave heights were consistently reduced by shoaling (compared with the flat-bottom values).

At the farther wave gage, the water depth was usually about three times the peak wave height (η_{m_2}) for the sloped bottoms, and η_{m_2} usually increased slightly (compared with the flat-bottom values). For the contoured-bottom shots, the water depth was usually less than twice as large as η_{m_2} and η_{m_2} was larger than for shots over the flat bottom. It can be seen from the measured wave trains (Figs. 45 through 54) that the shoaling effect caused the waves to become peaked, i.e., the crests became higher than the trough depths at the second wave gage, where the shoaling effect was most pronounced. Comparison of the farther wave gage records for Shots 37, 49, and 51, for example, shows that as the water depth at the gage was reduced from 48 to 5.7 to 3.9 in., the peak wave height increased from 1.5 to 2.0 to 2.1 in. and the crests became much higher than the troughs. Shoaling caused the number of discernible waves to decrease and tended to produce a few large spilling crests. For Shots 50 through 55 over the contoured bottoms, a surf zone was produced in the wedge tank.

EFFECT OF SAND BOTTOM

Shots 56 through 63 were fired over a sandy bottom to determine the effect of bottom cratering on the water cavity and waves, all of which was visible through the transparent sidewall of the wedge tank. The sand was a coarse, washed Ottawa (Flint shot) sand with nearly pure silica particles. The particles had rounded shapes with 30 percent retained on a No. 30 sieve (0.0234 in.) and 60 percent retained on a No. 40 sieve (0.0165 in.). The sand filled the region from the apex of the wedge tank to a radial distance of 9 ft and down to the concrete floor 8 ft below the water surface. The top surface of the sand was made flush with the flat steel plate, which extended beyond the 9-ft radius so that the water depth was constant for each shot. The charge was half submerged for all of the shots over the sand bottom. The data in Table 1 show the following effects of a sand bottom on the cavities and waves generated in shallow water as compared with those for a hard steel bottom.

Effects for a Water Depth of 4 ft

The data for Shots 56 and 57, compared with those for Shots 36 and 37, show that the water cavity was slightly deeper over the sand, but it did not touch bottom and the peak wave height was slightly smaller. There was hardly any cratering of the sand, but the bottom rose about 6 in. as the water cavity collapsed.

Effects for a Water Depth of 3 ft

The expanded cavities just touched both the sand and steel bottoms (Shots 48, 59, 34, 35, 38, and 39). There was still hardly any motion of the sand, however, except for a slight mounding as the cavity collapsed. The cavity radius and wave heights were the same for all the shots within experimental scatter.

Effects for a Water Depth of 2 ft

The data for Shots 60, 61, and 31 show that there was little difference in the water cavities or peak wave heights; but in this case the expanded water cavity produced a dry area about 2 ft in radius over the bottom, and the sand was compressed under the expanded cavity to form a crater about 1/2 ft deep. The shallow crater subsequently disappeared as the cavity collapsed and the water washed back over it.

Effects for a Water Depth of 1 ft

Shots 62 and 63, compared with 31, 33, and 40, show that the water cavities were somewhat larger over the sand bottom. The cavities spread about 3 ft over the bottom and formed shallow craters in the sand, which subsequently disappeared. For the sand bottom the peak wave heights were slightly smaller close in and slightly larger farther away from the source.

The foregoing data show that the effect of the sand bottom, compared with a hard bottom, is nearly insignificant for the water cavities and waves generated by explosions at the water surface. Even in water so shallow that

the water cavity diameter was over eight times larger than the water depth, only a very shallow crater was produced in the bottom. The crater subsequently disappeared and caused little effect on the water motion and wave generation.

Section 5
CALCULATED WAVE TRAINS

METHOD OF CALCULATION AND RESULTS

In order to predict the wave trains theoretically, they will be assumed to originate from an initially motionless cavity shape represented mathematically by a truncated parabola, as shown in Fig. 66. For this cavity shape, the equations for predicting the wave trains can be found in Ref. 7. First the final system of equations used to compute the wave train will be presented, and then their derivation will be given.

In dimensionless form, the final equation for the wave height η at range R and time t can be expressed as

$$H = F\,G\cos\theta$$

where

$$H = \sigma^2 \frac{R\eta}{R_c d_w} \tag{1}$$

$$F = \text{a function of } \sigma = \sqrt{\frac{\sigma\phi(\sigma)}{-\phi'(\sigma)}} \tag{2}$$

$$G = \text{a function of the cavity shape and } \sigma \tag{3}$$

$$\theta = 2\pi\left(\frac{t}{\tau} - \frac{r}{\lambda}\right) \tag{4}$$

$$\lambda = \text{wavelength} = \frac{2\pi d_w}{\sigma} \tag{5}$$

$$\tau = \text{wave period} = \frac{2\pi}{\left(\frac{g}{d_w}\,\sigma\tanh\sigma\right)^{1/2}} \tag{6}$$

For a given initial cavity shape, time t, and range R, all of the listed variables can be found in terms of σ alone. The value of σ is determined by the following expression [Eq. (14) of Ref. 7]

$$2\phi(\sigma) \equiv \frac{2R}{\sqrt{gd_w}\,t} = \left(\frac{\tanh\,\sigma}{\sigma}\right)^{1/2} + \frac{(\sigma/\tanh\,\sigma)^{1/2}}{\cosh^2\,\sigma} \tag{7}$$

At any specified time and range, one can find ϕ, then σ, and finally the wave height η, from the foregoing equations.

Now the variables F, C, and θ will be written explicitly as functions of σ, r, and t. By the substitution of λ and τ into θ, one gets directly

$$\theta = \left(\frac{g}{d_w}\,\sigma\,\tanh\,\sigma\right)^{1/2} t - \frac{\sigma R}{d_w} \tag{8}$$

By differentiating ϕ and substituting into the expression for F, one finds that

$$F = \sigma\sqrt{\frac{2\,(1 + D)}{(1 - D)^2 + 4\sigma^2 C}} \tag{9}$$

where

$$C = \operatorname{sech}^2\,\sigma \tag{10}$$

$$D = \sigma\,\operatorname{csch}\,\sigma\,\operatorname{sech}\,\sigma \tag{11}$$

Finally the variable G can be derived as follows. Equation (1) corresponds to Eq. (13a) of Ref. 7, which was derived by the "method of stationary phase." In the present nomenclature, this equation can be written as

$$R\eta(r,t) = \frac{\bar{\eta}_c}{d_w}\,F\cos\,\theta \tag{12}$$

Thus by comparison with Eq. (1), it can be seen that

$$G = \frac{\sigma^2 \bar{\eta}_c}{R_c d_w^2} \tag{13}$$

where $\bar{\eta}_c$ is the zero-order Hänkel transform of the initial cavity shape shown in Fig. 66, or

$$\bar{\eta}_c = \int_0^\infty \eta_c \, J_o\left(\frac{\sigma}{d_w} r_c\right) r_c dr_c \tag{14}$$

The following equations corresponding to Eq. (6) of Ref. 7 will be used to describe the cavity shape when the cavity touches bottom, as shown in Fig. 66.

$$\begin{aligned} \eta_c &= -d_w \quad \text{if} \quad r_c < R_a \\ &= \frac{-R_c^2 \, d_w}{R_c^2 - R_a^2} \left(1 - \frac{r_c^2}{R_c^2}\right) \quad \text{if} \quad R_a \leq r_c \leq R_b \\ &= 0 \quad \text{if} \quad r_c > R_b \end{aligned} \tag{15}$$

The water will be assumed incompressible, so that the volume of the cavity is equal to that of the elevated lip. By integrating Eq. (15) to find the cavity volume and then setting the volume equal to zero, one gets

$$R_a^4 = 2R_b^2 R_c^2 - R_b^4 \tag{16}$$

or

$$(R_b^2/R_c^2 - 1)^2 = 1 - (R_a/R_c)^4$$

In addition, it will be assumed that the untruncated parabolic cavity has a maximum depth equal to R_c. In this case (with $\eta_c = R_c$ when $r_c = 0$), Eq. (15) gives $R_c d_w = R_c^2 - R_a^2$. If the water is deep enough that the cavity does not touch bottom ($d_w > R_c$), then R_a is set equal to zero, and $R_b = \sqrt{2}\, R_c$.

By substitution of these equations into Eq. (14) and integration, one finds that corresponding to Eq. (6) of Ref. 7

$$G = \frac{\sigma^2 \overline{\eta}_c}{R_c d_w^2} = (r_b^2 - 1)\, \sigma_b\, J_1(\sigma_b) - 2r_b^2\, J_2(\sigma_b) + 2r_a^2\, J_2(\sigma_a) \qquad (18)$$

where

$$r_{a,b} = R_{a,b}/R_c \qquad (19)$$

$$\sigma_{a,b} = \left(\sigma/d_w\right) R_{a,b} \qquad (20)$$

$$J_n = \text{Bessel functions of } n^{th} \text{ order} \qquad (21)$$

Thus all of the remaining variables in the foregoing equations, and particularly the wave height, η_2, can be found in terms of three independent dimensionless variables, R_c/d_w, R/d_w, and $\sqrt{g/d_w}\, t$. In other words, a wave gage record (η versus t) can be calculated for given values of water depth, initial cavity radius, and gage range. Two such wave records are shown in Fig. 67.

To illustrate the behavior of the subsidiary variables some additional plots have been prepared. By dividing Eq. (8) by R/d_w and then substituting Eq. (7) for R/t, one gets

$$\frac{d_w \theta}{R} \equiv \sigma_K = \sigma \frac{\sinh \sigma \cosh \sigma - \sigma}{\sinh \sigma \cosh \sigma + \sigma} \qquad (22)$$

Figure 68 shows how the variable σ varies with σ_K or with θ for fixed values of d_w and R. The two variables F and G are plotted versus σ in Fig. 69.

The wave envelope is given by

$$\frac{FG}{\sigma^2} = \frac{R\eta_w}{d_w R_c} \tag{23}$$

where η_w gives the absolute value of η at the wave crests or troughs as shown in Fig. 67. This quantity can be calculated from the foregoing equations as a function of the two variables R_c/d_w and $\sqrt{g/d_w}\,t$. The peak values of the wave envelope, η_{max}, shown in Fig. 67 can be calculated versus the single independent parameter R_c/d_w, and the values given in Table 6 are obtained. It can be seen that the first peak in the wave envelope is usually higher than the second, but not when $R_c/d_w \simeq 2$.

COMPARISON WITH MEASURED DATA

Wave trains computed from the foregoing equations are compared with the measured wave trains in Figs. 10, 14 through 18, 20 through 29, 34, 36, 37, and 40. The time scales in Figs. 9 through 63 are measured from detonation of the charge, whereas the time for the theoretically predicted wave trains starts with the collapse of the expanded cavity. The calculated and measured wave trains were matched by adding the constant time increment T to the computed values t and by multiplying all of the calculated wave heights by the factor K. The constants T and K were chosen so that one of the prominent measured waves (usually the highest wave) superimposed on a comparable calculated wave, as shown in the foregoing figures. The empirical values of T and K are listed in Table 5. One would expect T to be about +1/4 sec (i.e., the observed time required for the cavity to form in Table 1). However, it can be seen from Table 5 that T is generally about -2 sec. The value of K generally ranged between 0.4 and 0.8, as shown in Fig. 70, where this value from Table 6 is plotted versus water depth. There is no discernible trend of K with water depth, even though the depth ranged between about one-third to twice the cavity radius.

The calculated wave trains agree rather well with those measured (after the application of the factors K and T), particularly at the second wave gage, as shown in Figs. 10 through 40. However, for the shallowest water depth of 1 ft, the agreement is less satisfactory (Figs. 27 through 29, and Fig. 34). The agreement between the measured and calculated wave trains exists only for the first peak (or lobe) of the wave envelope, the second peak is always observed to be much smaller than predicted.

Section 6
PREDICTION TECHNIQUE

The peak wave height generated by explosions at the surface of shallow water can be predicted by the following technique based on the agreement between the measured data and the calculations for a lipped parabolic cavity in Section 5. An average value for the ratio of measured to predicted peak wave height is taken as K = 0.6 from Table 5 and Fig. 70. Then the predicted peak wave height is taken as 0.6 times the maximum height of the first lobe of the calculated wave envelope. This height is given by Table 6 or Fig. 71. Although the wedge tank data consistently show that the cavity radius and wave height increase slightly with depth of burst in shallow water, this variation is believed to be due to the presence of the ceiling and sidewalls in this tank, as described earlier. Thus the prediction technique will assume that this variation is negligible for explosions in open shallow water. The effect of bottom material and slope will also be assumed negligible based on the data in Section 4. Thus the predicted peak wave height is given by the curve in Fig. 71 after η_{max} is reduced by the factor 0.6. This curve can be approximated by the two solid straight lines given in Fig. 4 of Ref. 4 as shown in Fig. 71, where they are replotted.

The foregoing technique predicts the peak wave height in terms of the cavity radius R_c, rather than the yield of the explosive charge. The wedge tank data cannot be used to accurately predict R_c in terms of the charge yield as explained earlier. However, the data show that R_c is nearly independent of water depth for shallow depths of burst and has an average value of 3.7 ft for W = 1 lb (Table 1). The water column diameters measured at Mono Lake and for nuclear explosions at shallow depth of burst are also nearly independent of water depth, as mentioned in Ref. 2.

In the absence of information regarding how R_c scales with yield, it will be assumed that the potential energy of the cavity is a fixed fraction of the charge yield, so that $R_c \approx W^{1/4}$ for a fixed ratio of d_w/R_c.

Thus the cavity radius and peak wave height for explosions at shallow depth of burst can be predicted by the following empirical rules.

The cavity radius is

$$R_c(ft) = 3.7\left[W(lb)\right]^{1/4} = 140\left[Y(kt)\right]^{1/4} \qquad (24)$$

The peak wave height (given by the straight lines in Fig. 71) is

$$\eta_m R(ft)^2 = \frac{5}{8}\left(\frac{d_w}{R_c}\right)R_c^2 = 8.5\left(\frac{d_w}{R_c}\right)\sqrt{W} = 2.3\, d_w W^{1/4} = 87\, d_w Y^{1/4} \qquad (25)$$

if

$$d_w \leq \frac{3}{4} R_c = 2.8\, W^{1/4} = 105\, Y^{1/4}$$

or

$$\eta_m R(ft)^2 = 0.47\, R_c^2 = 6.4\sqrt{W} = 0.90 \times 10^4\sqrt{Y} \qquad (26)$$

if

$$d_w \geq \frac{3}{4} R_c$$

These rules agree with the wedge tank data and nuclear data within the experimental scatter as shown in Fig. 3 of Ref. 4 and Fig. B-3 of Ref. 2. However, the water column radii and peak wave heights generated by the large H.E. explosions at Mono Lake were considerably larger than the values predicted by these rules (Ref. 4). The observed radius of a water column may continue to expand to a value larger than the radius of the expanded cavity as shown in Figs. 4, 5, 7, and 8. The variations between the wedge tank, Mono Lake, and nuclear data cannot be ascribed to yield scaling alone, since there are energy losses in the wedge tank (because of the ceiling and sidewalls) and energy losses from a nuclear explosion at shallow depth of burst due to

radiation. The "nuclear – TNT equivalence" for surface wave generation in shallow water apparently is about the same as the wedge tank equivalence to uncontained TNT explosions. The TNT equivalence of shallow nuclear and wedge tank explosions is probably less than unity only for the cavity generation process Eq. (24) . The TNT equivalence during the generation of surface waves by the collapse of the cavity appears to be about unity, as shown by the agreement of the data from the wedge tank, Mono Lake, and nuclear tests with the prediction curves in Fig. 71 or Eqs. (25) and (26) . The peak wave height estimates on Page 6-8 of Ref. 9 are considerably larger than the predictions herein for a 1-lb charge. The yield scaling rules in Ref. 9 also differ from the Froude scaling implied by Eqs. (25) and (26).

Section 7

CONCLUSIONS AND RECOMMENDATIONS

The following conclusions and recommendations are drawn from the wedge tank data reported herein.

1. The horizontal radii of the expanded water cavities generated by explosives at shallow depth in the wedge tank are nearly independent of the water depth and depth of burst.

2. The shapes of the expanded cavities are nearly hemispherical, except that the bottoms of the cavities are truncated in shallow water.

3. In deep water, the cavities in the wedge tank are about the same size and shape as those for a 1-lb TNT sphere in open water. However, for the wedge tank, the water column impinges on the ceiling; there is no evidence of jet impingement on the bottom of the expanded cavity (Fig. 64); and there are shock wave losses through the tank sidewalls.

4. The foregoing anomalies occur early during the expansion of the water cavity and they appear to affect mainly the variation of peak wave height with depth of burst, such that the upper critical depth effect is hardly visible in the wedge tank. The peak wave heights in the wedge tank agree with WES data for a 1-lb TNT sphere when they are averaged over depth of burst.

5. The peak wave height in deep water (where the cavity does not touch bottom) corresponds closely with that predicted by the Kranzer-Keller theory for an initially motionless parabolic cavity without a water column or lip.

6. All of the wave trains measured in the wedge tank for water of constant depth can be correlated reasonably well with those predicted theoretically in the first lobe of the wave envelope corresponding with a lipped parabolic cavity. All of the measured wave heights are about 0.6 times those predicted. The agreement becomes poorer when the water depth becomes less than one-third the radius of the expanded cavity.

7. All of the peak wave heights measured in the wedge tank over water of constant depth correlate onto one curve ($R\,\eta_{max}/R_c^2$ vs. d_w/R_c in Fig. 71). Mono Lake data and nuclear data also correlate onto this curve when the water column radius is used for R_c. The

horizontal cavity radius R_c appears to be nearly independent of the charge depth, water depth, bottom material, and bottom slope over wide ranges of these parameters. The cavity radius appears to scale reasonably well with the fourth root of the charge yield, but there is uncertainty about the nuclear–TNT equivalence for shallow explosions due to the upper critical depth effect and energy losses from radiation.

8. When a surf zone was created in the wedge tank over a contoured bottom, the shoaling wave crests became higher and sharper compared with waves over a flat bottom, but the number of waves was reduced.

It is recommended that the comparison of wedge tank data and theoretically predicted wave trains be extended to include those from an unlipped parabolic cavity. The agreement with measured data should improve since the lipped cavity used herein gives waves about two times higher than measured in the first lobe of the wave envelope and much higher in the second lobe. It is also recommended that the cavity and wave data from exploding wires at shallow depths (generated recently at Engineering Physics Company under ONR sponsorship) should be reduced and compared with existing data from explosions to illustrate the TNT equivalence of simulated nuclear explosions. It is finally recommended that the URS wedge tank be used to generate data for water velocity fluctuations and the erosion of simulated sedimentary bed loads under gently spilling breakers. These data can be generated conveniently by photography of dye and particulate tracers made visible through the transparent sidewall of the tank.

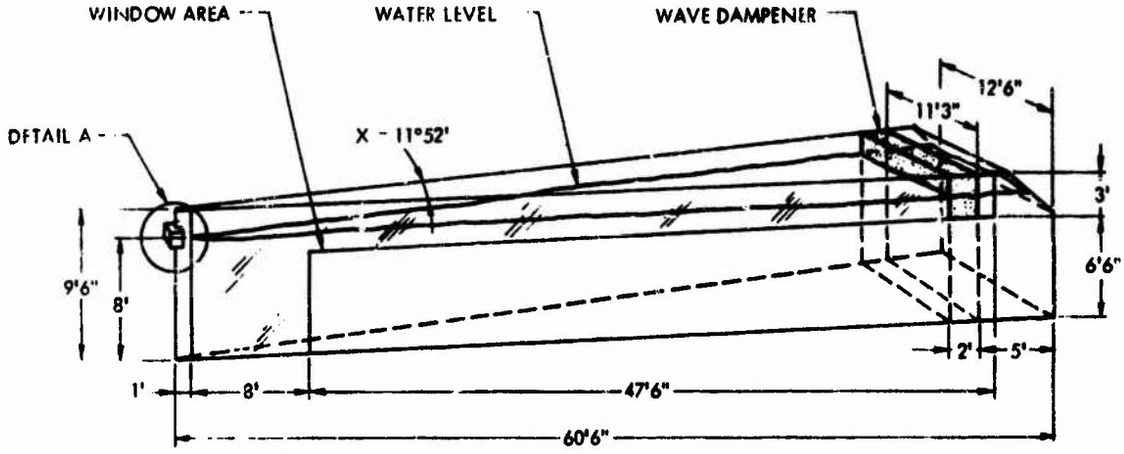

URS WEDGE TANK

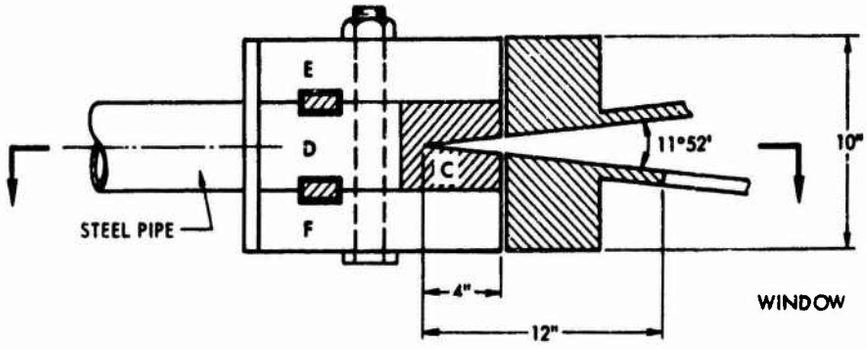

TOP VIEW

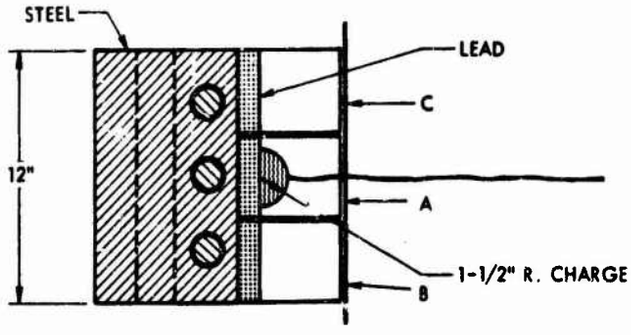

SIDE SECTIONAL VIEW

DETAIL A - CHARGE HOLDER

Fig. 1 Sketch of Wedge Tank and Charge Holder

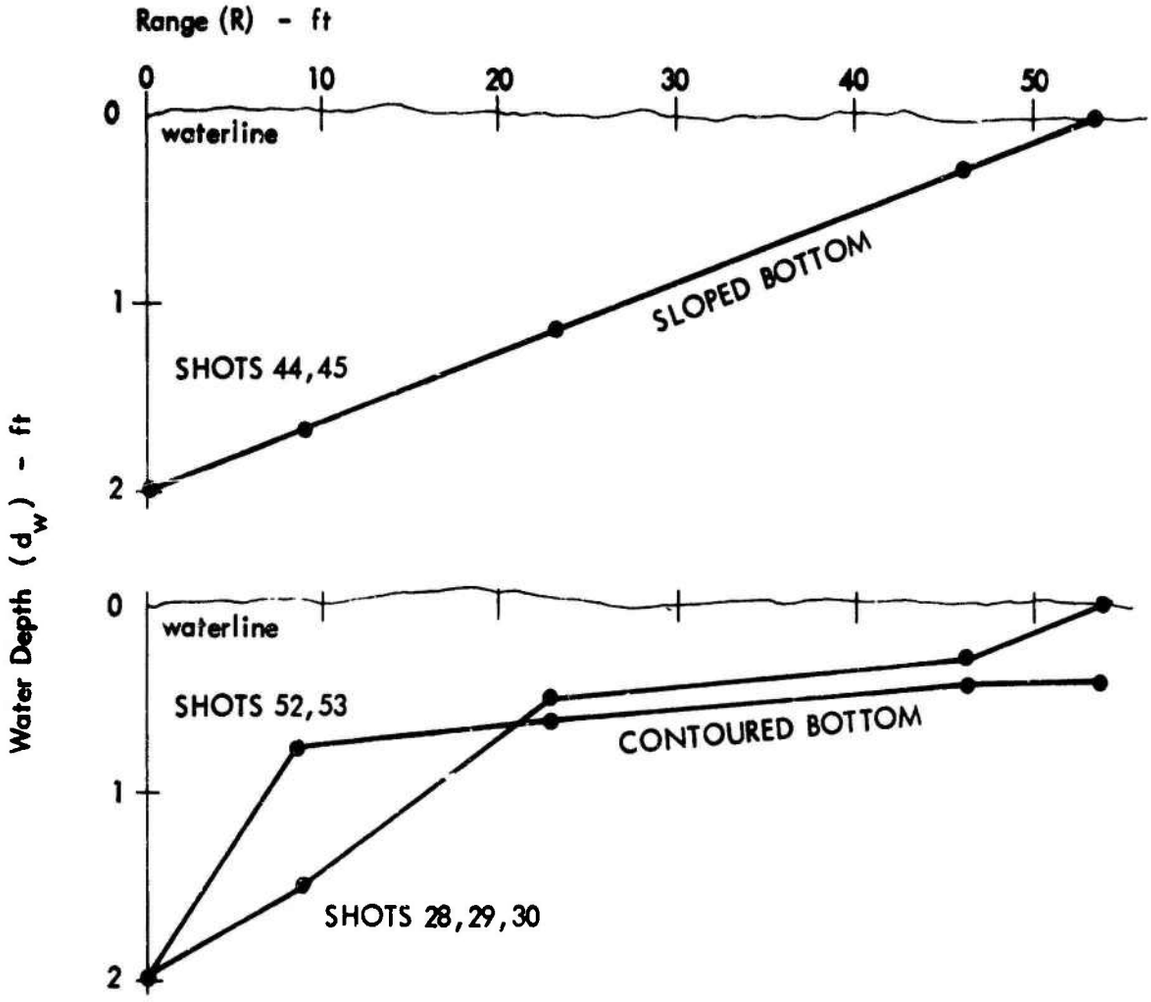

Fig. 2. Shapes of Sloped and Contoured Bottoms

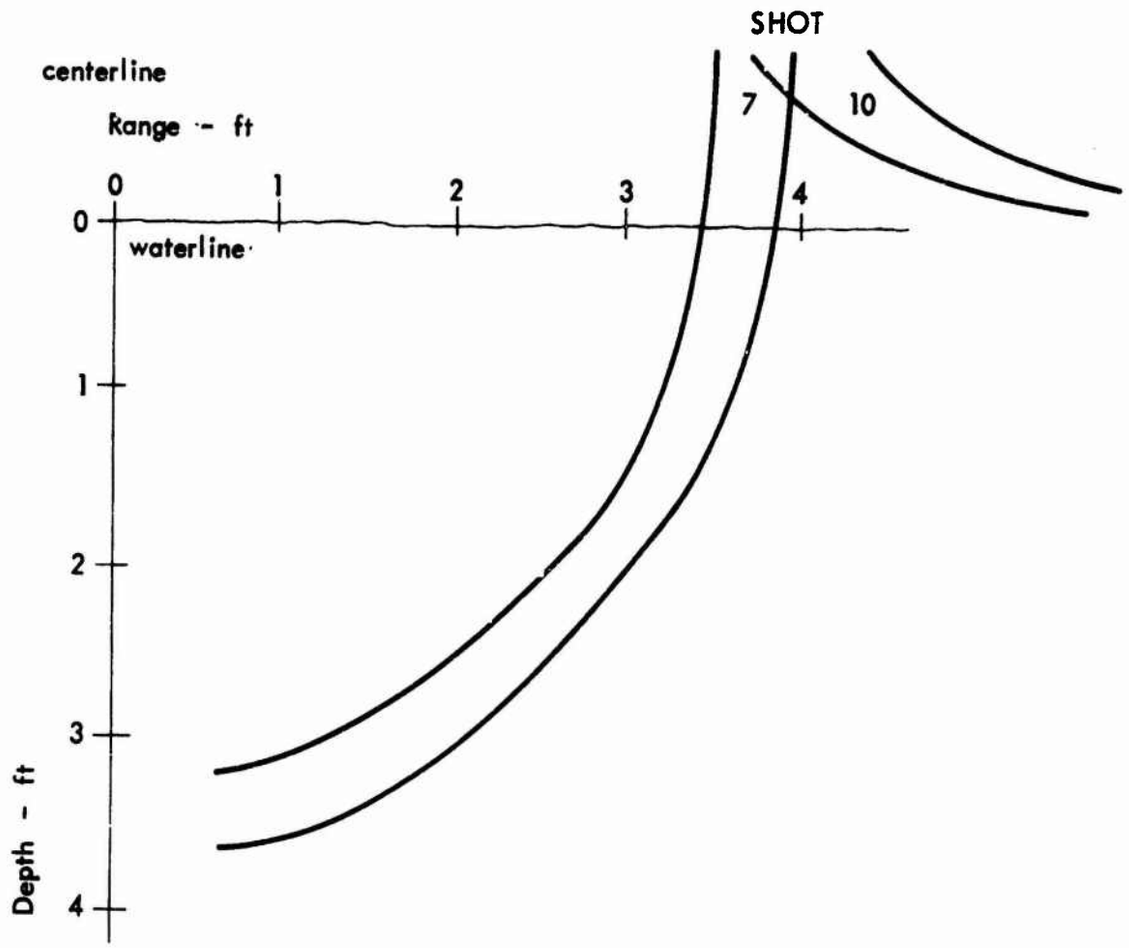

Fig. 3. Cavity Shapes With Water 8 Ft Deep

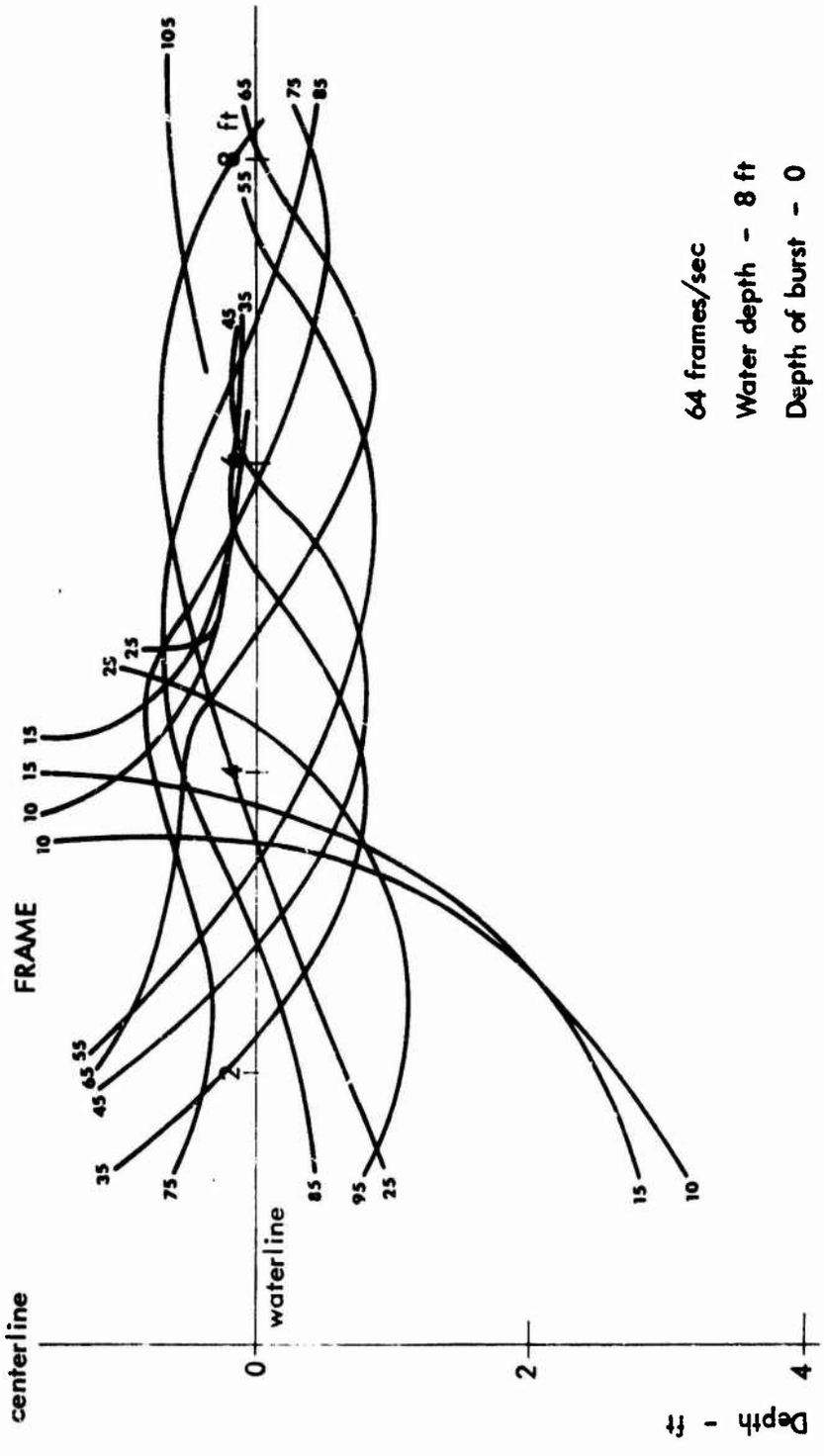

Fig. 4. Cavity Shape Versus T' e – Shot 6

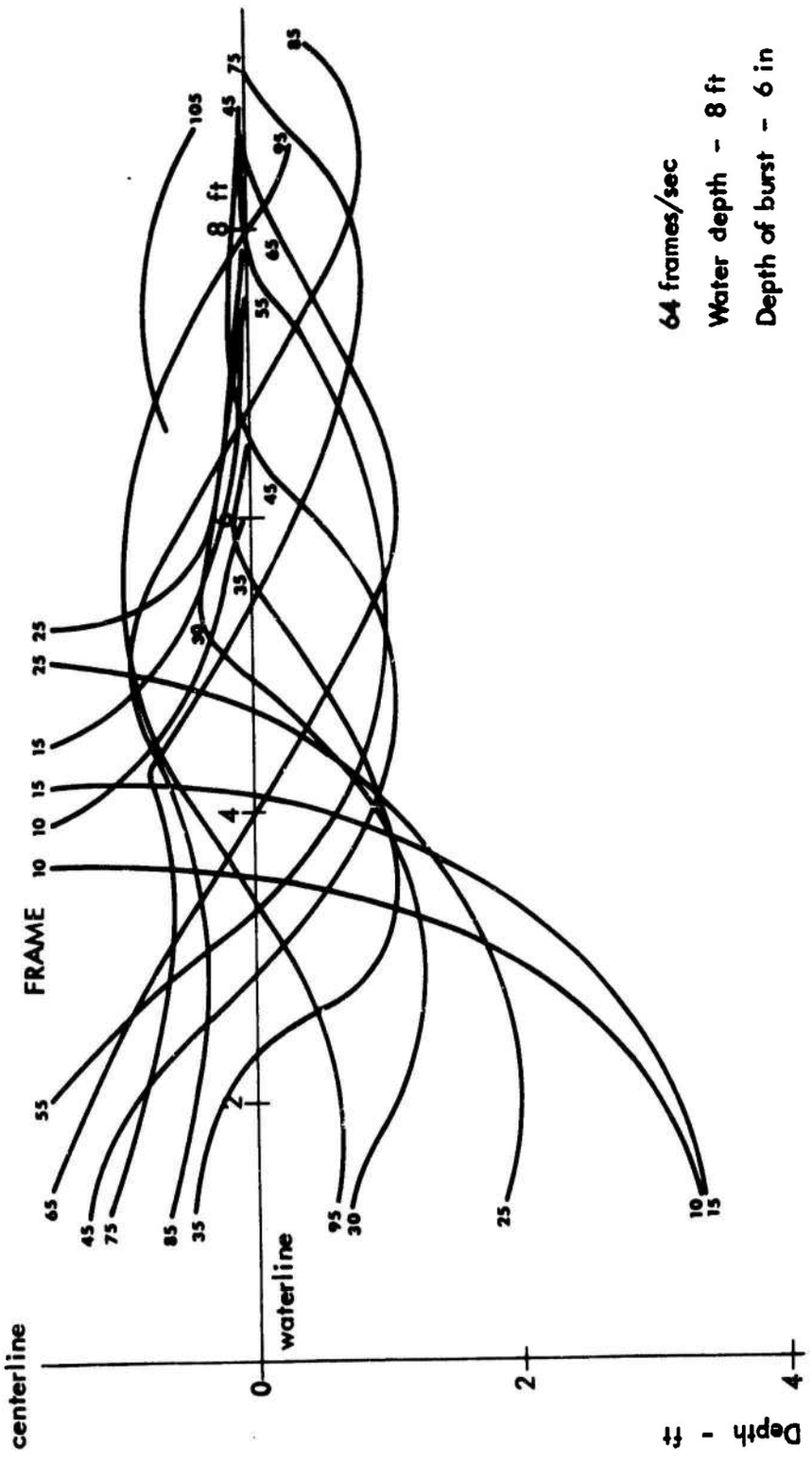

Fig. 5. Cavity Shape Versus Time — Shot 11

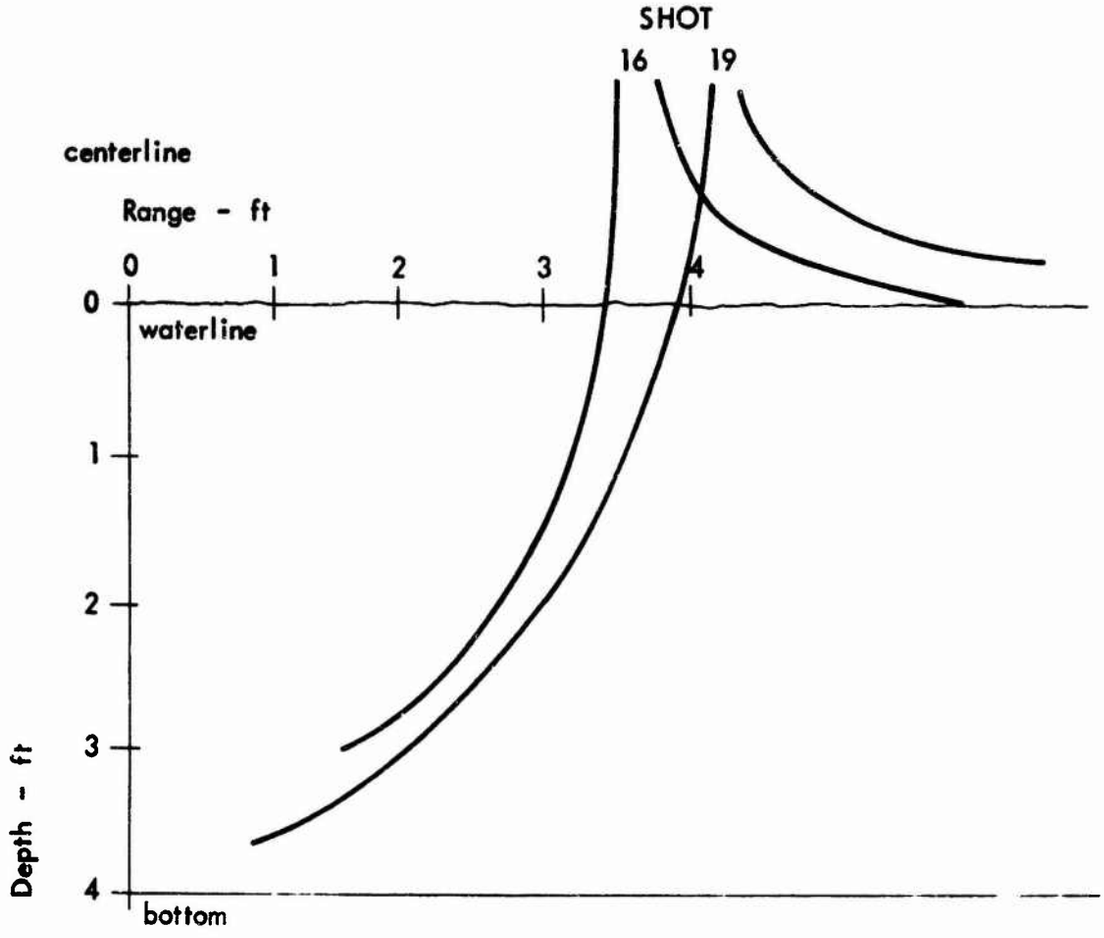

Fig. 6. Cavity Shapes With Water 4 Ft Deep

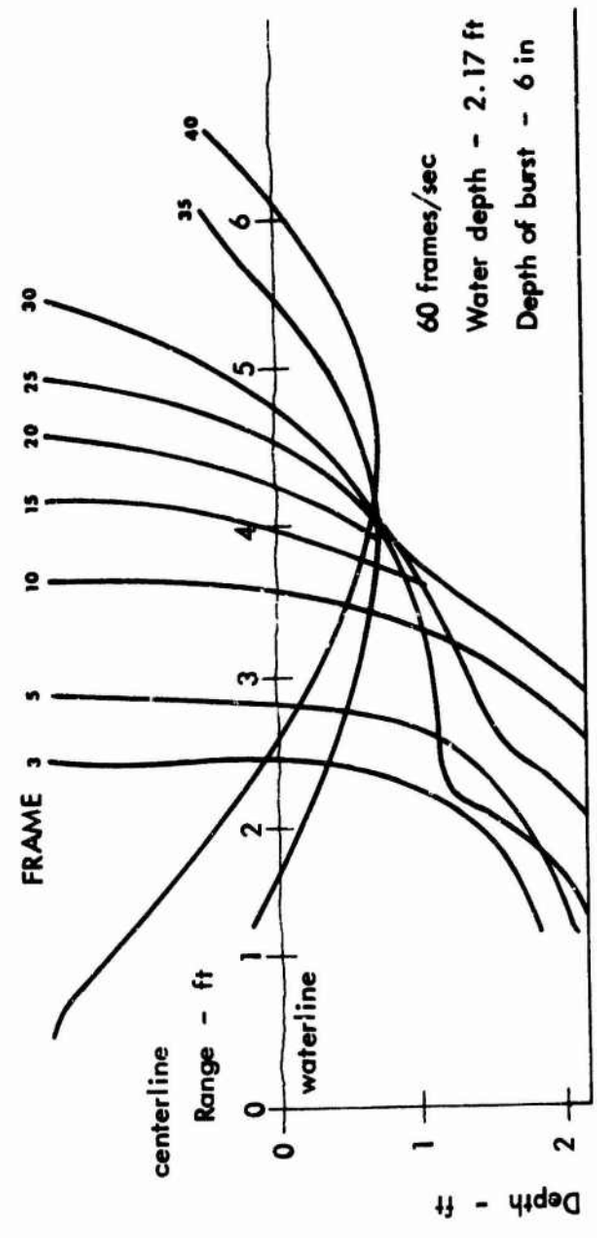

Fig. 7. Cavity Shape Versus Time — Shot 20

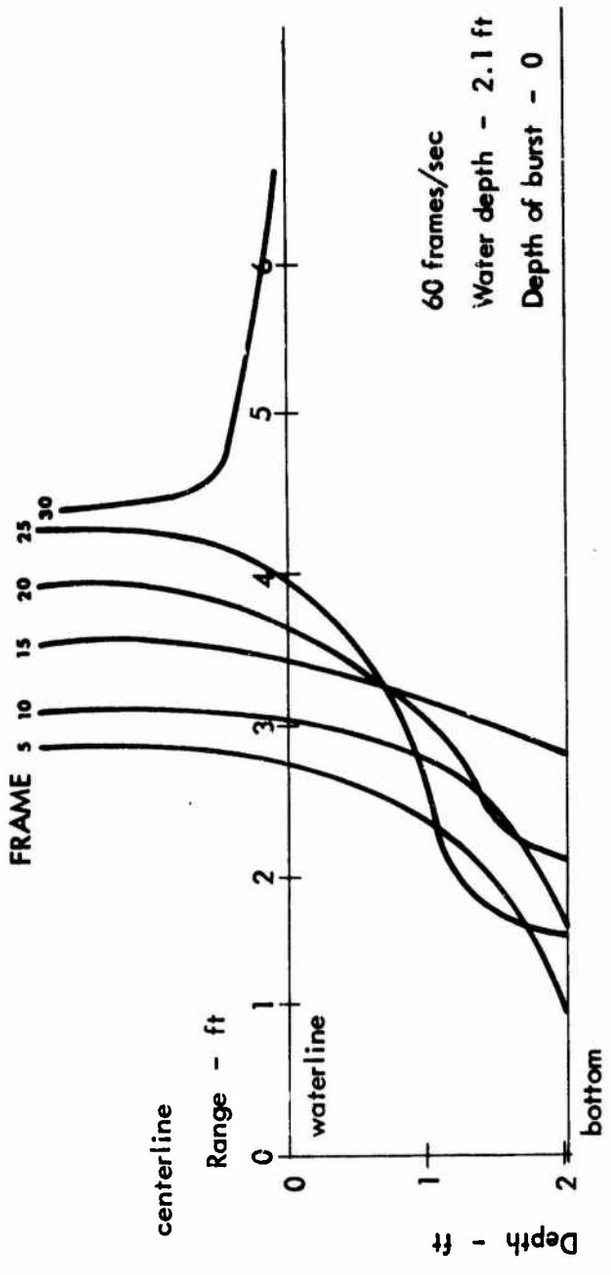

Fig. 8. Cavity Shape Versus Time — Shot 23

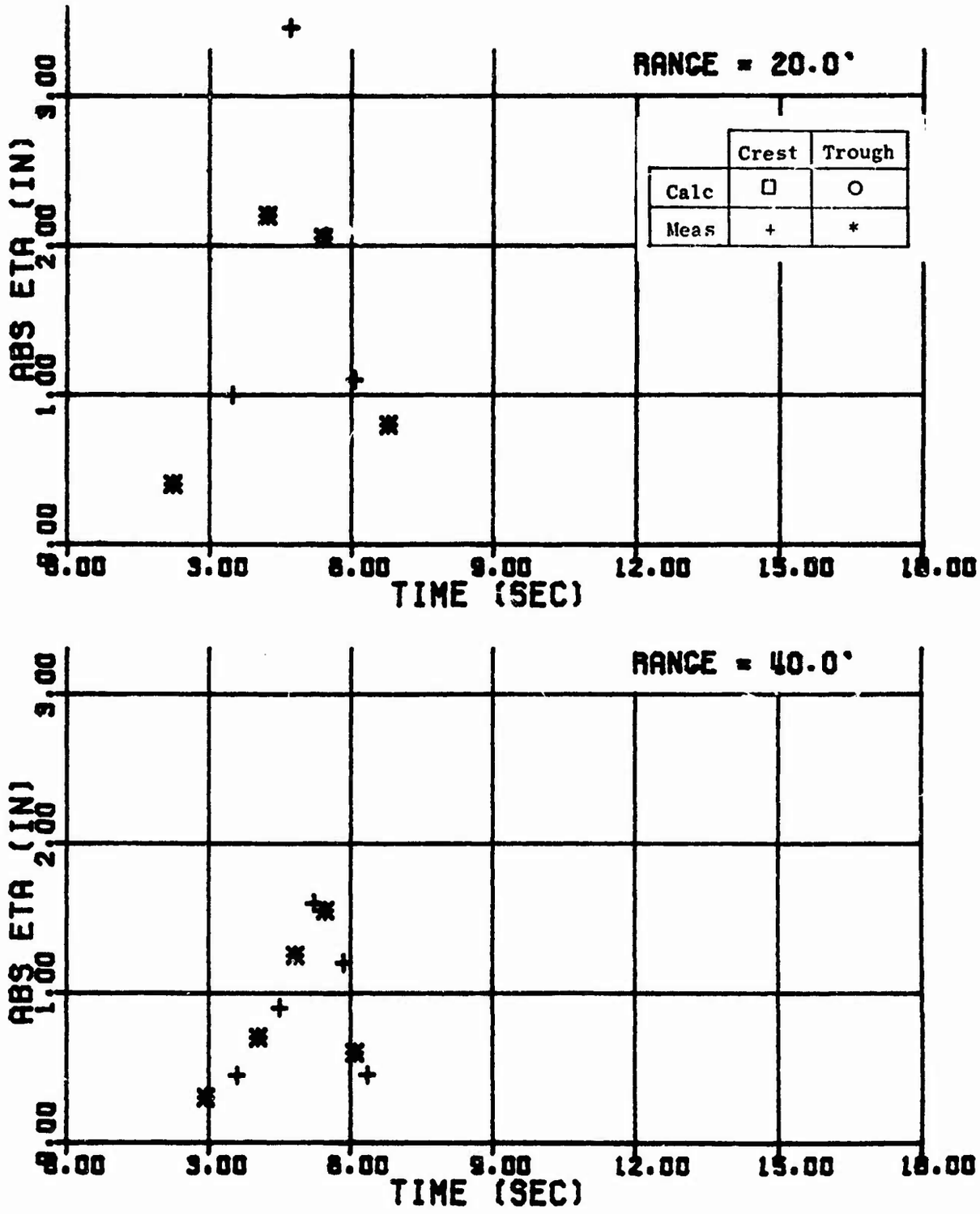

Fig. 9 Wave Trains - Shot 6

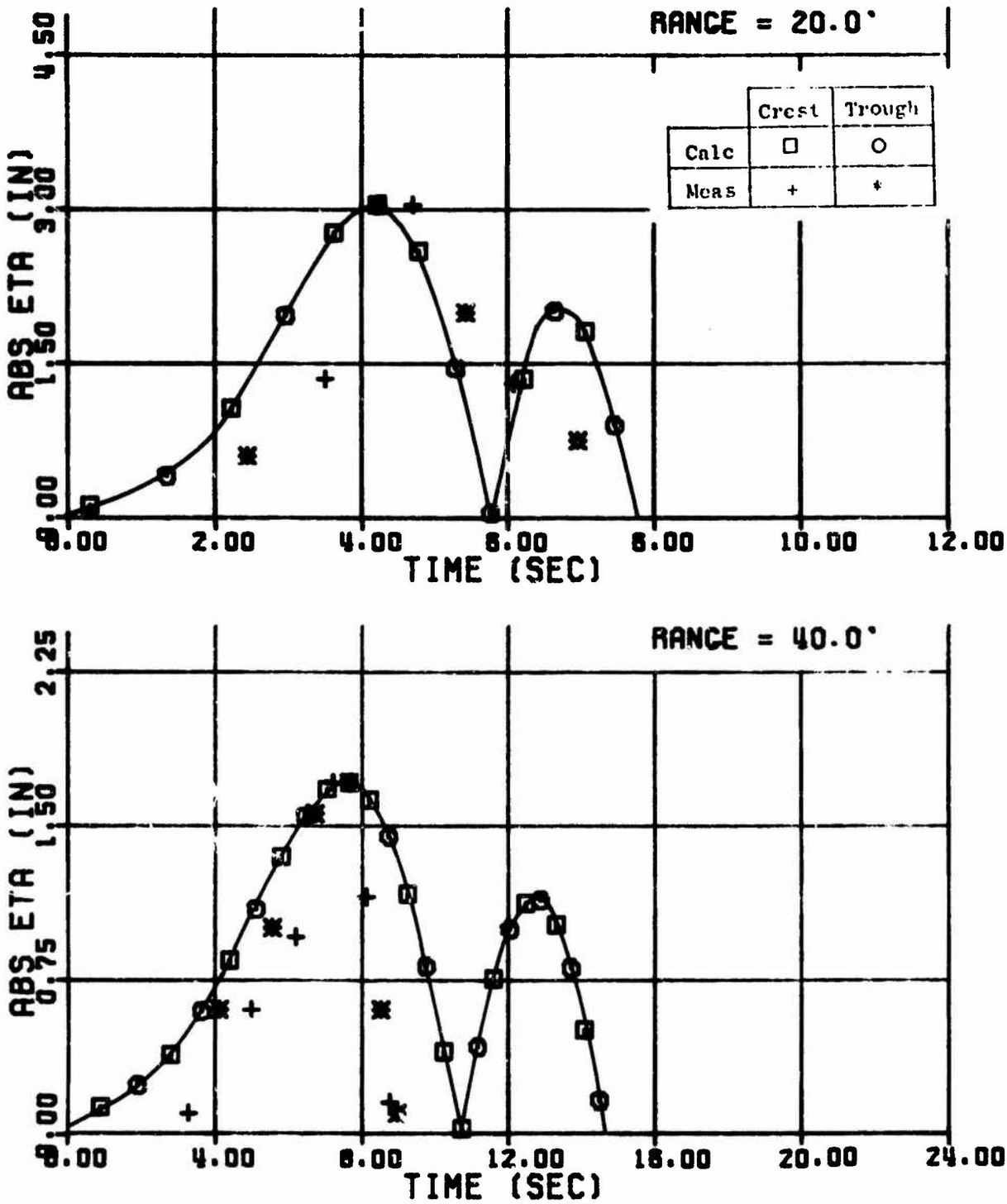

Fig. 10 Wave Trains - Shot 7

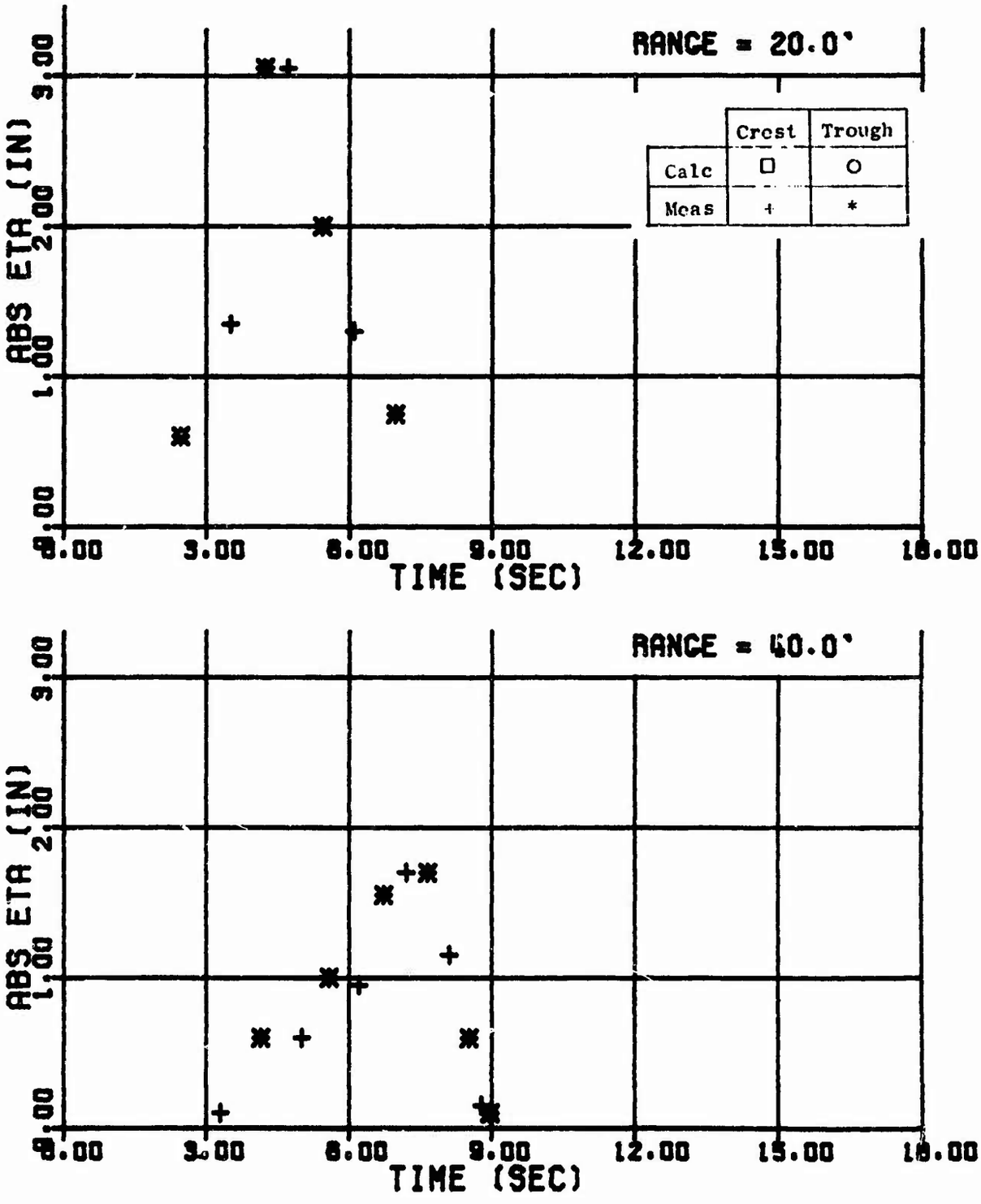

Fig. 11 Wave Trains - Shot 8

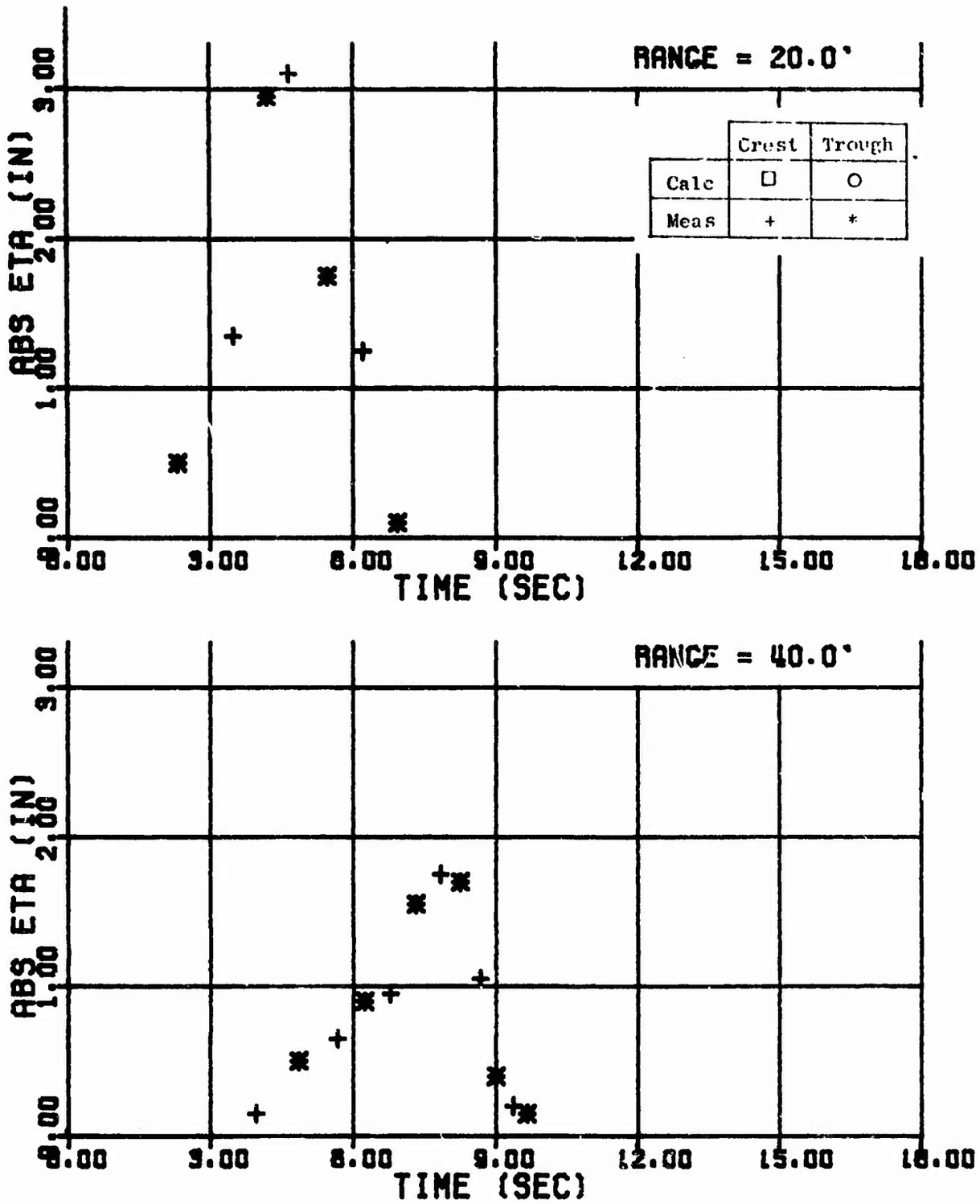

Fig. 12 Wave Trains - Shot 9

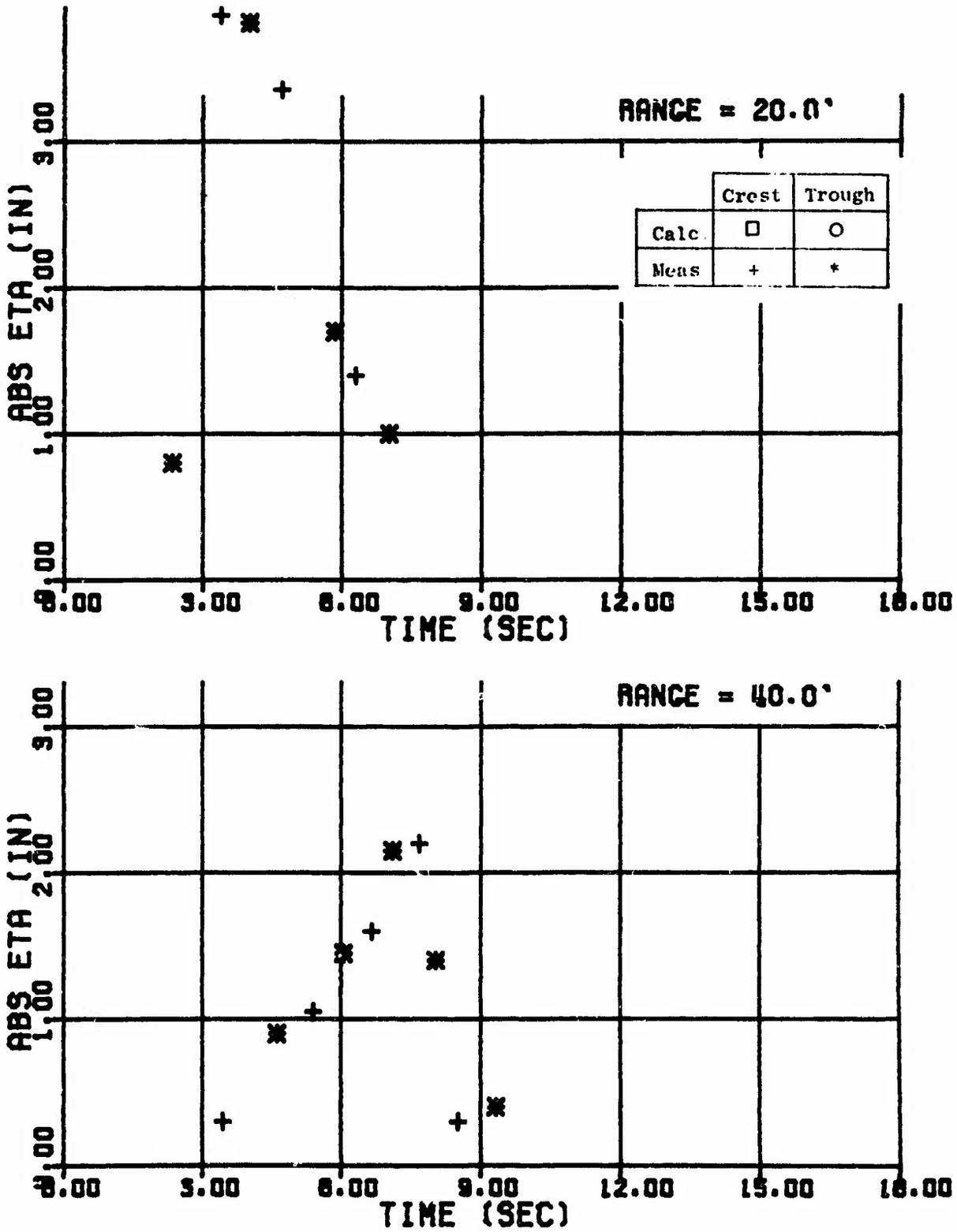

Fig. 13 Wave Trains - Shot 10

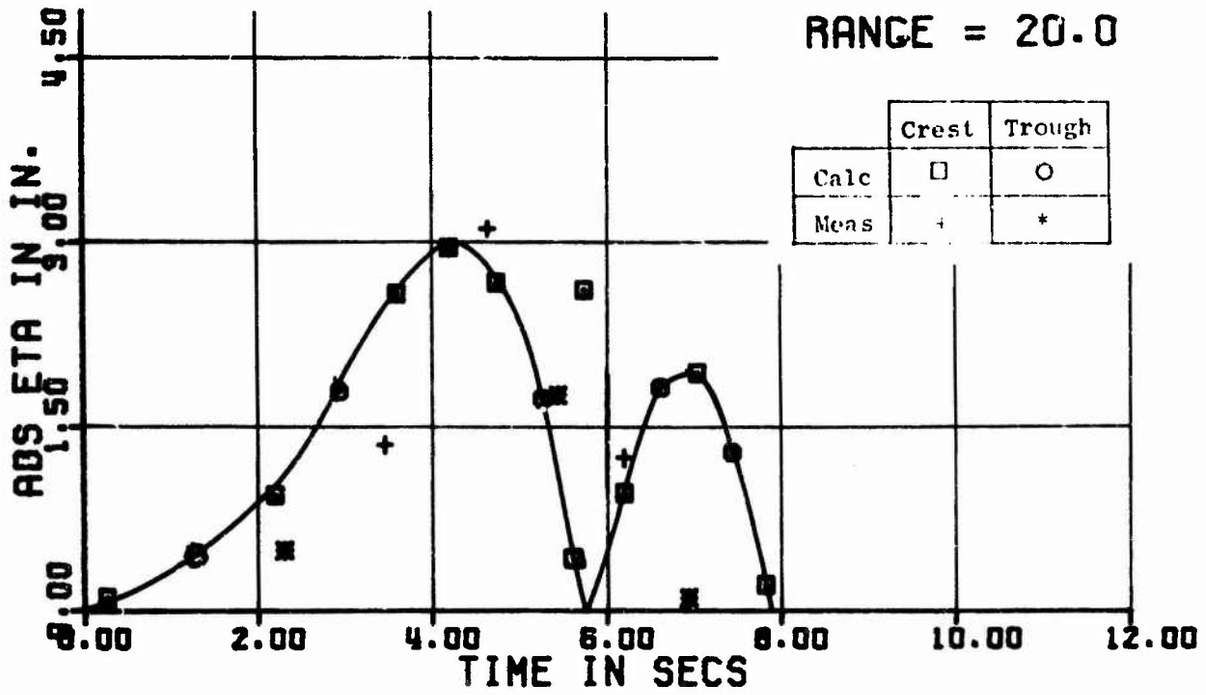

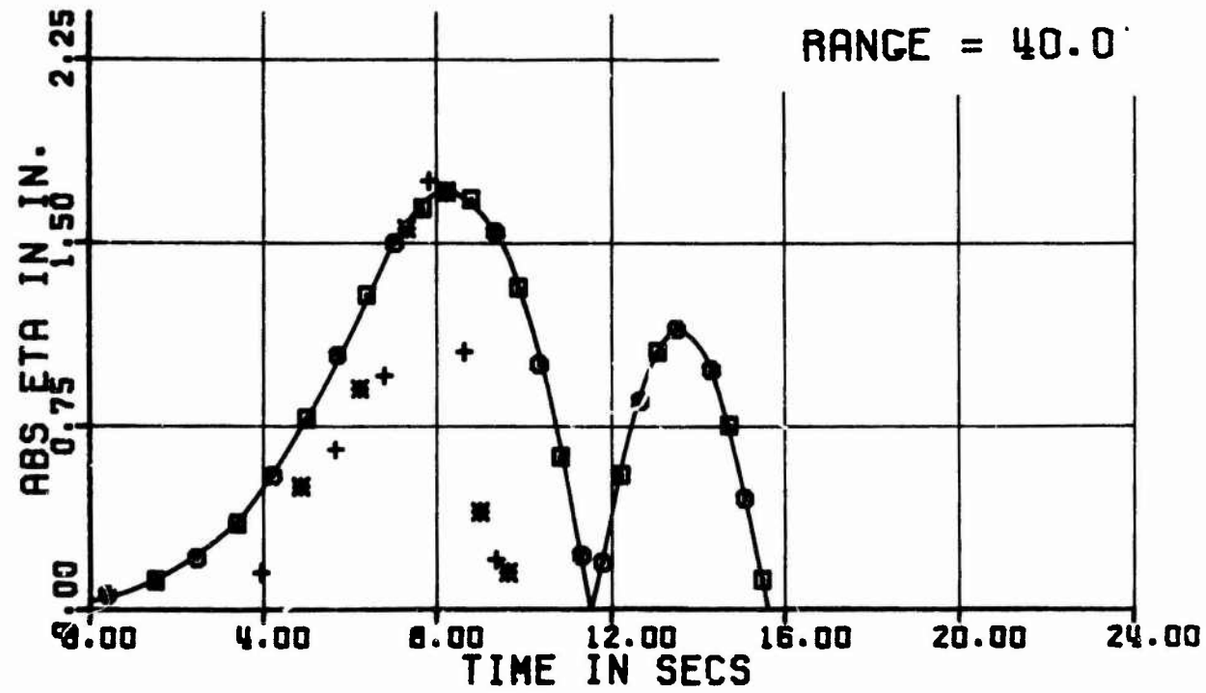

Fig. 14 Wave Trains - Shot 11

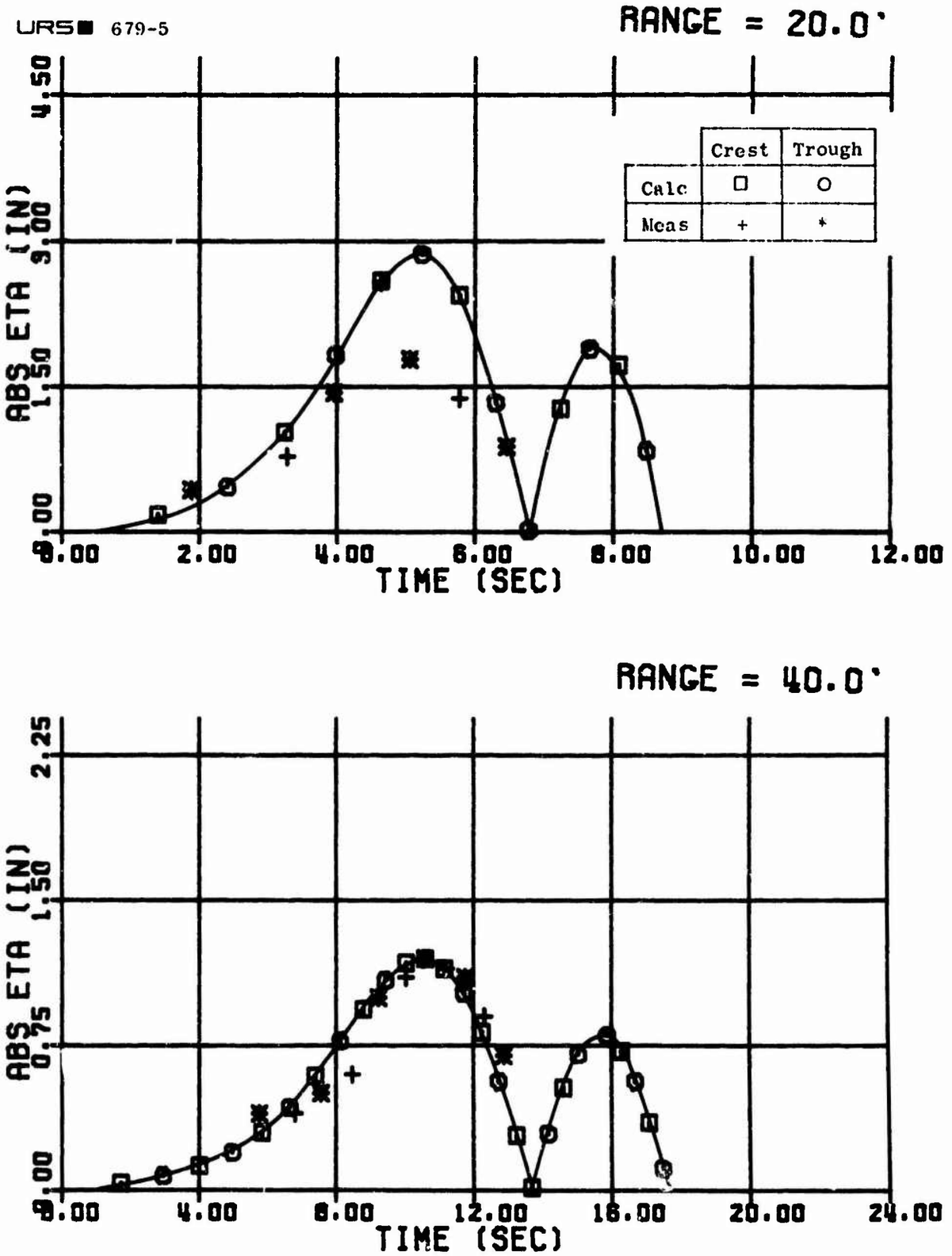

Fig. 15 Wave Trains - Shot 12

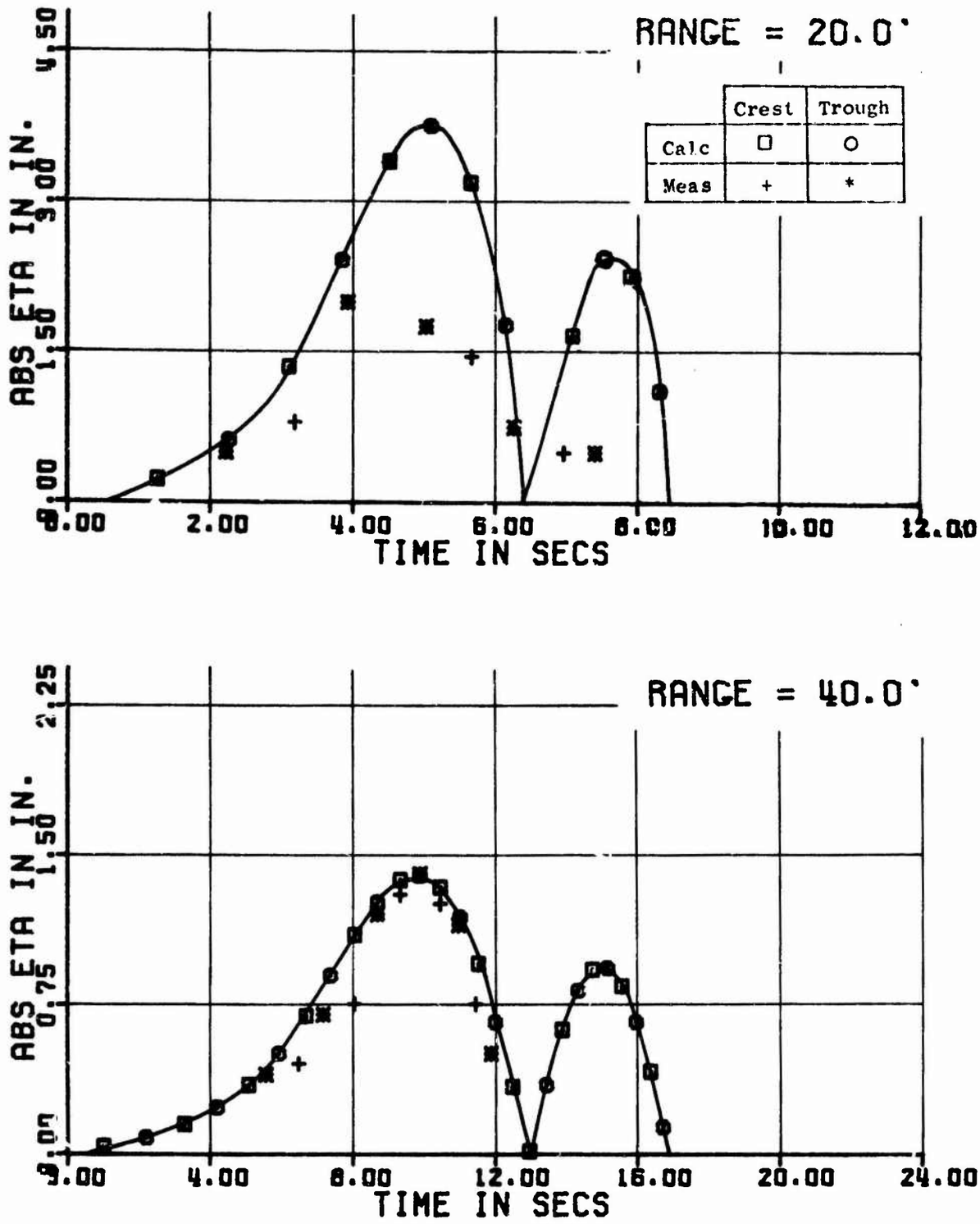

Fig. 16. Wave Trains - Shot 13

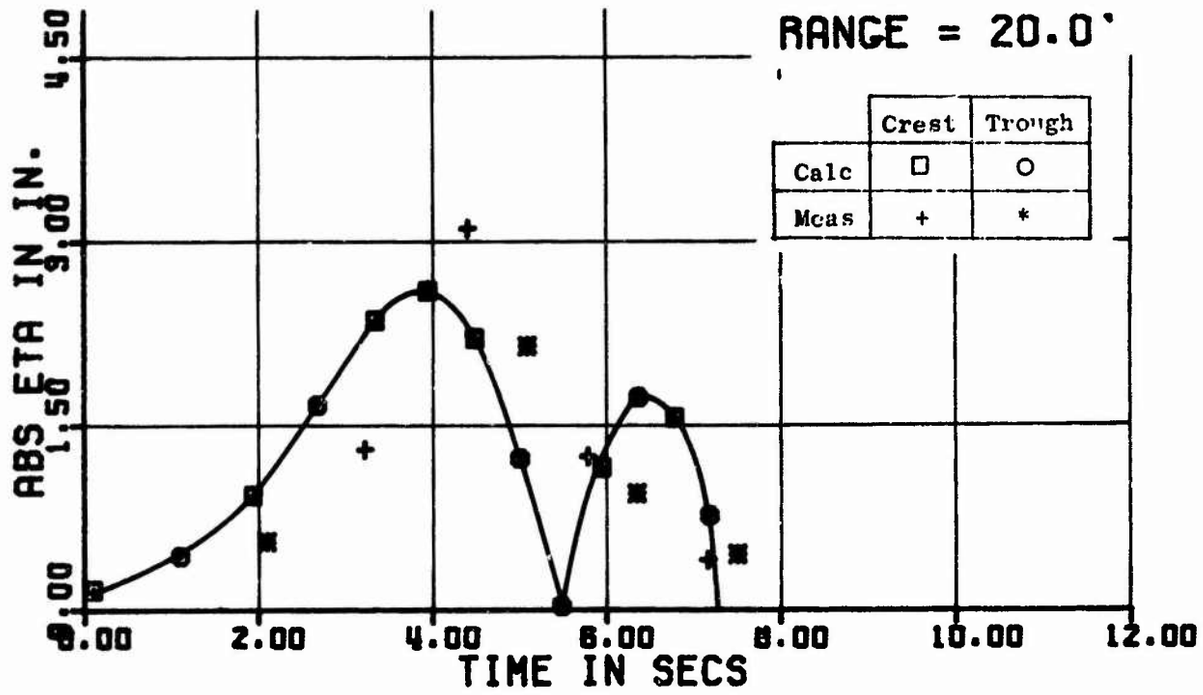

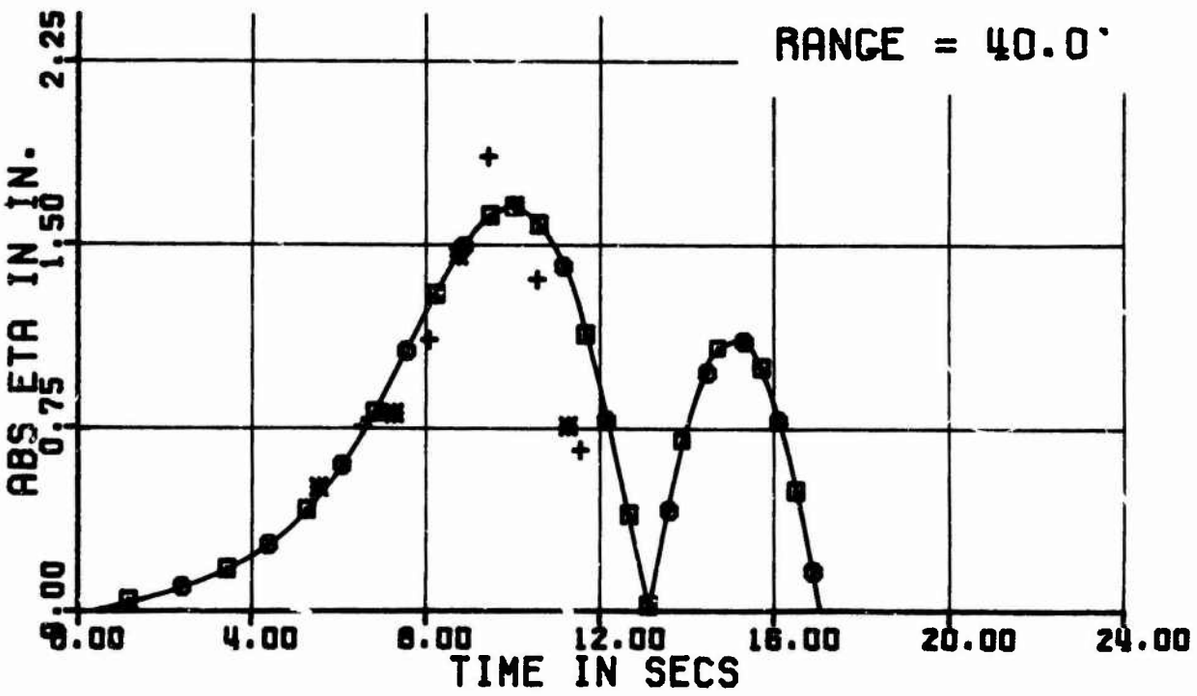

Fig. 17. Wave Trains - Shot 14

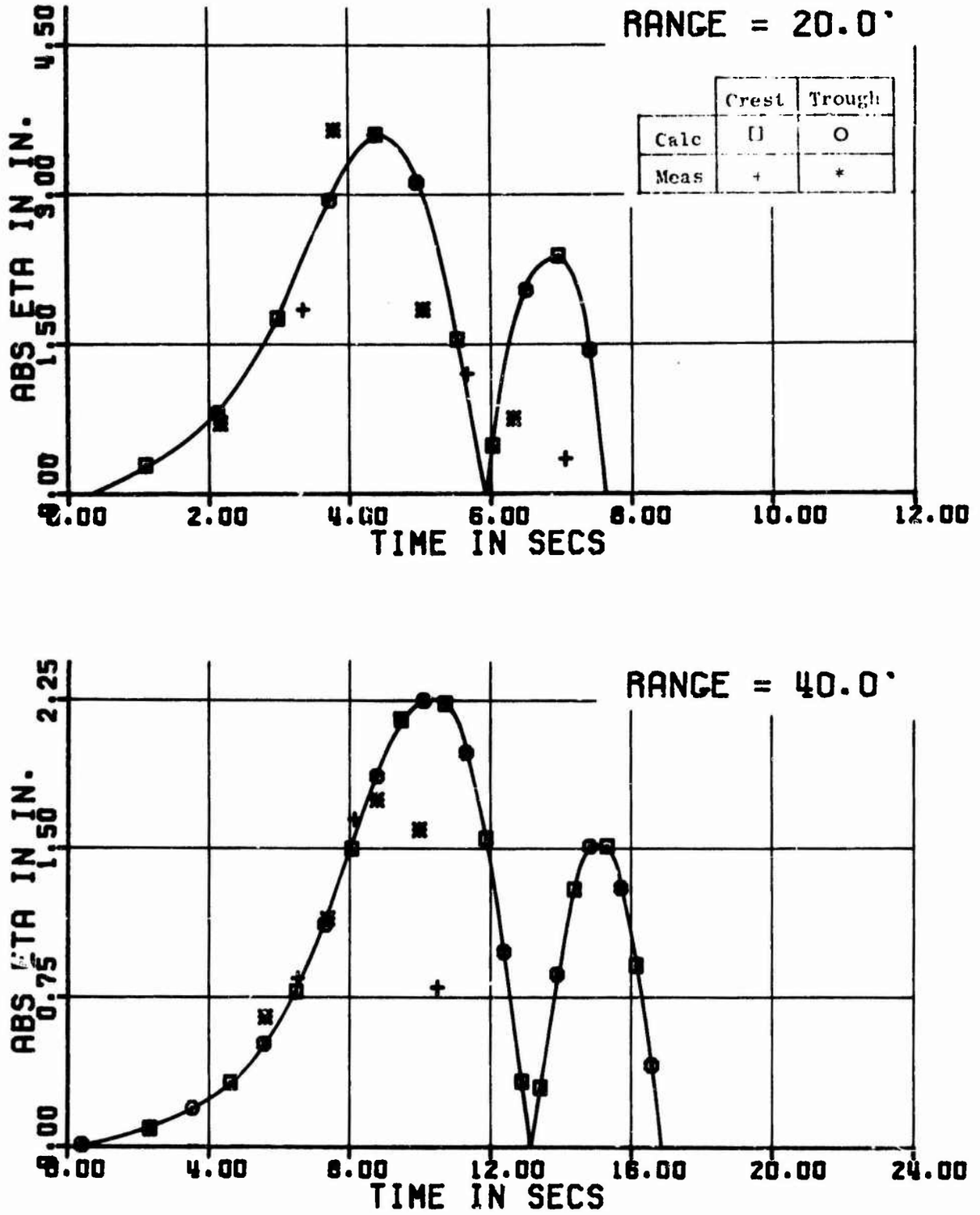

Fig. 18. Wave Trains - Shot 15

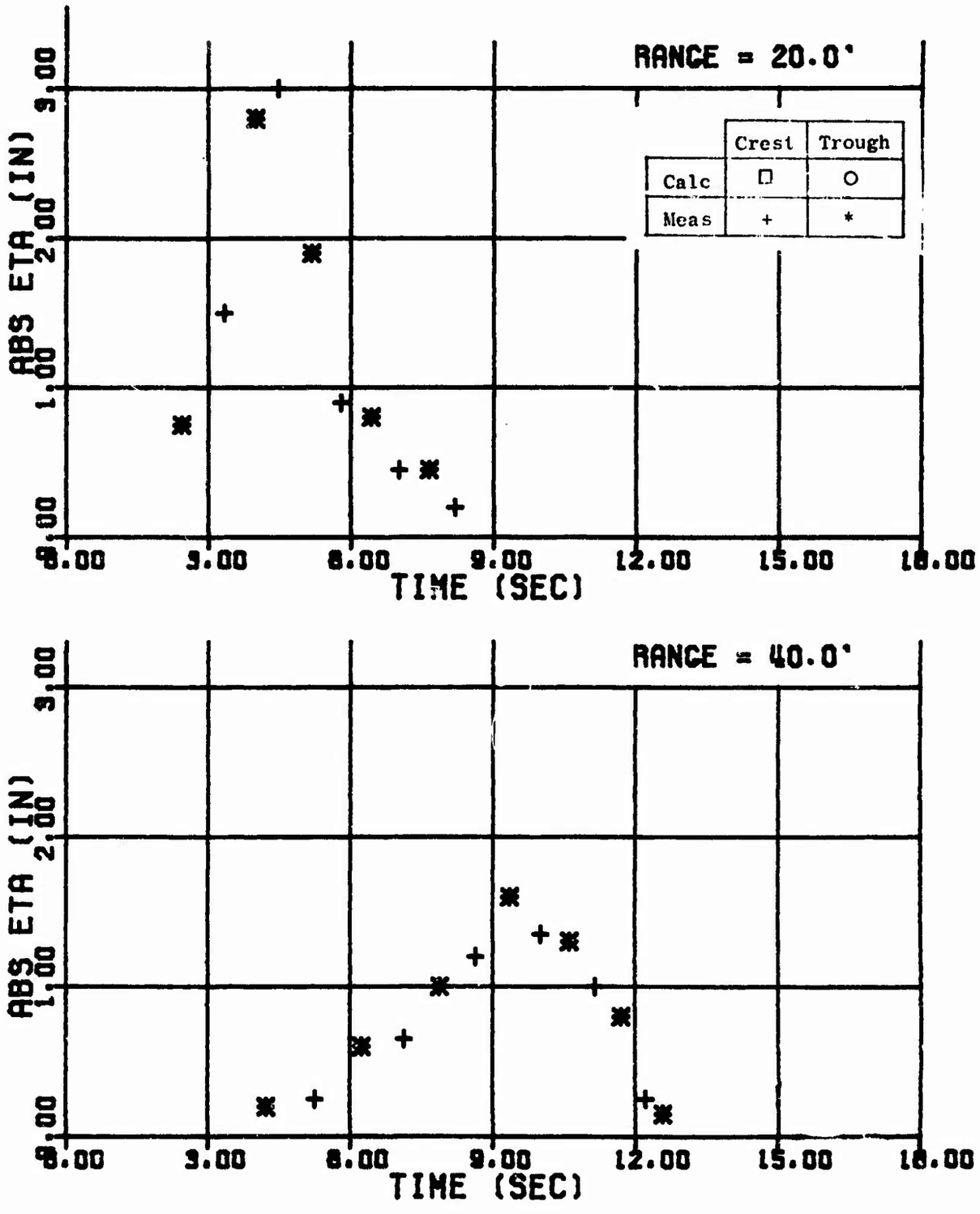

Fig. 19 Wave Trains - Shot 16

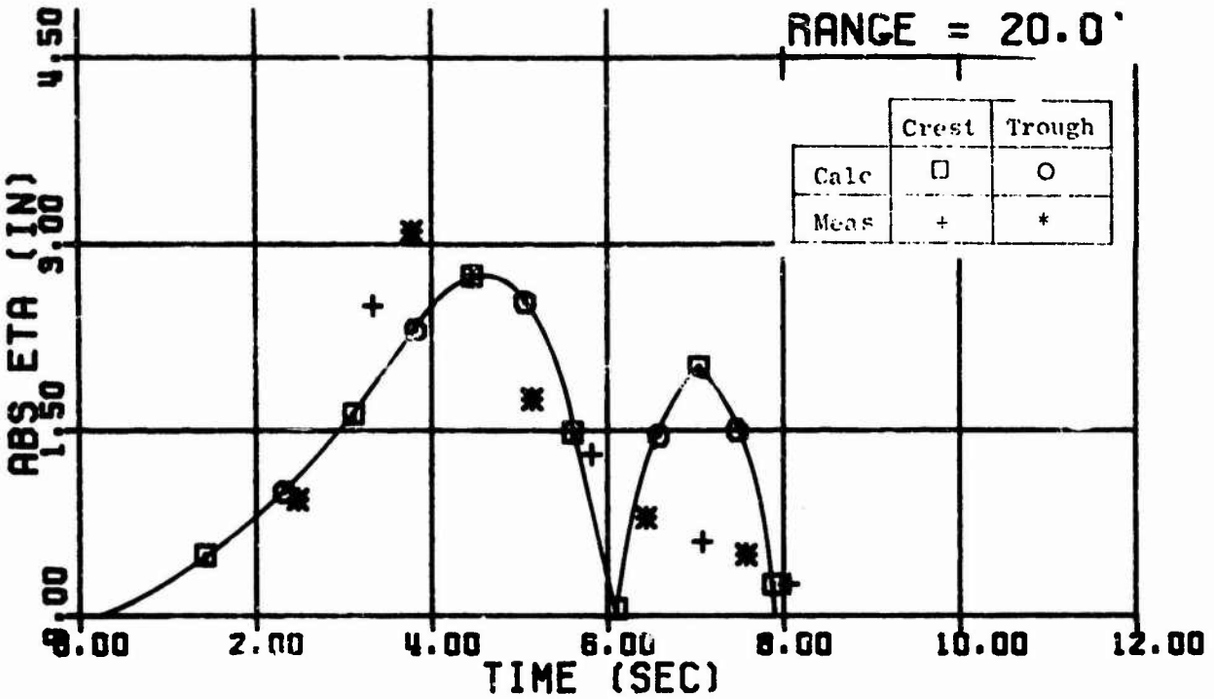

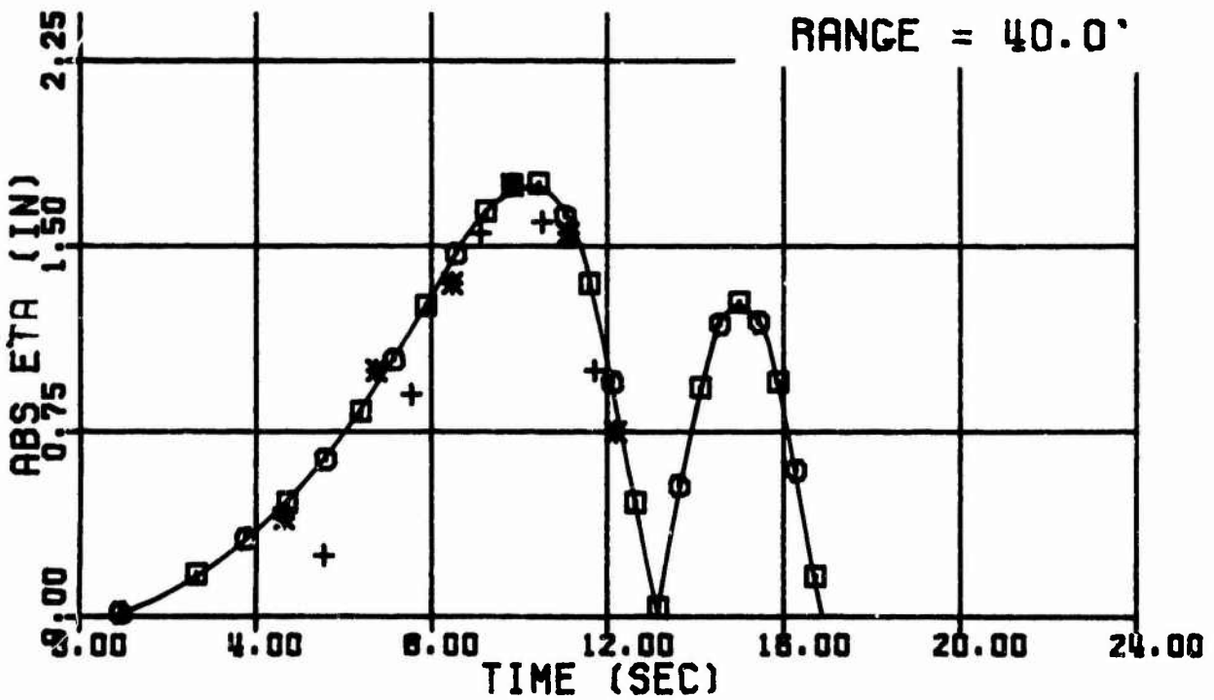

Fig. 20. Wave Trains - Shot 17

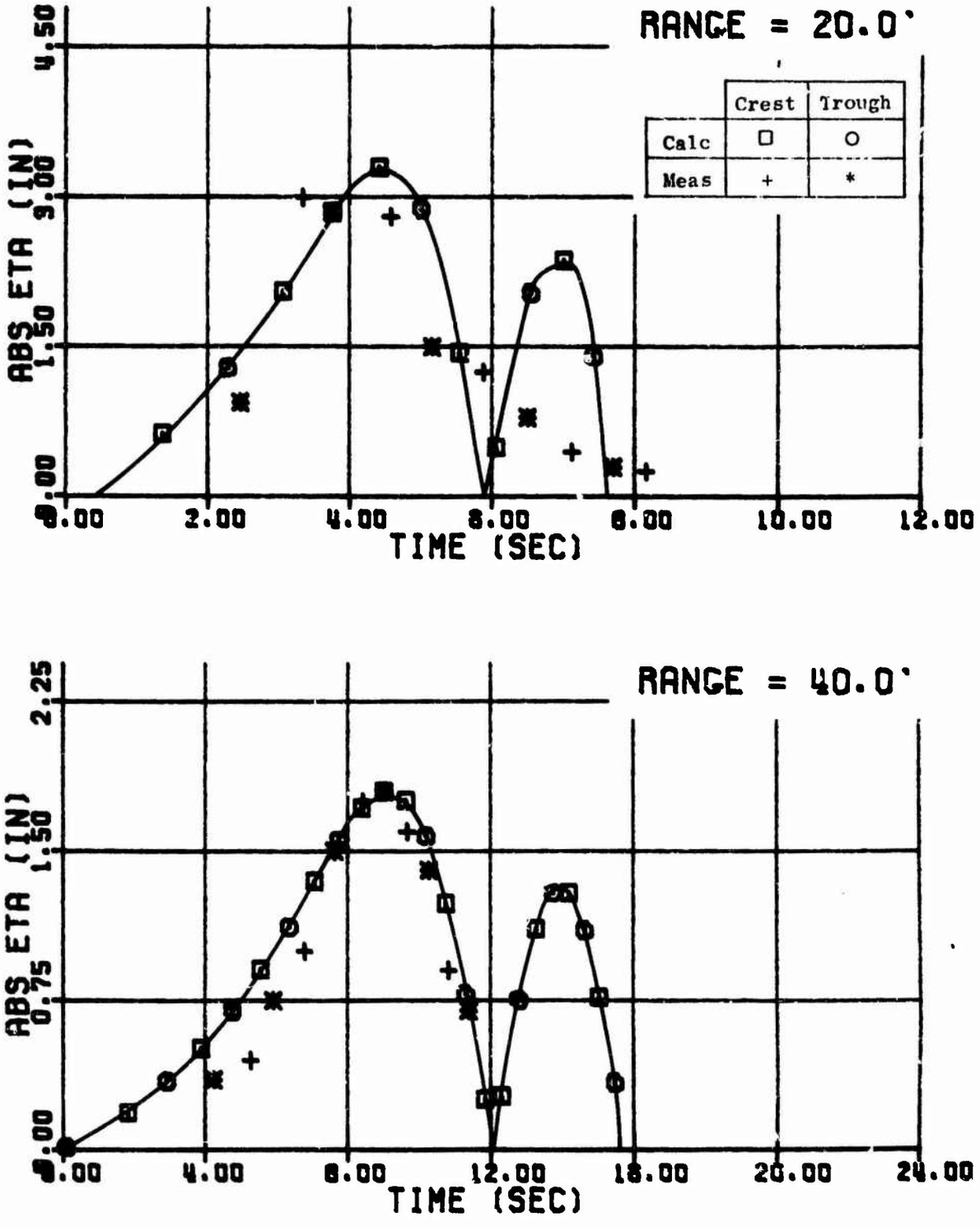

Fig. 21. Wave Trains - Shot 18

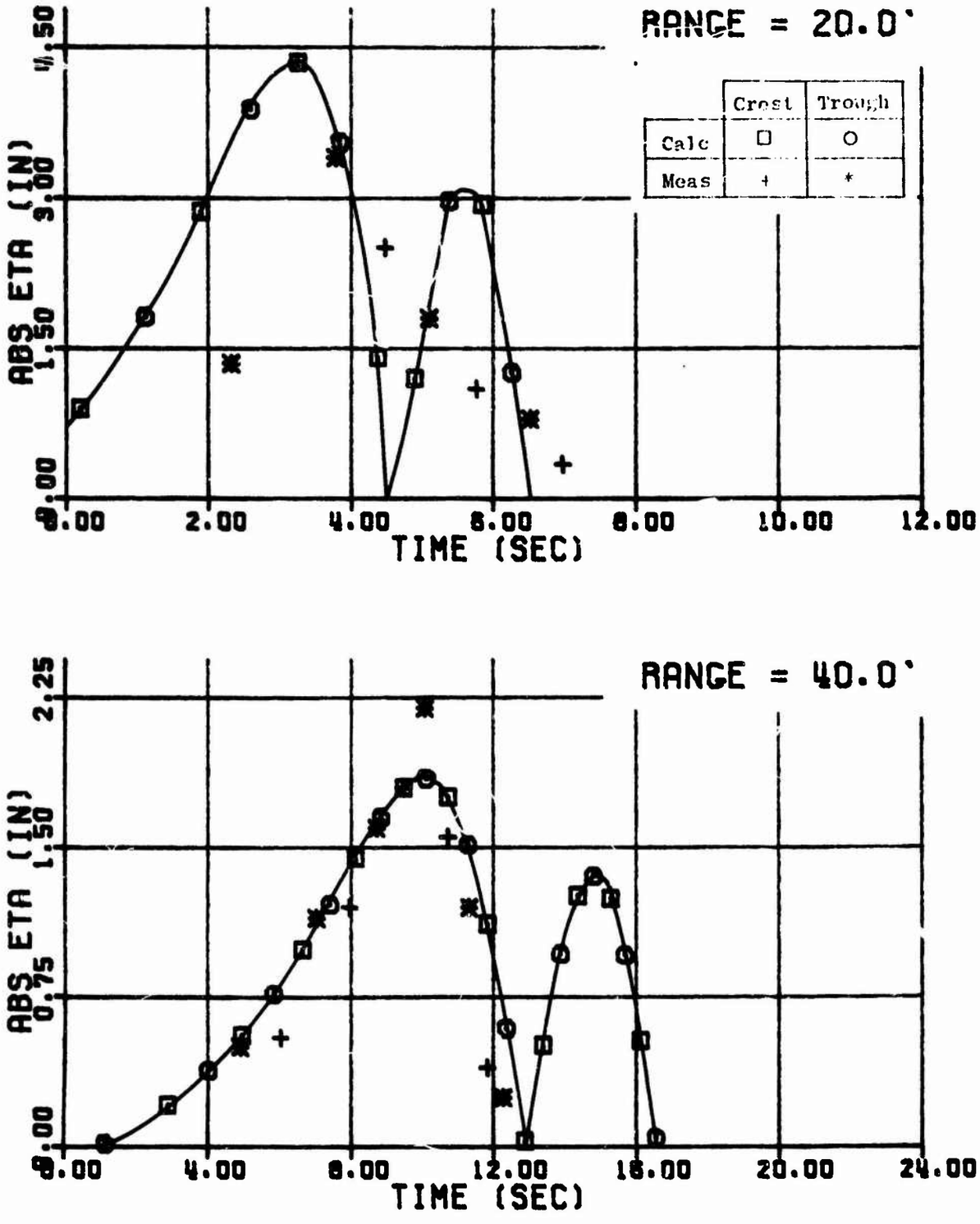

Fig. 22. Wave Trains - Shot 19

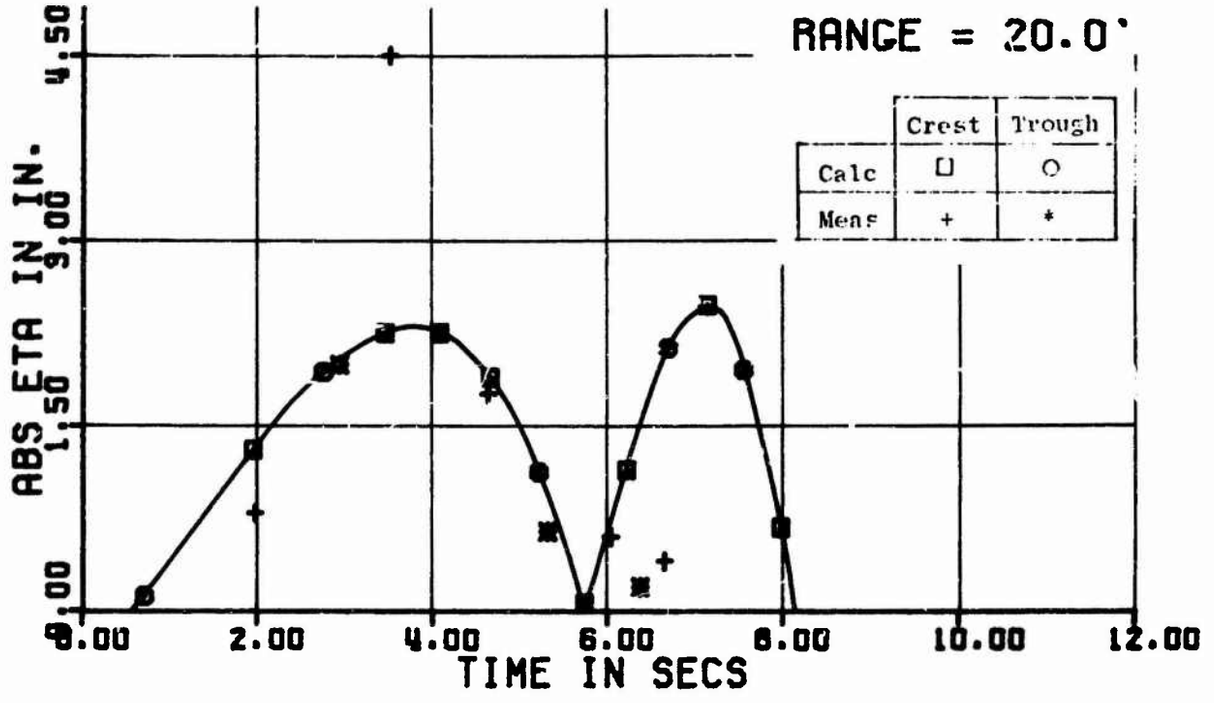

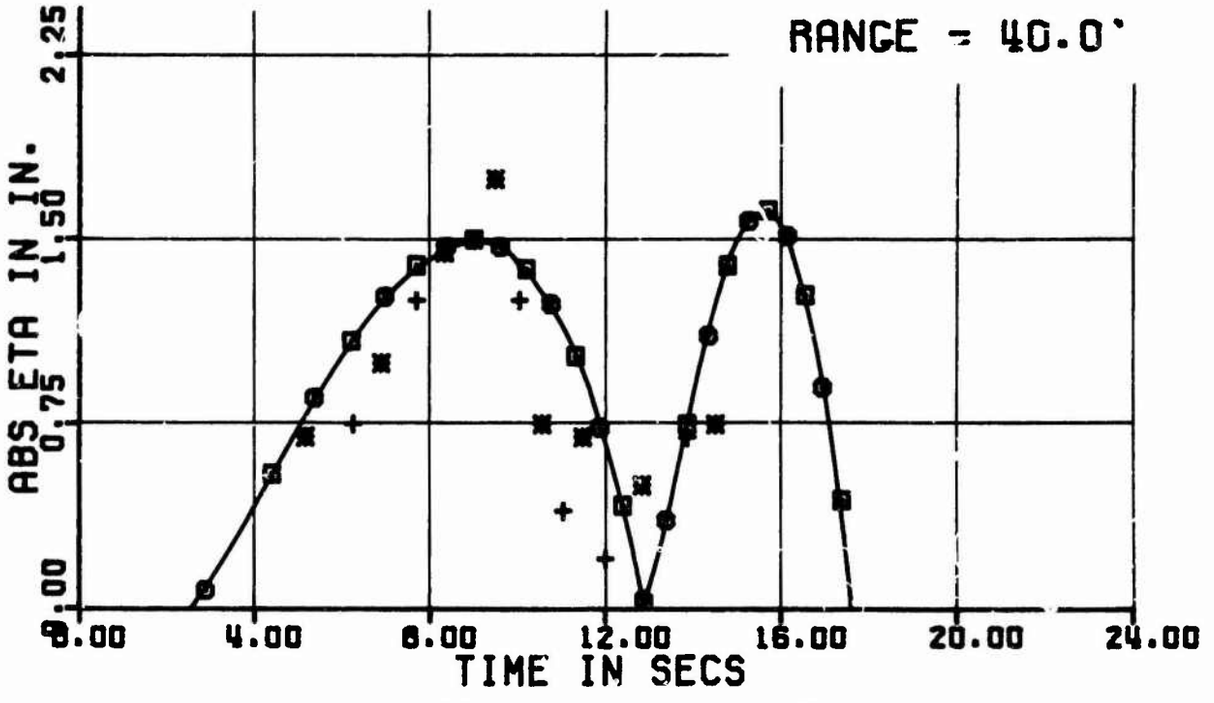

Fig. 23. Wave Trains - Shot 20

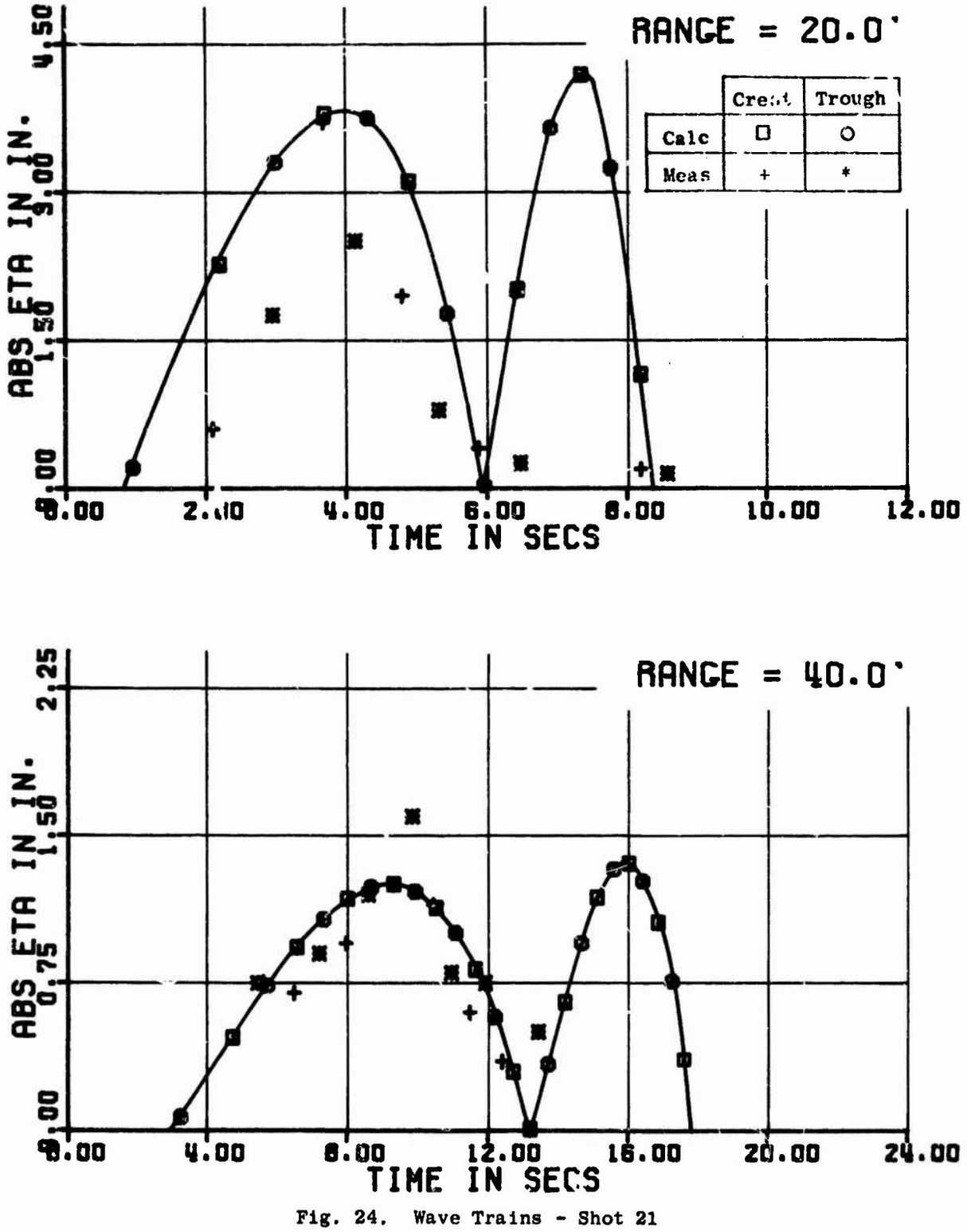

Fig. 24. Wave Trains - Shot 21

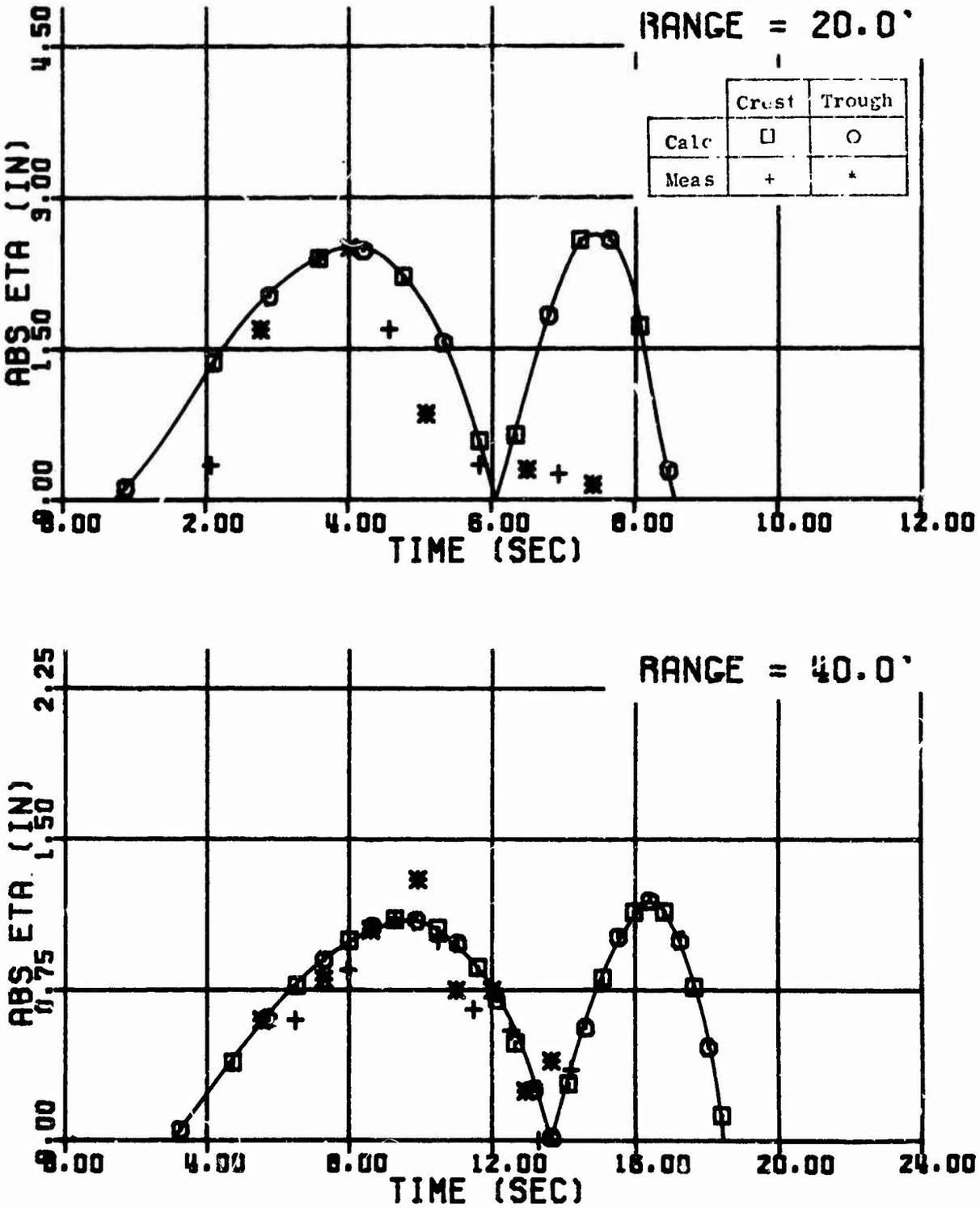

Fig. 25. Wave Trains - Shot 22

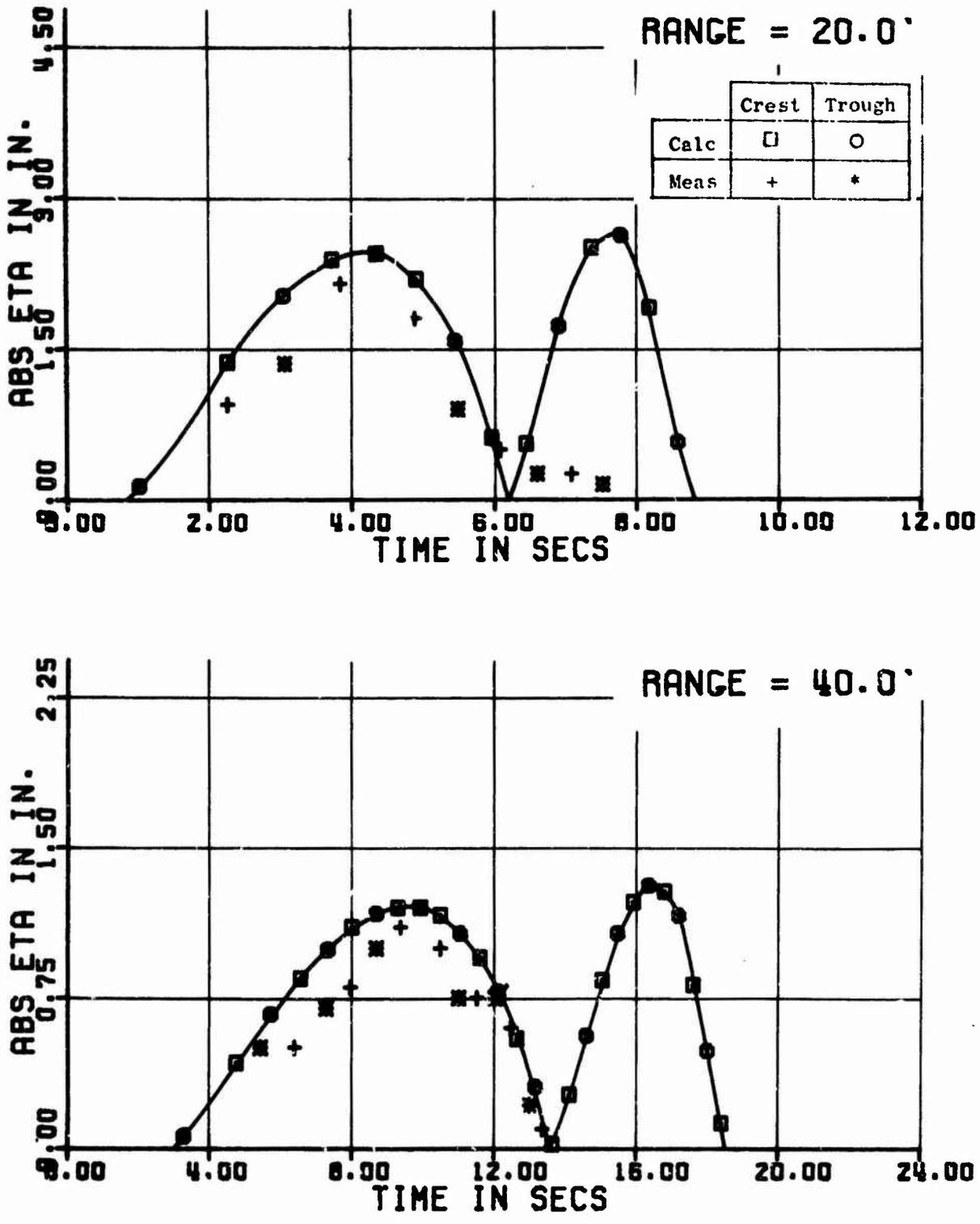

Fig. 26. Wave Trains - Shot 23

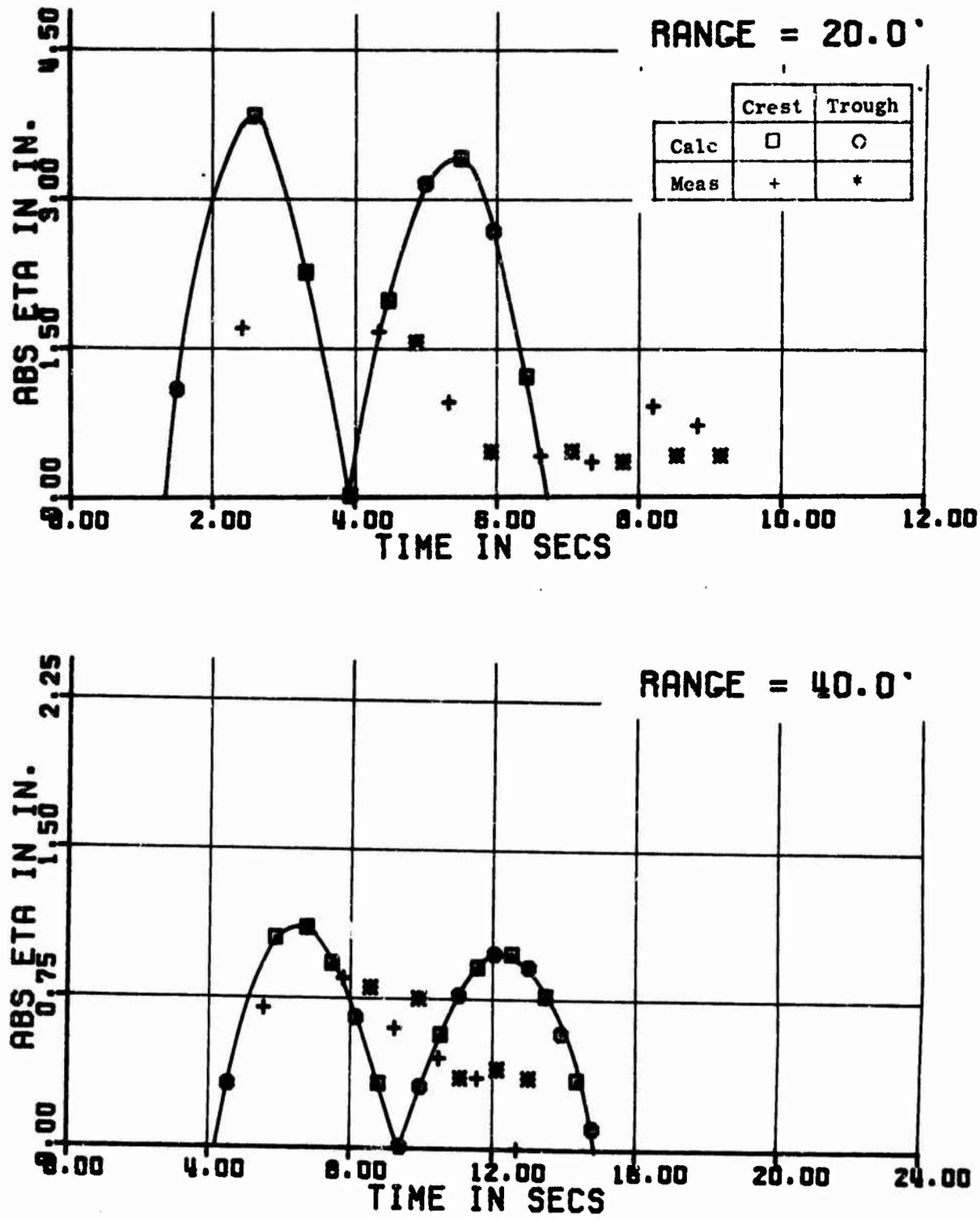

Fig. 27. Wave Trains - Shot 24

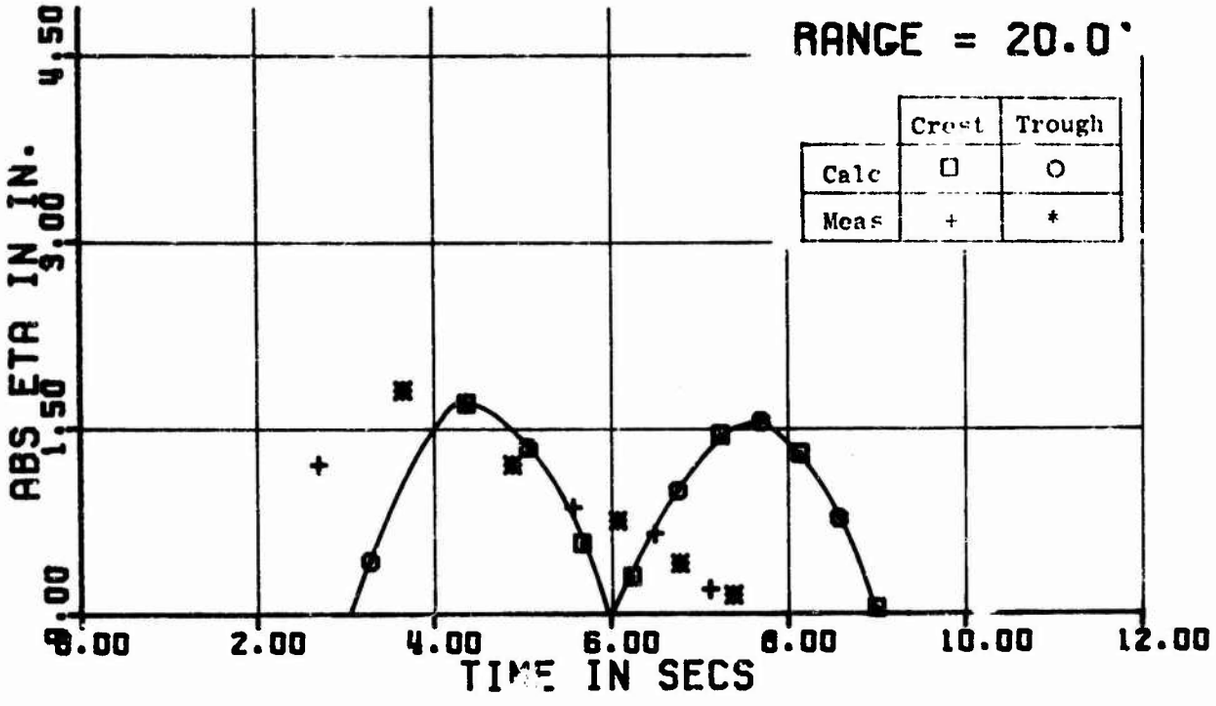

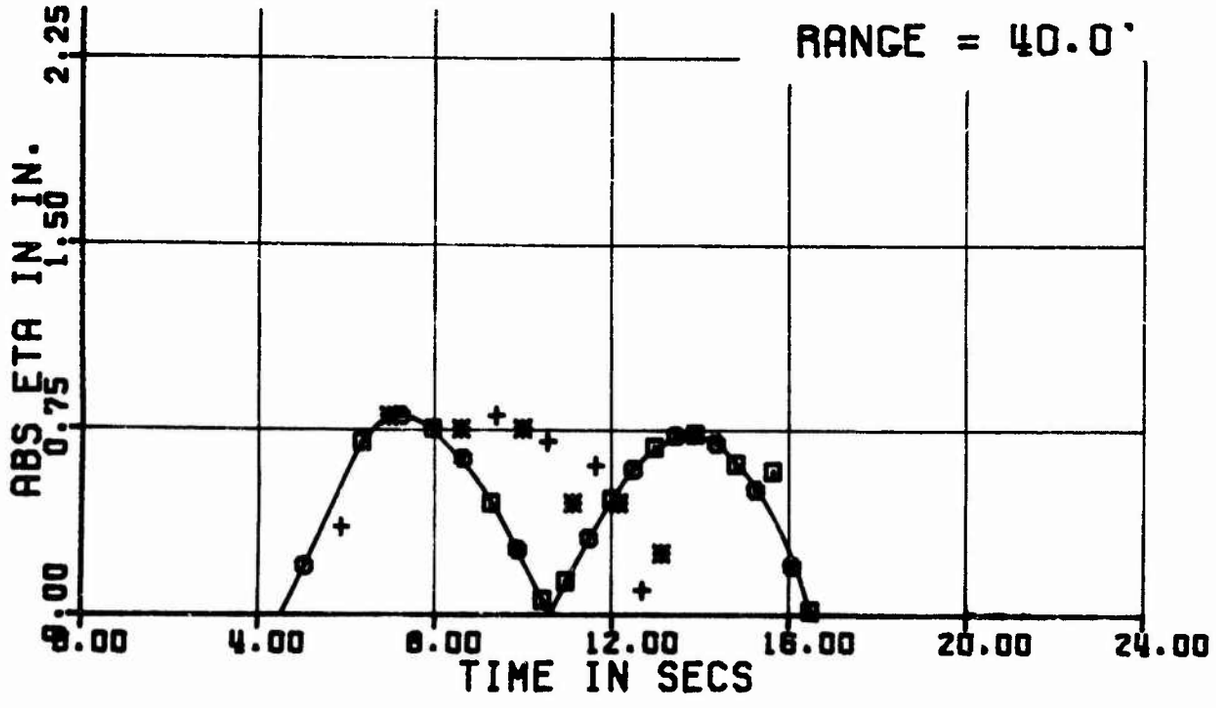

Fig. 28. Wave Trains - Shot 25

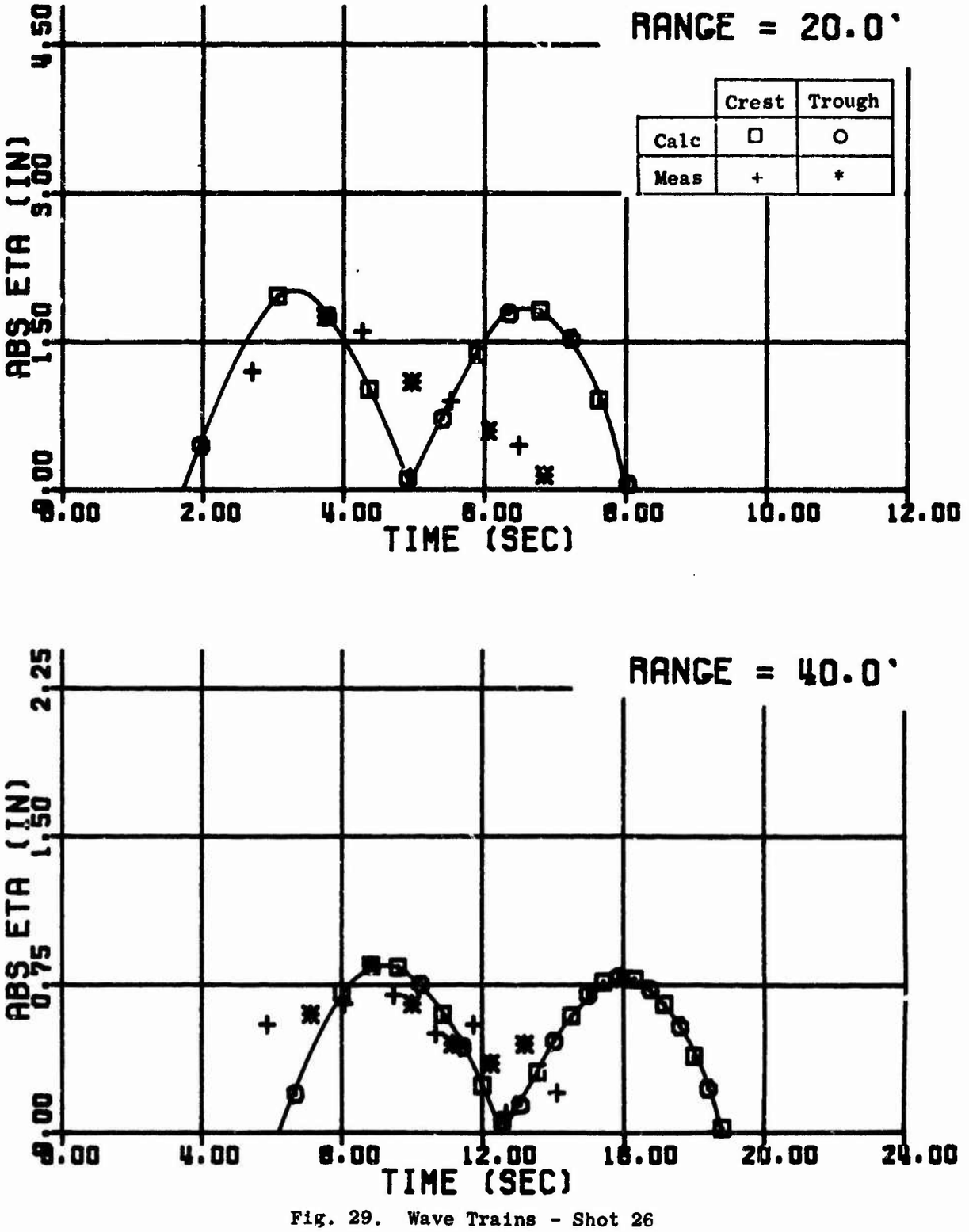

Fig. 29. Wave Trains - Shot 26

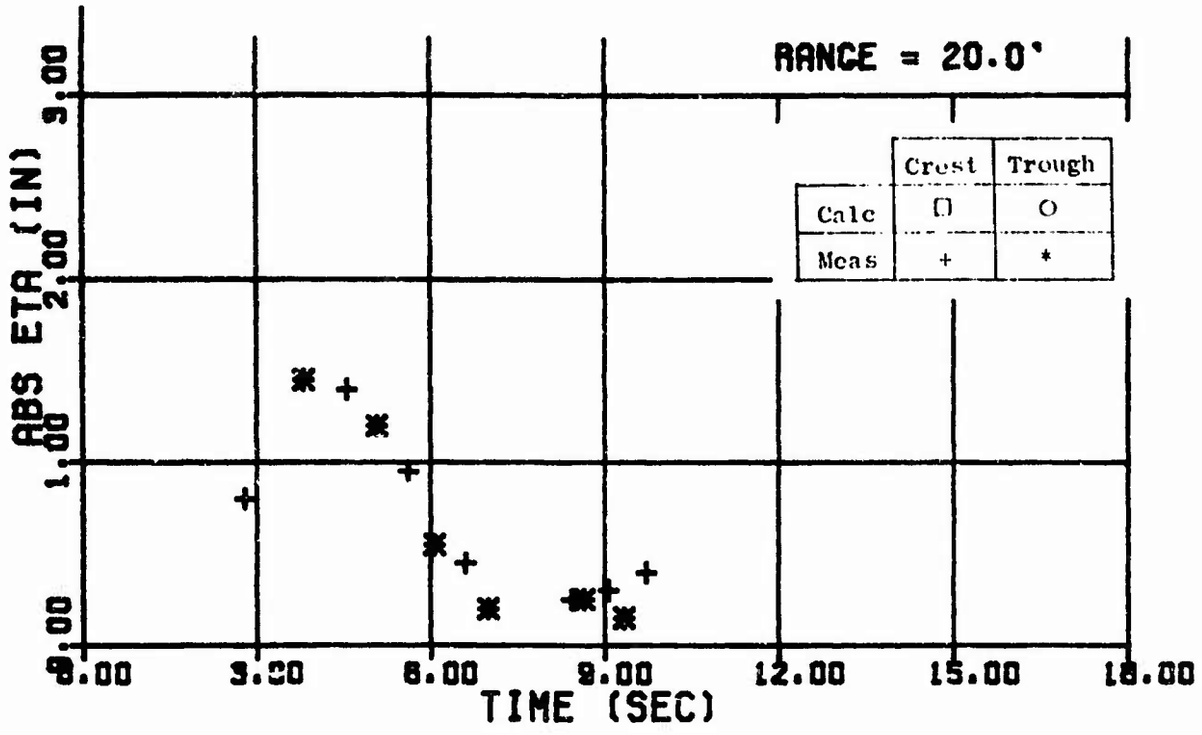

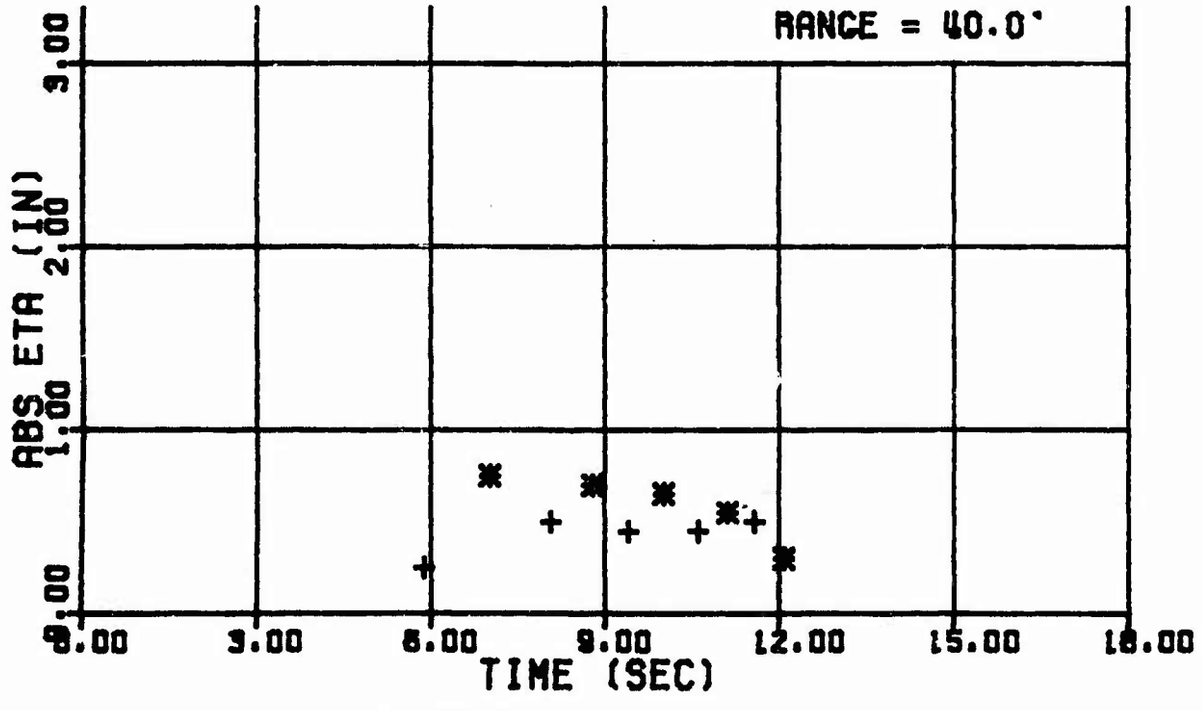

Fig. 30 Wave Trains - Shot 27

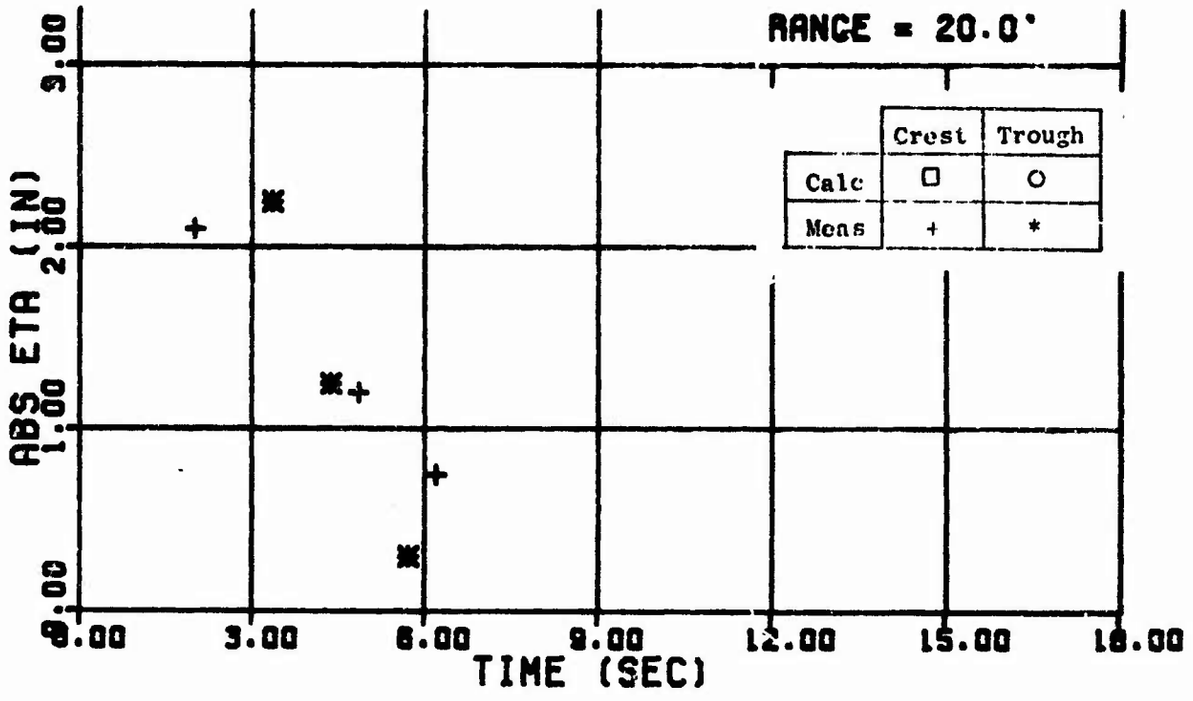

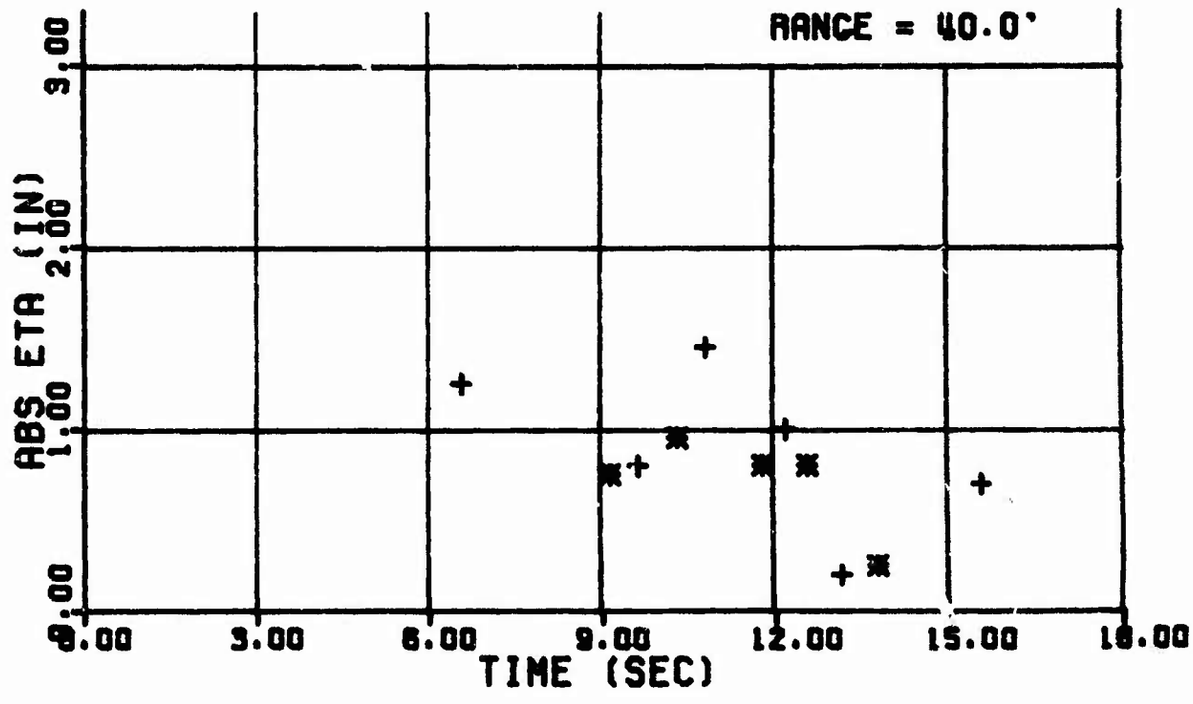

Fig. 31 Wave Trains - Shot 28

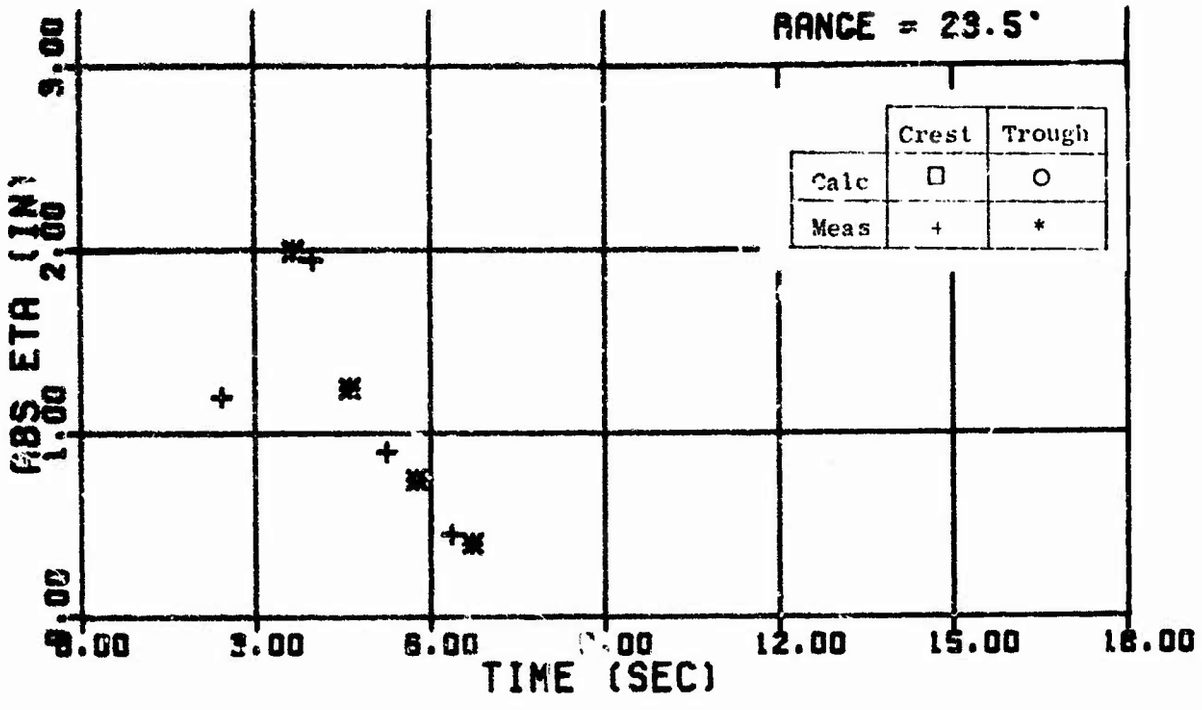

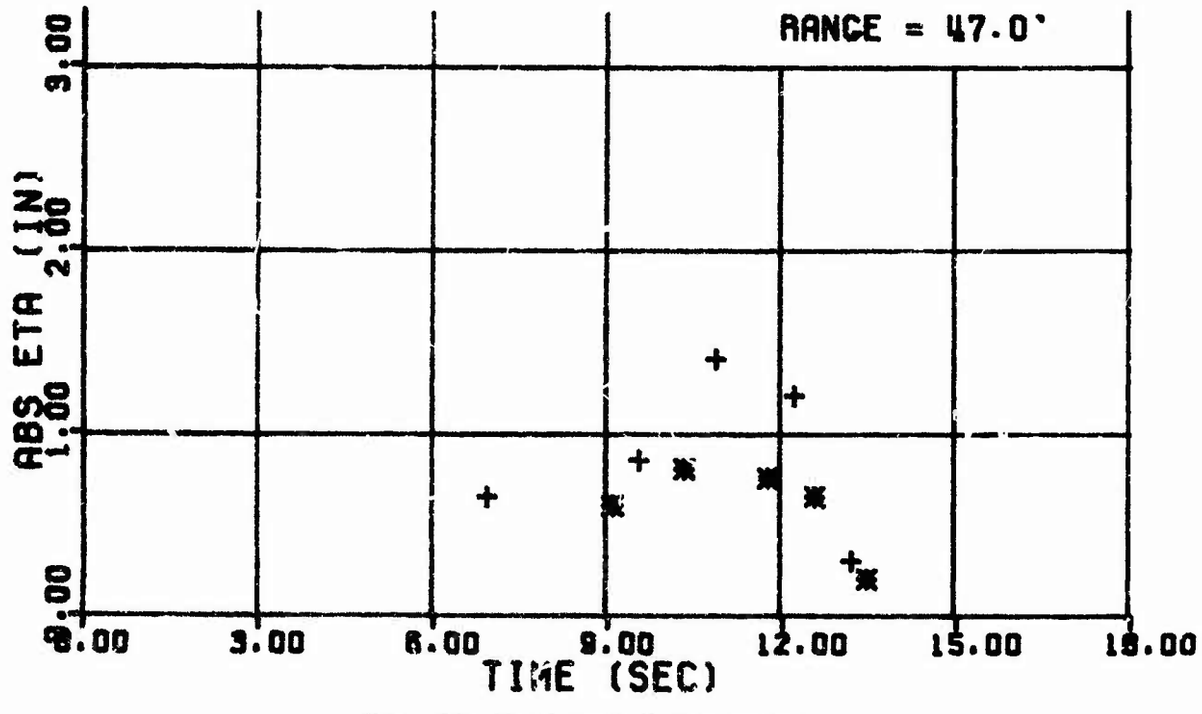

Fig. 32 Wave Trains - Shot 29

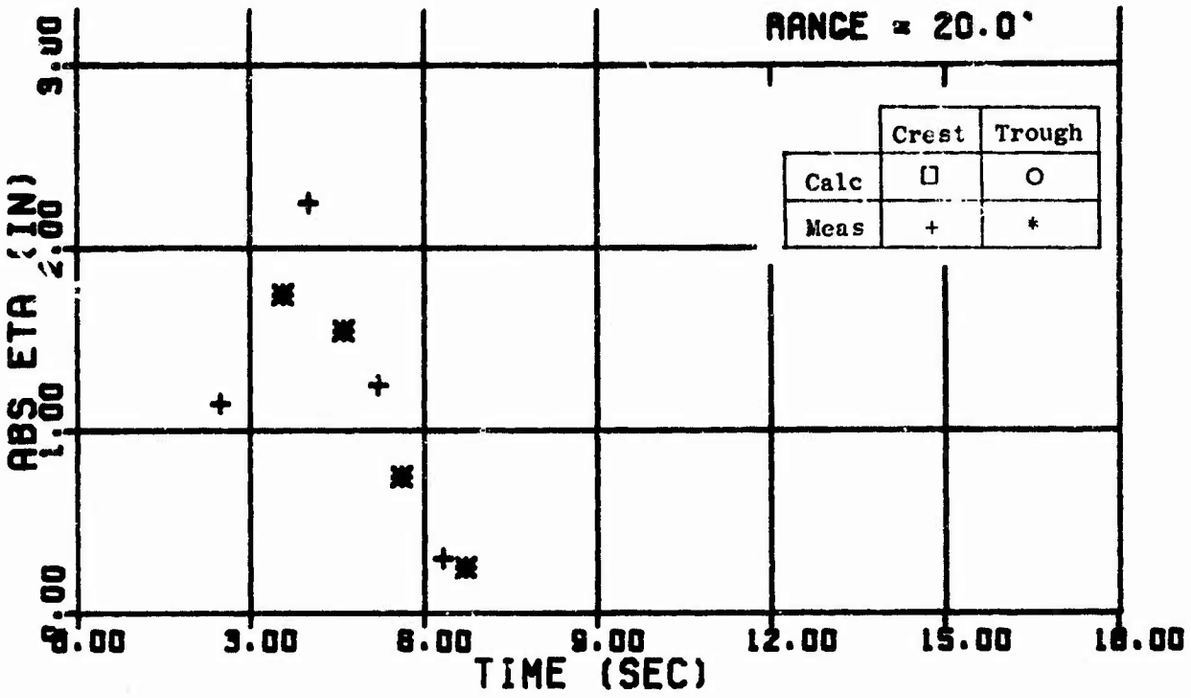

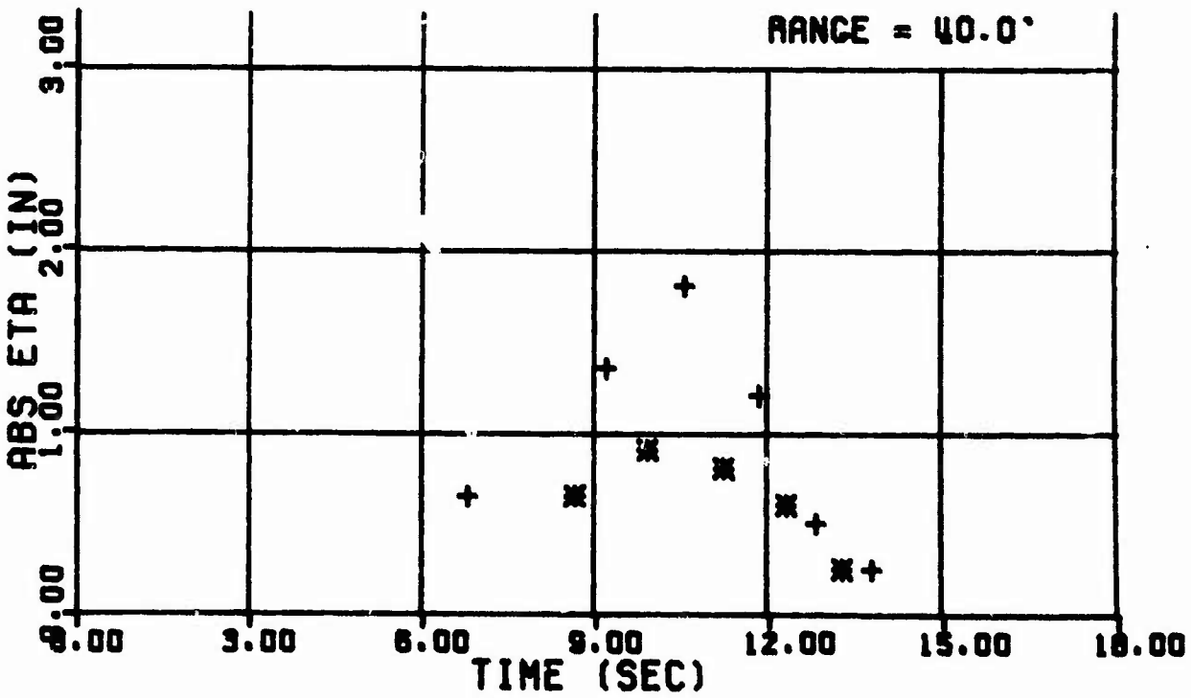

Fig. 33 Wave Trains - Shot 30

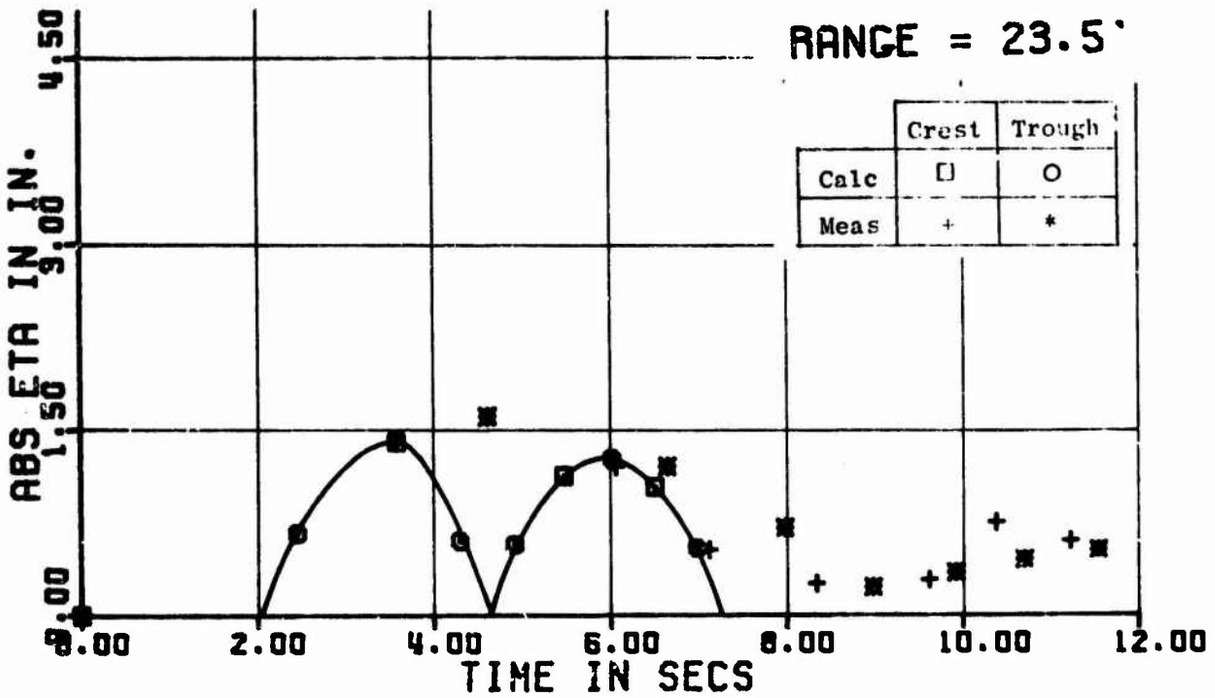

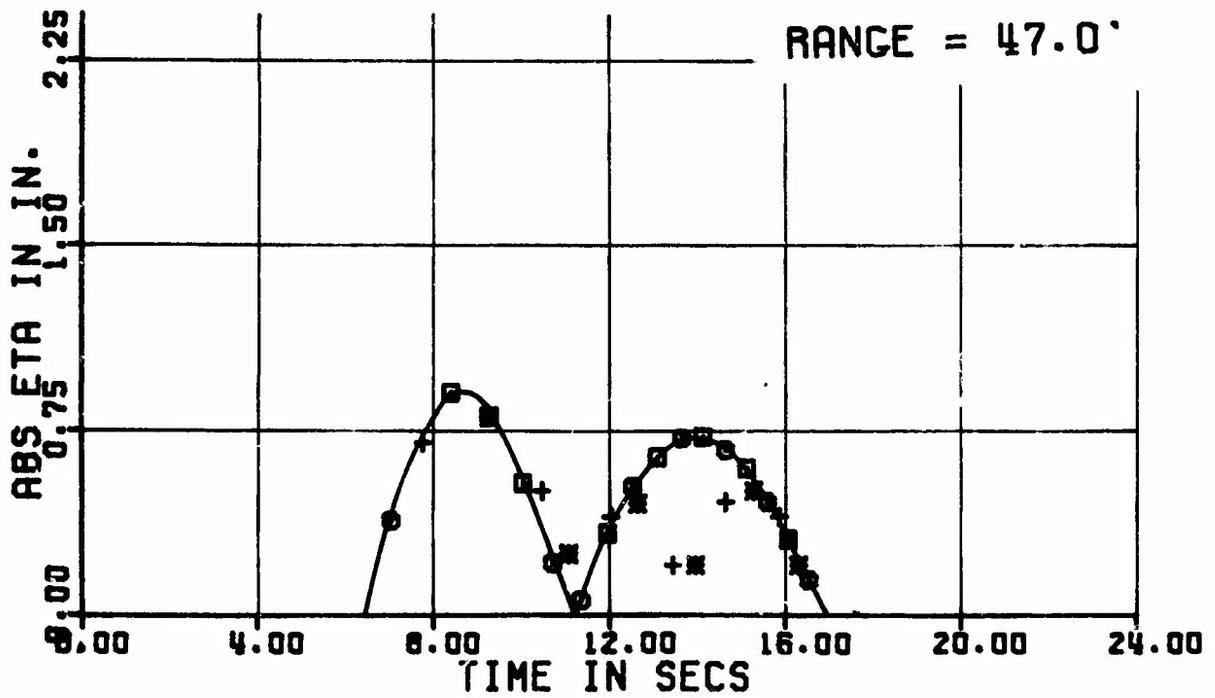

Fig. 34. Wave Trains - Shot 31

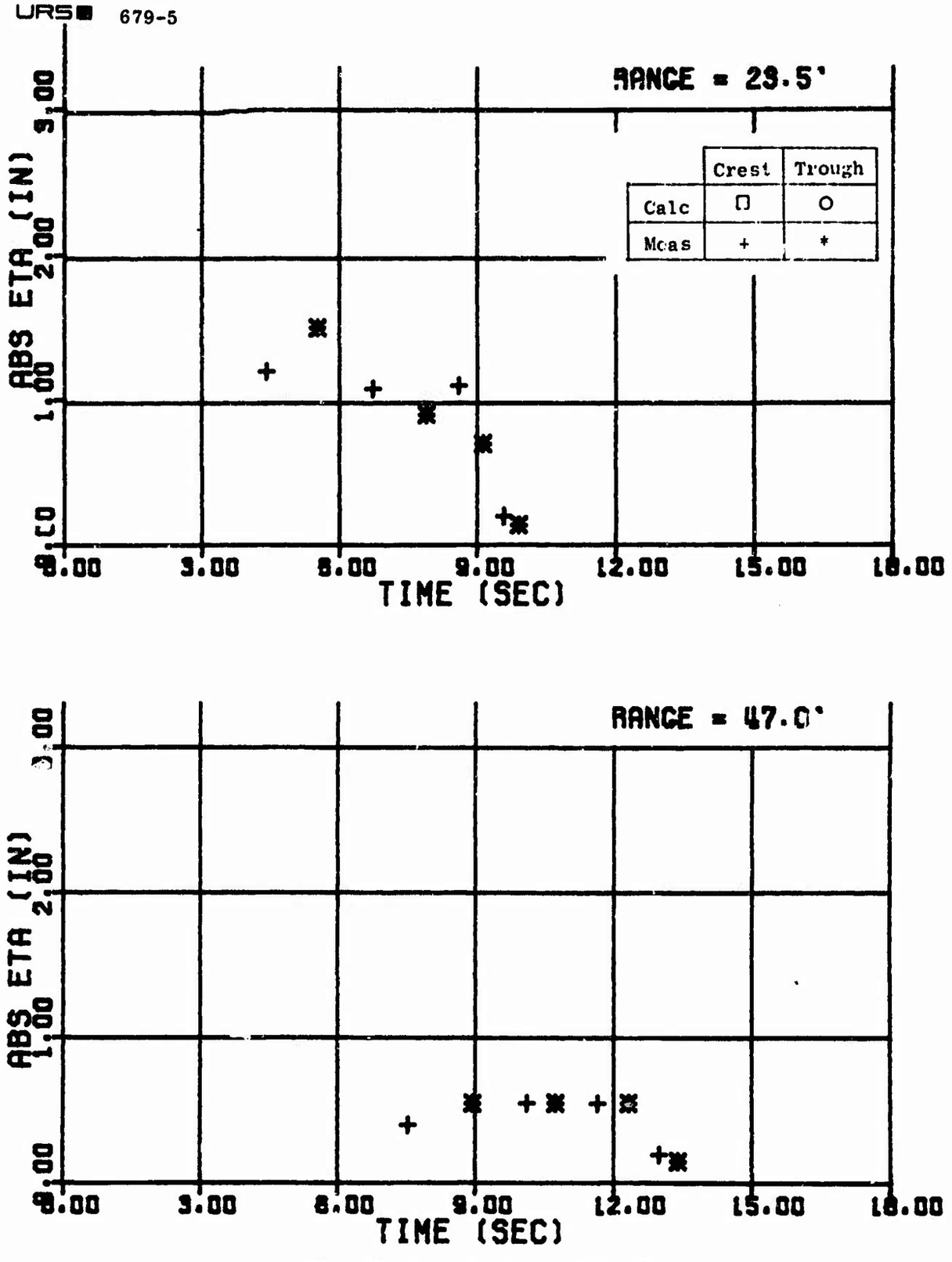

Fig. 35 Wave Trains - Shot 32

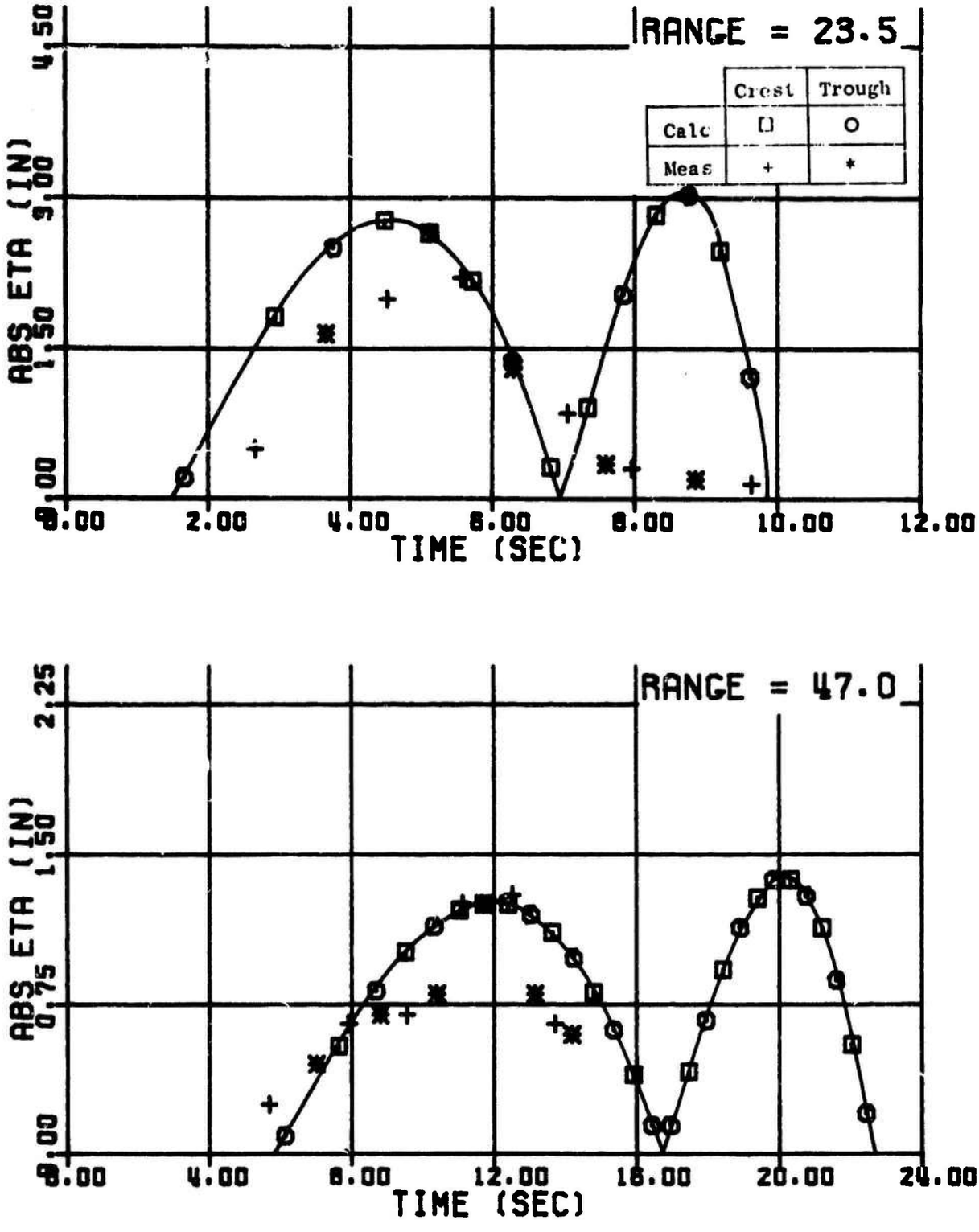

Fig. 36. Wave Trains - Shot 33

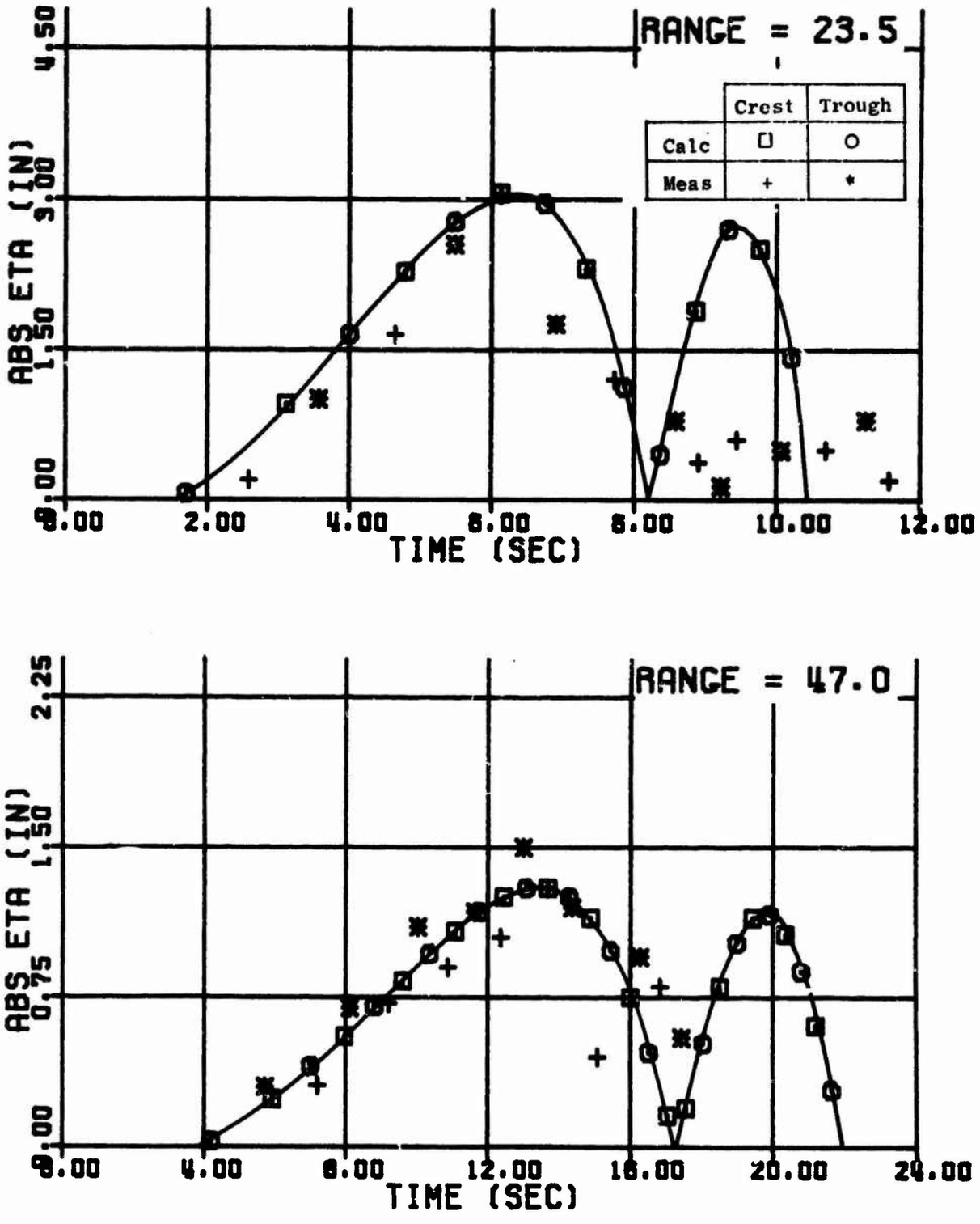

Fig. 37. Wave Trains - Shot 35

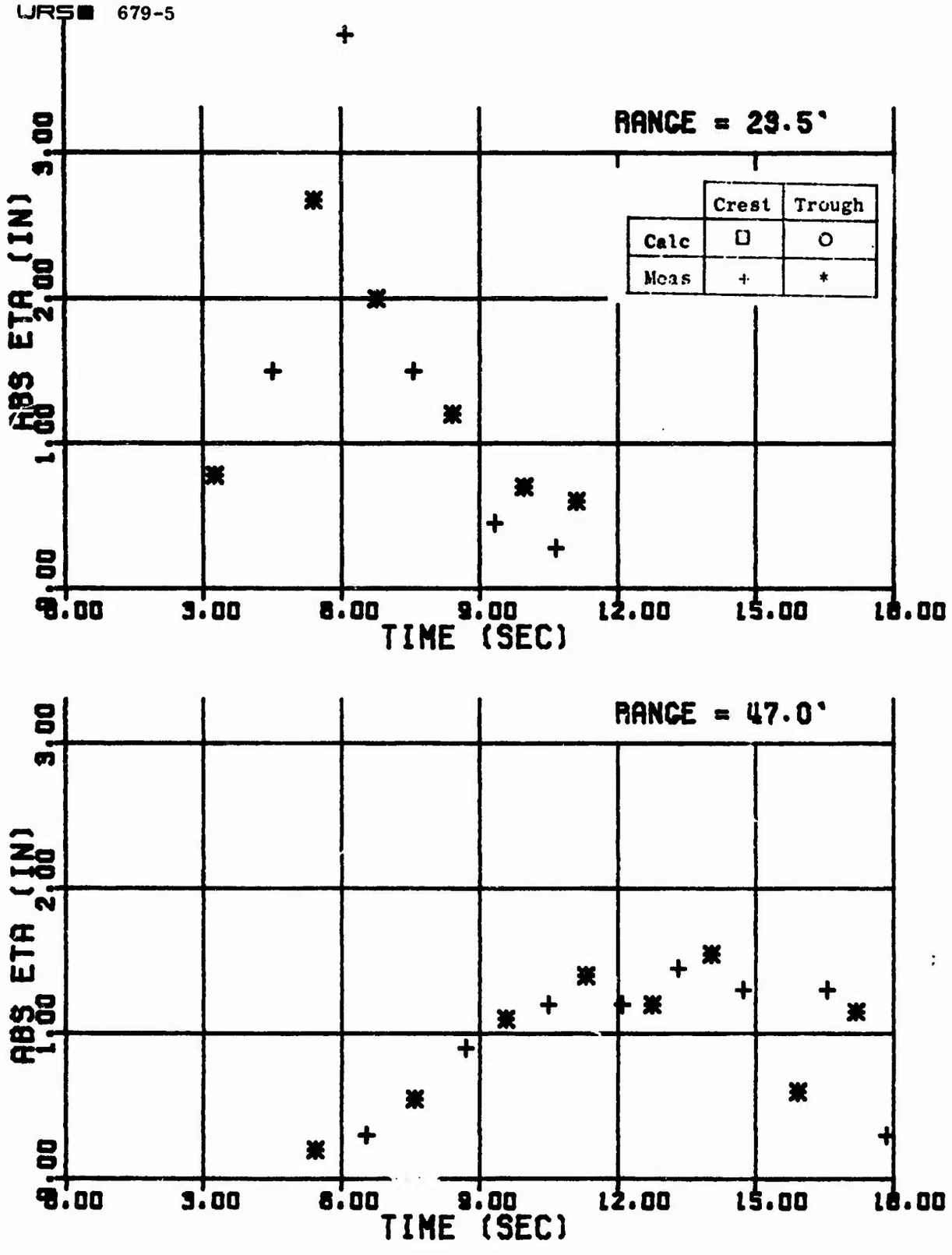

Fig. 38 Wave Trains - Shot 36

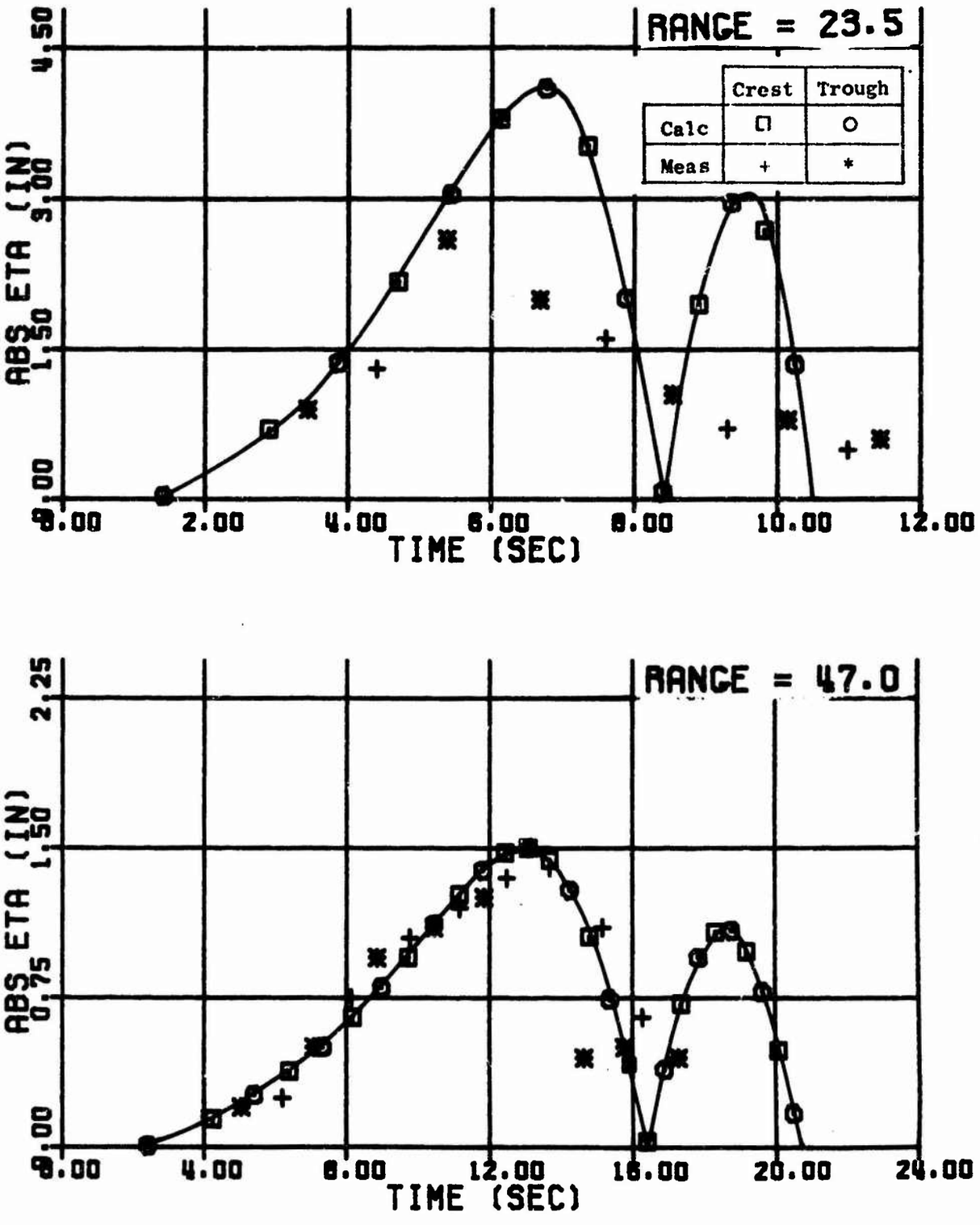

Fig. 39. Wave Trains - Shot 37

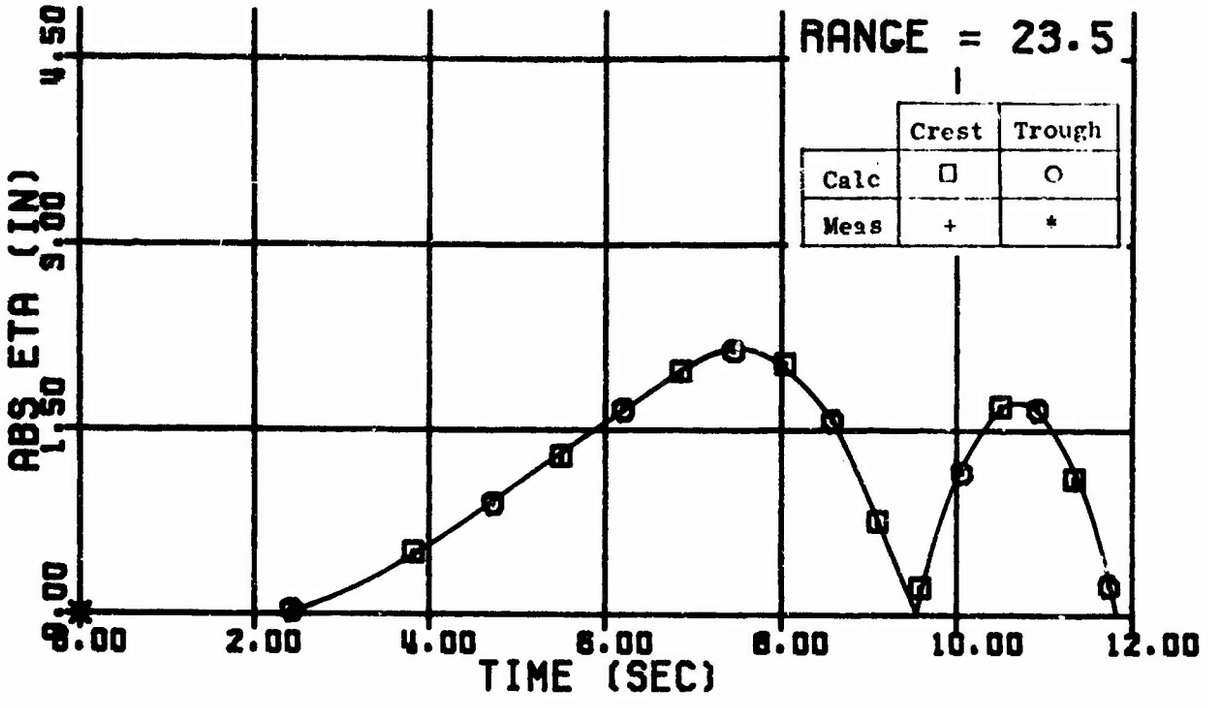

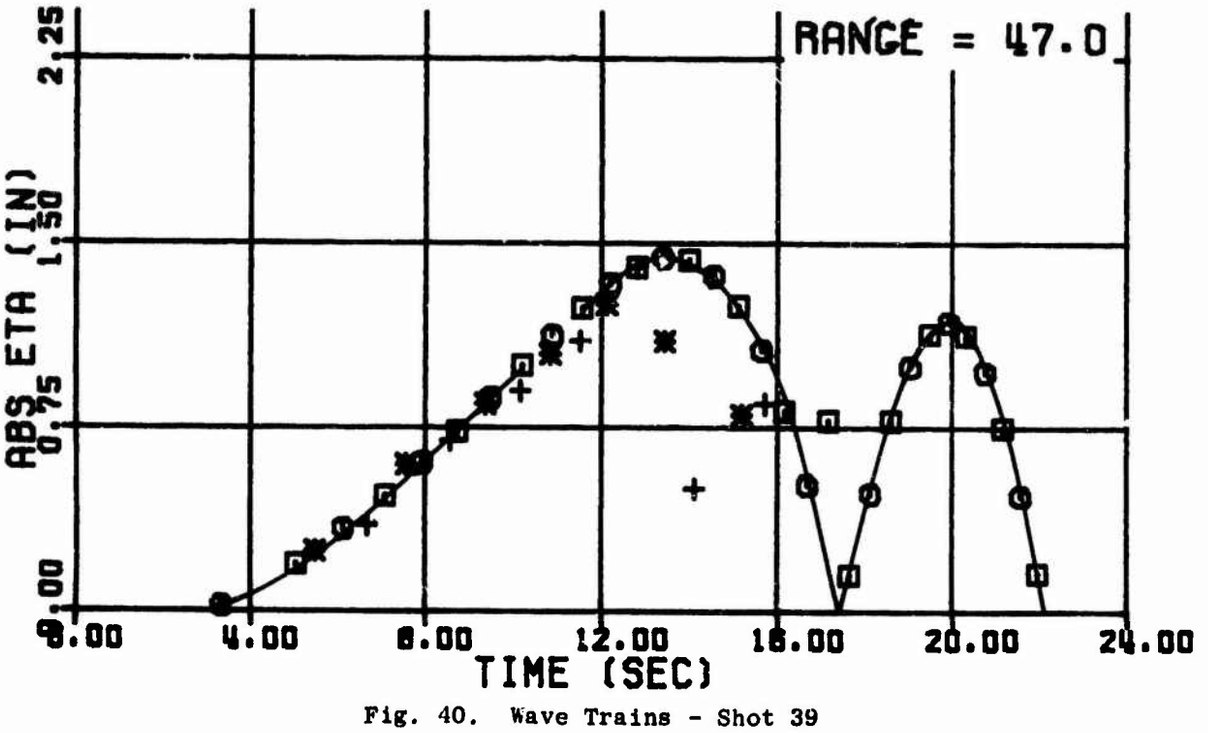

Fig. 40. Wave Trains - Shot 39

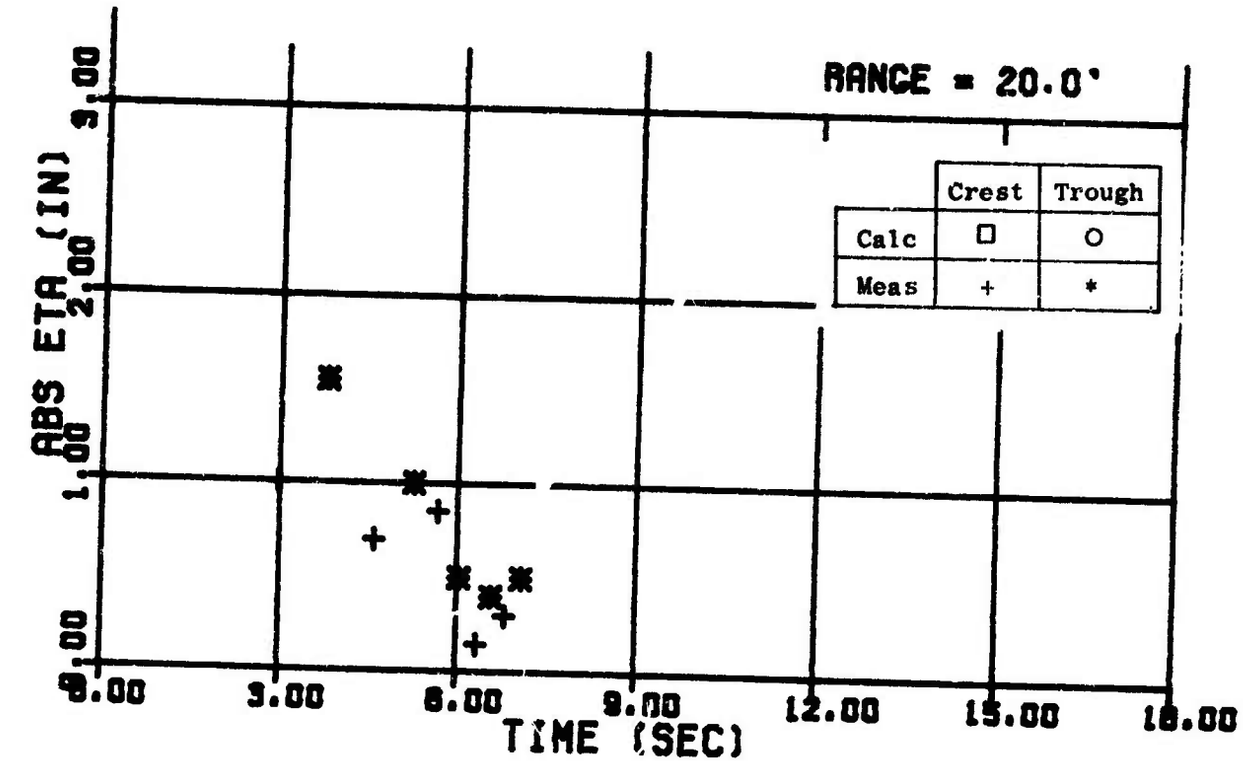

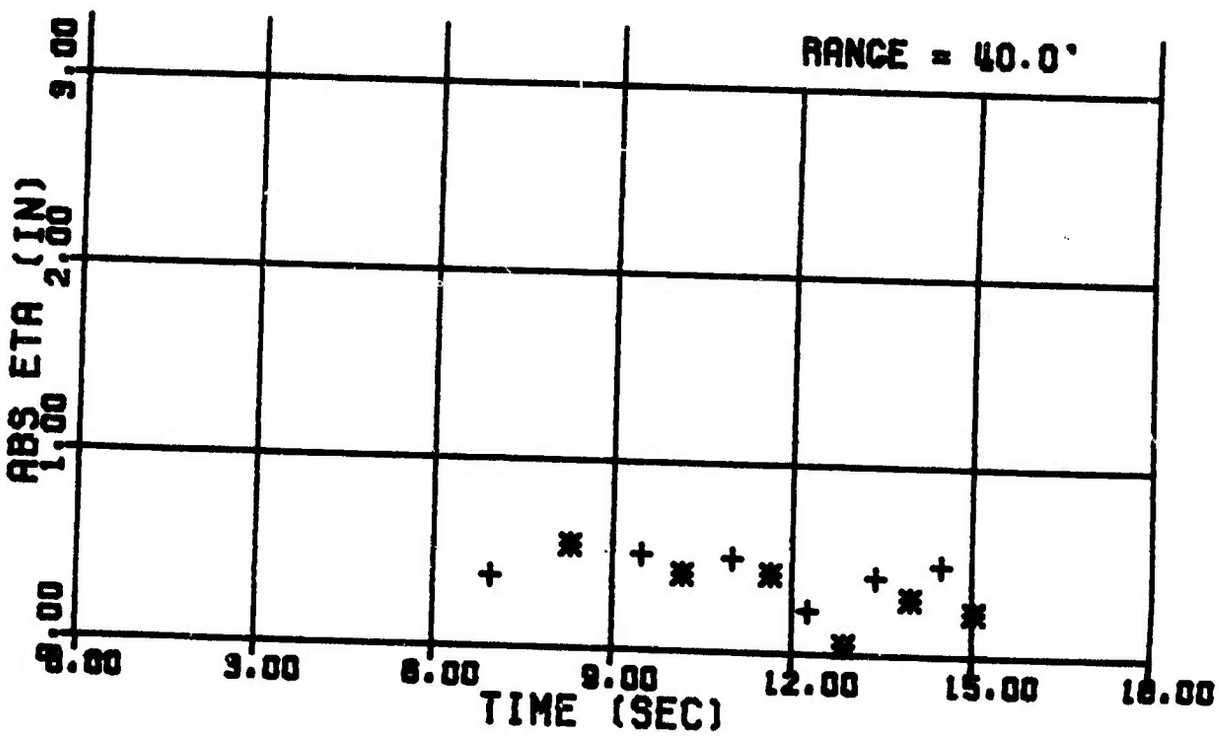

Fig. 41 Wave Trains - Shot 40

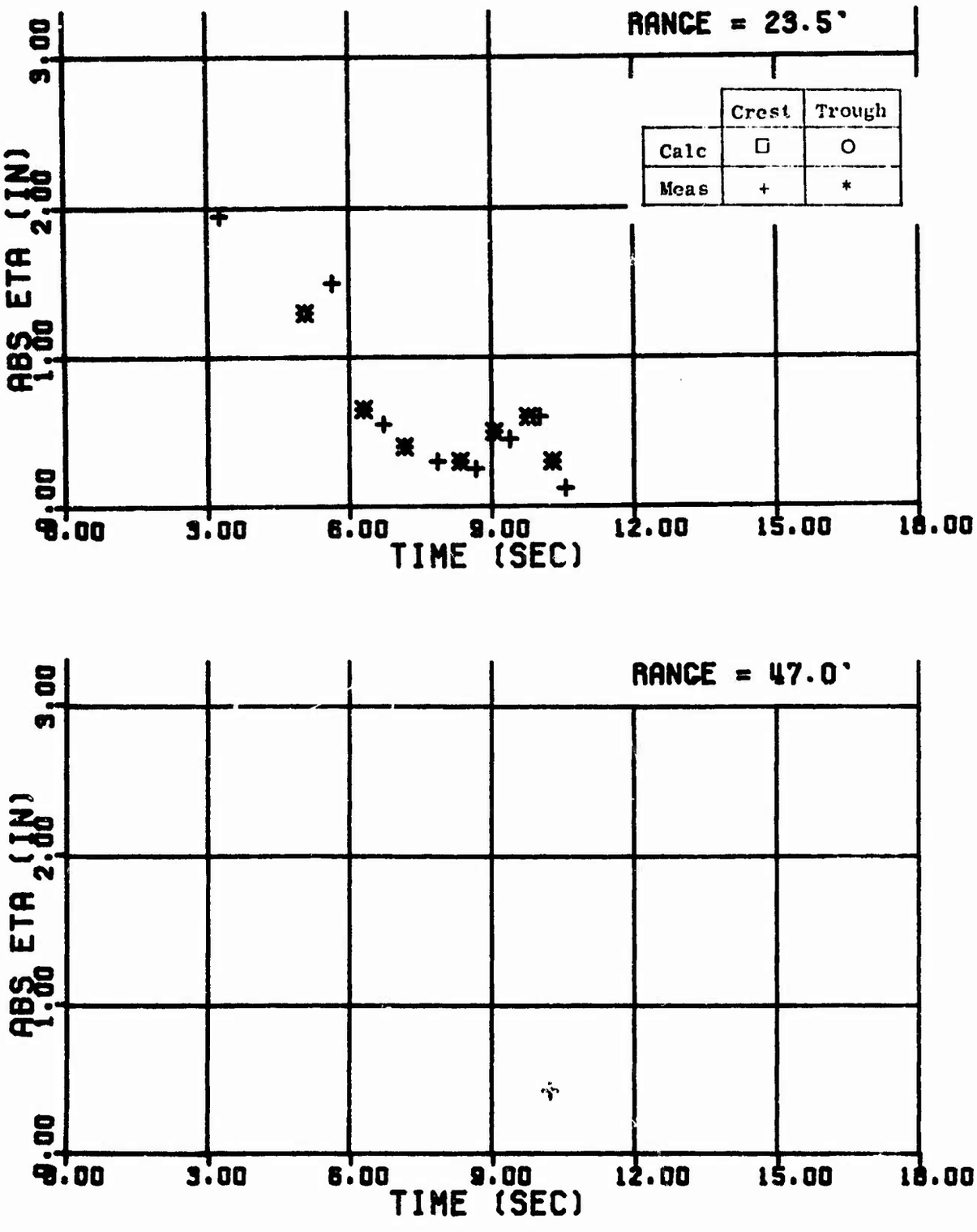

Fig. 42 Wave Trains - Shot 42

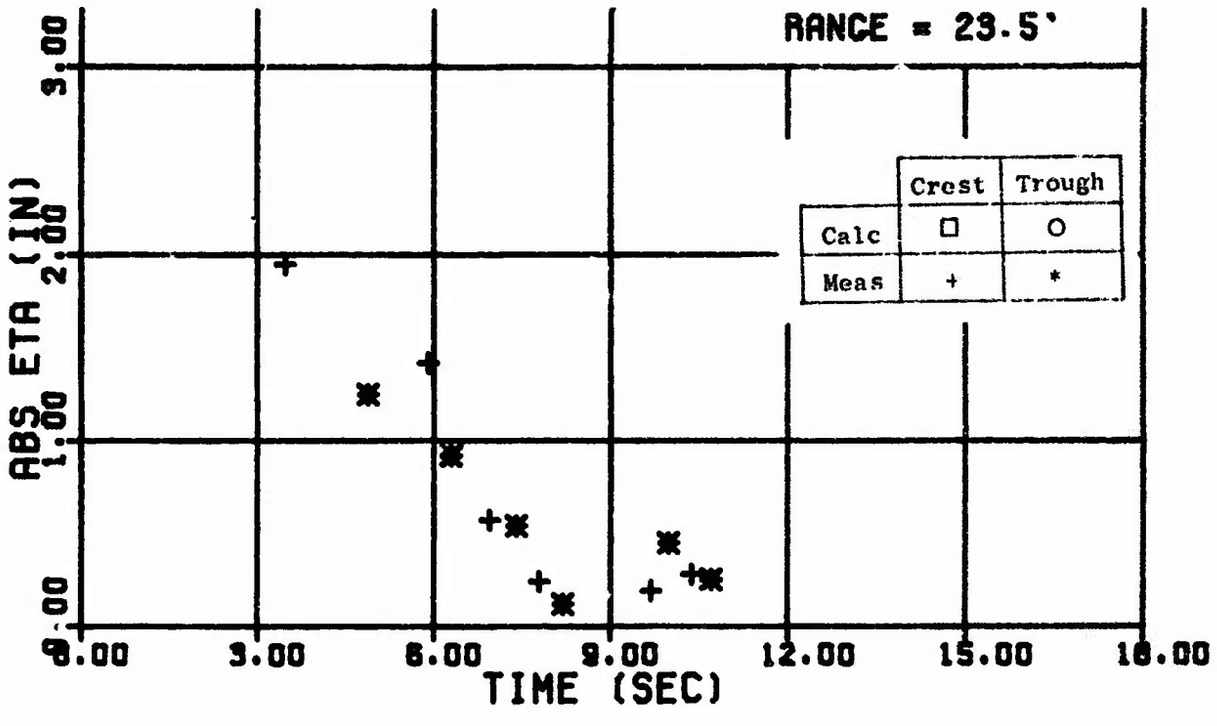

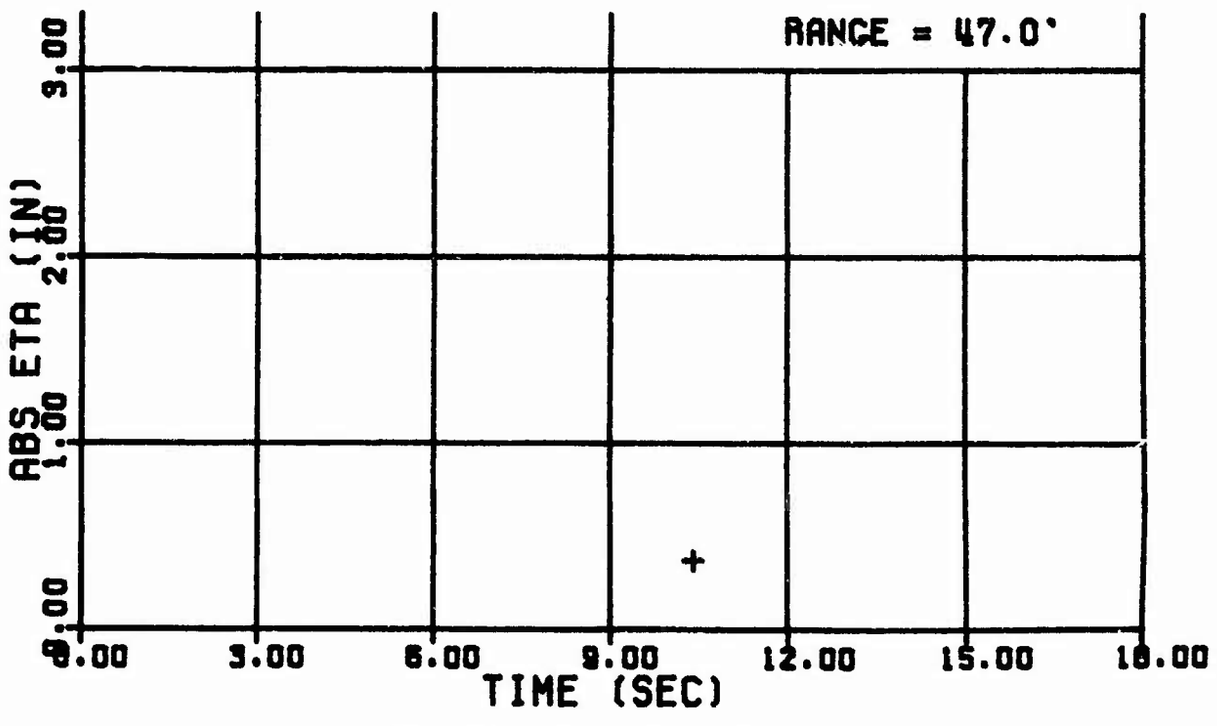

Fig. 43 Wave Trains - Shot 43

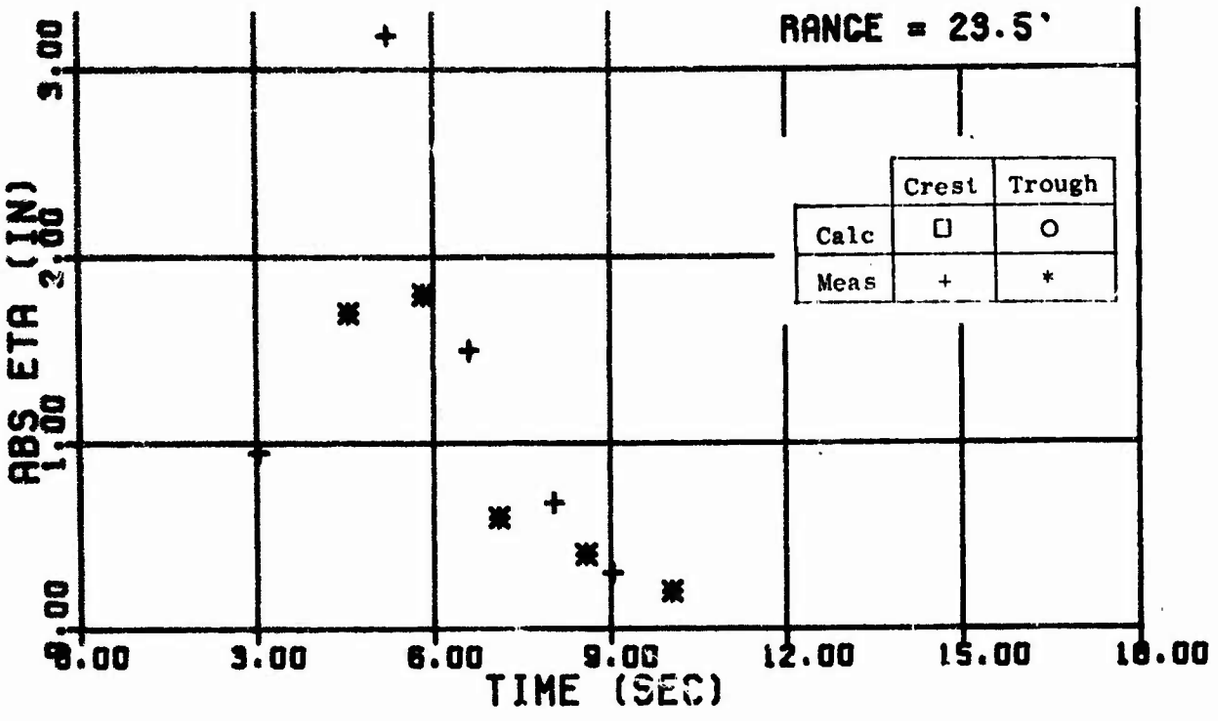

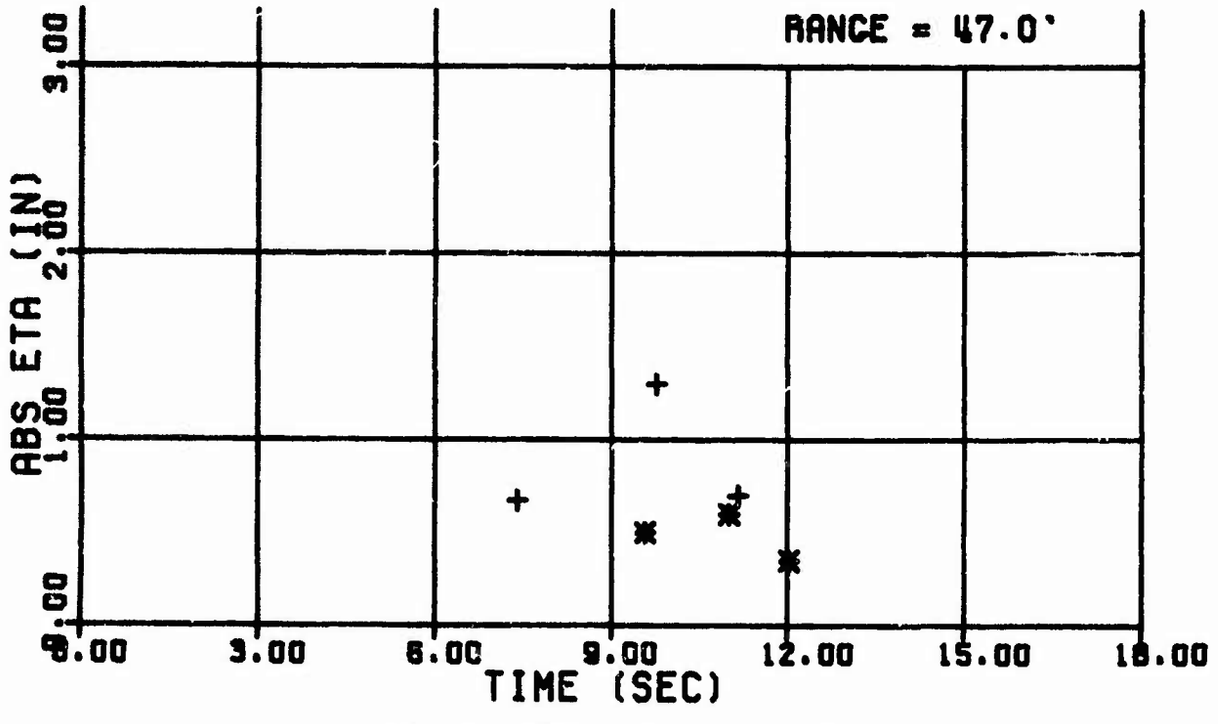

Fig. 44 Wave Trains - Shot 44

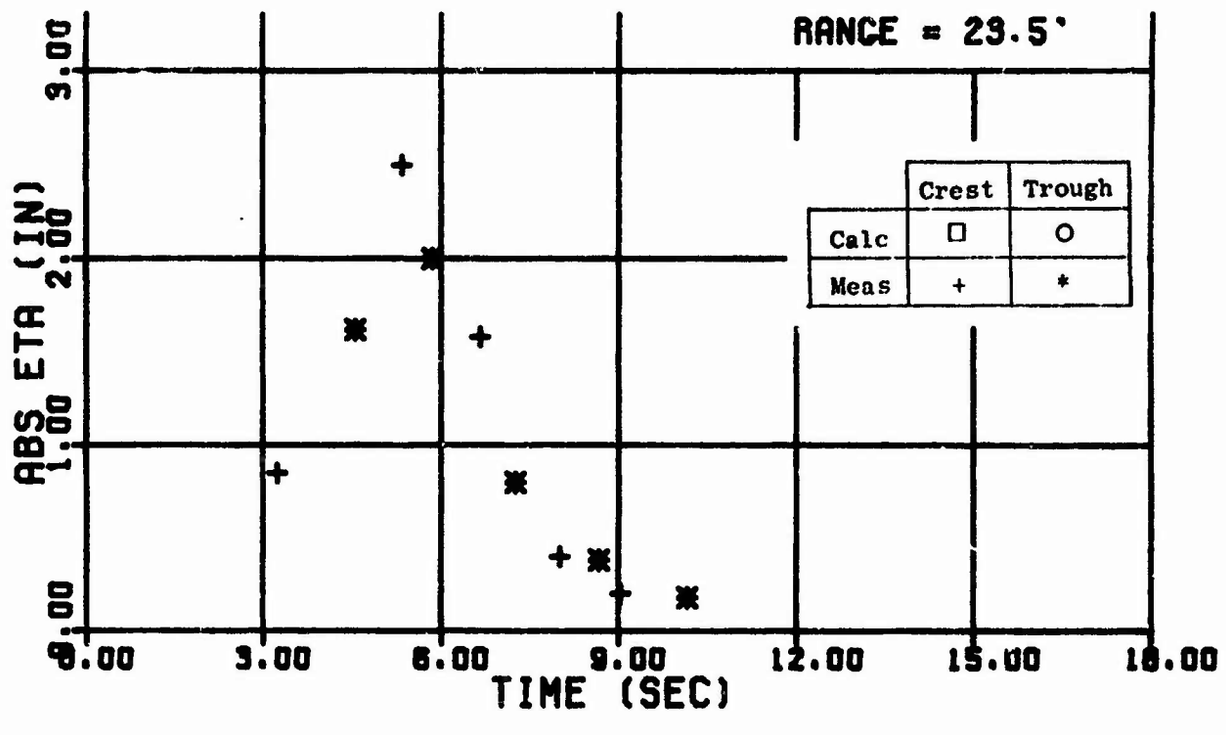

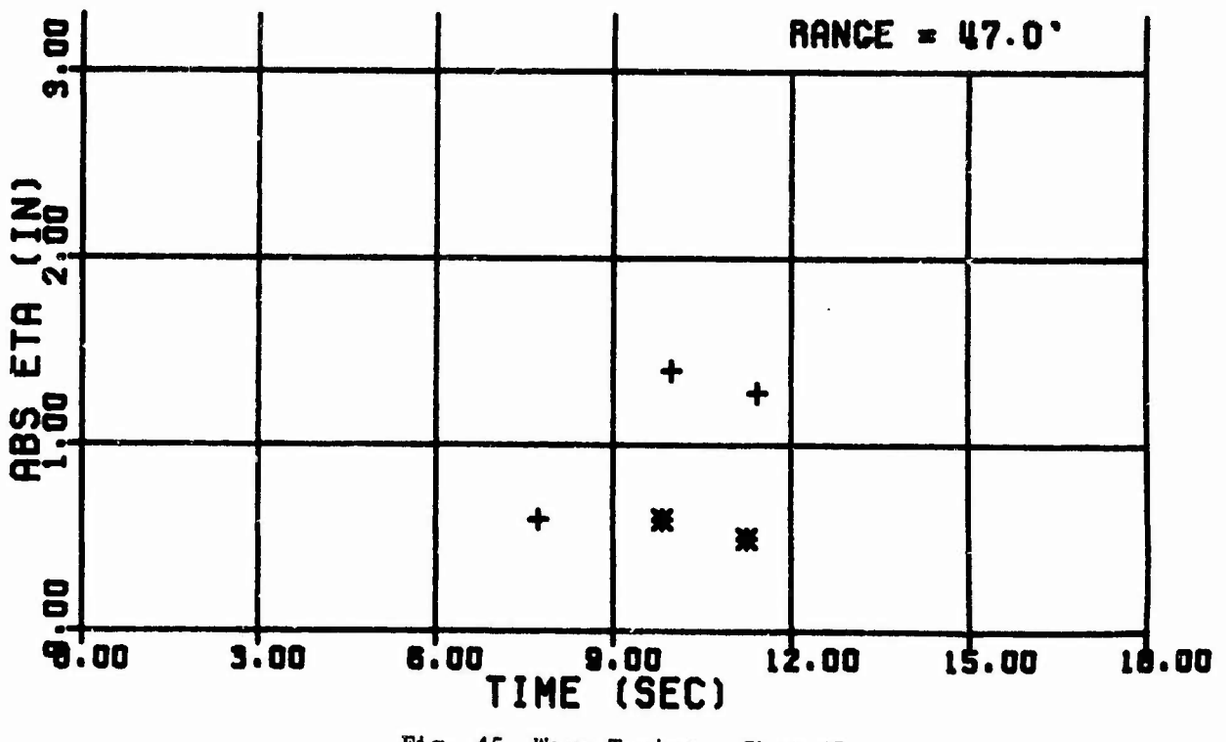

Fig. 45 Wave Trains - Shot 45

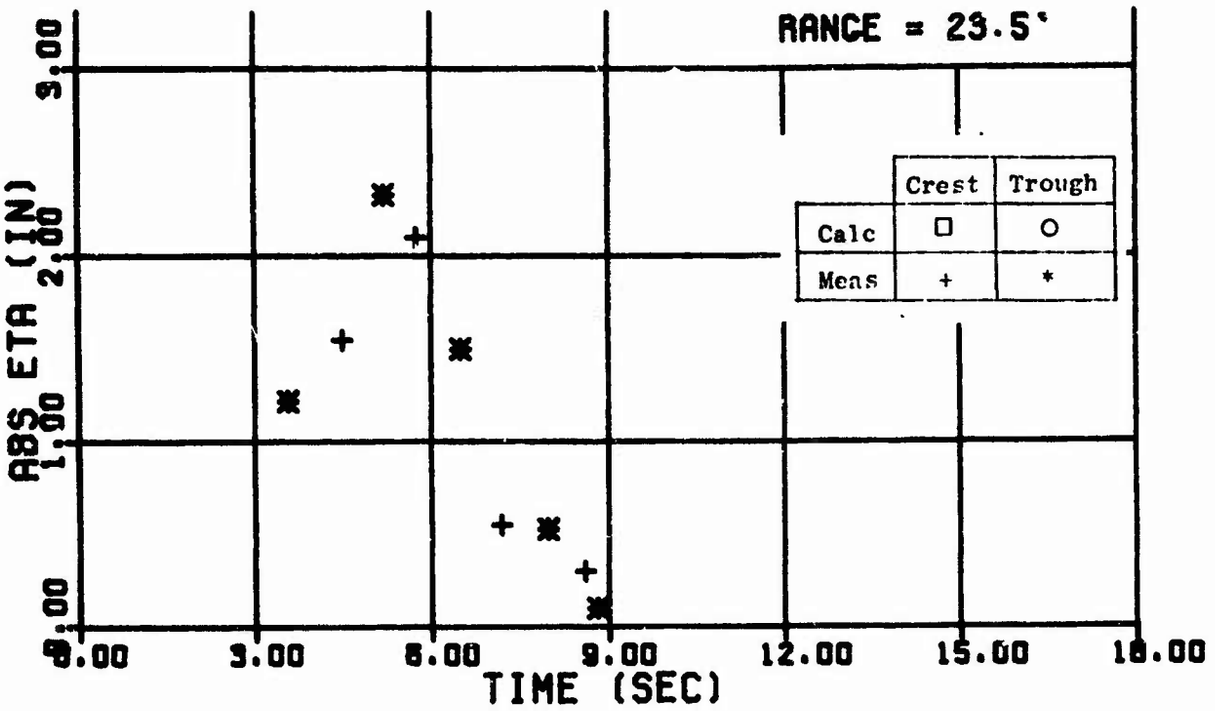

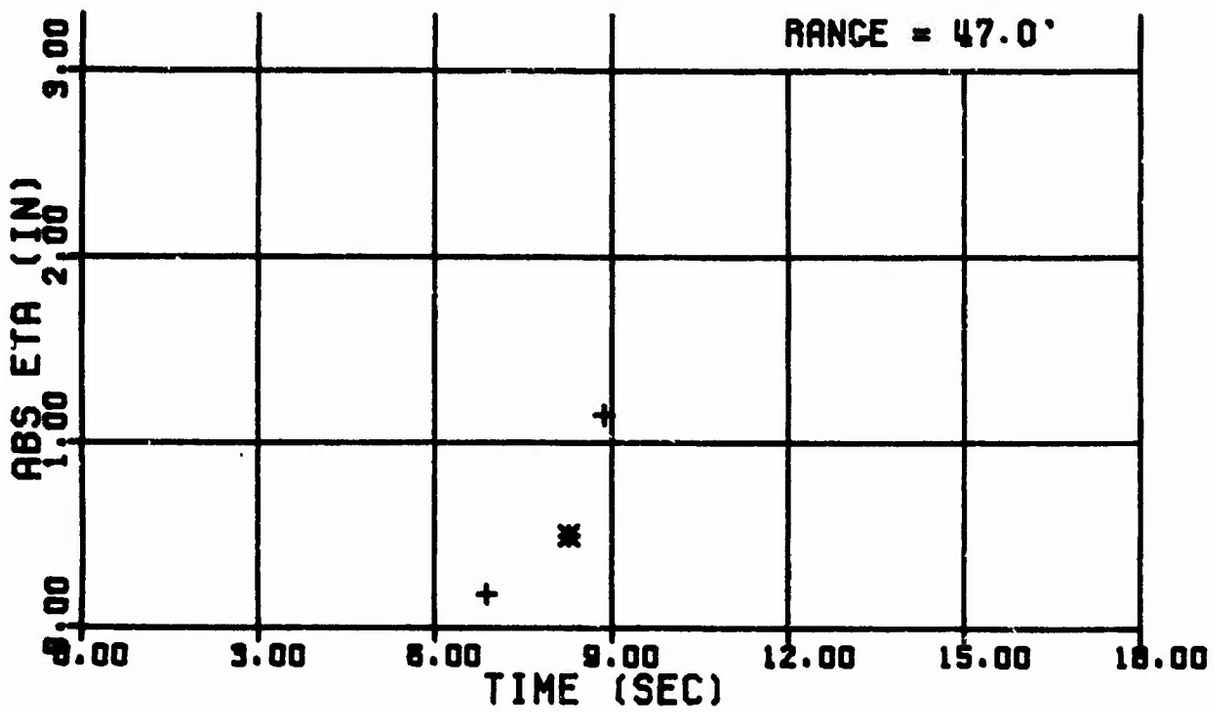

Fig. 46 Wave Train - Shot 46

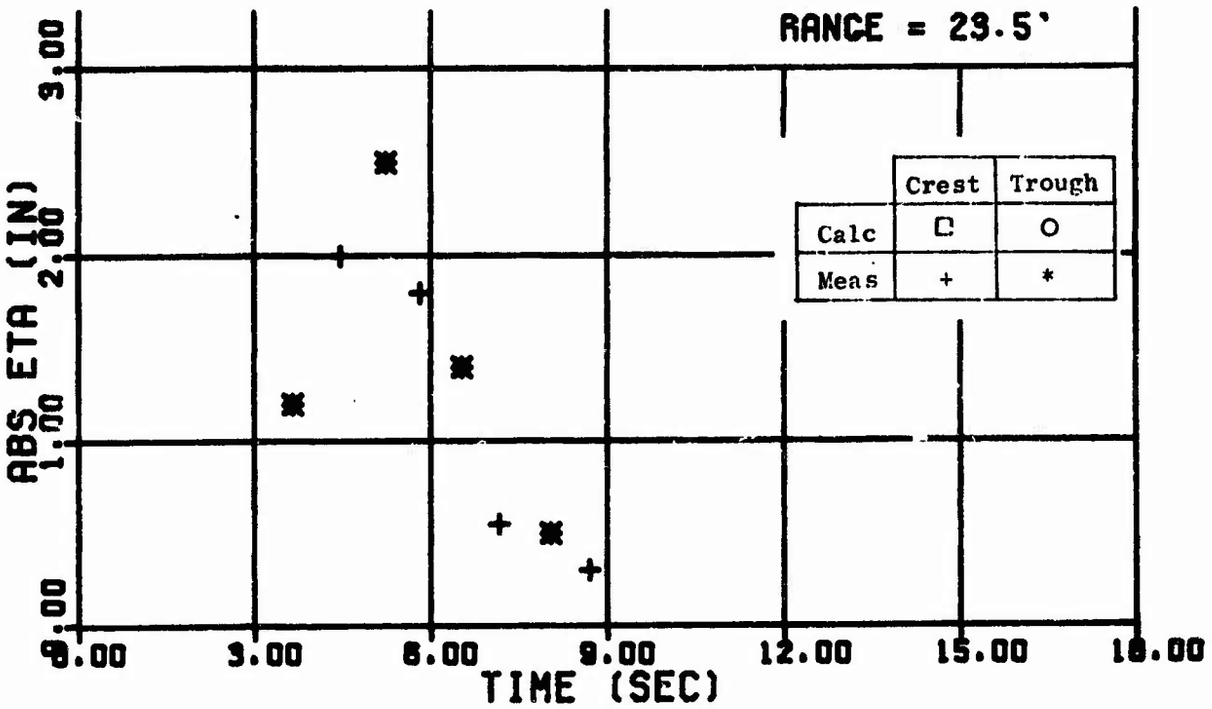

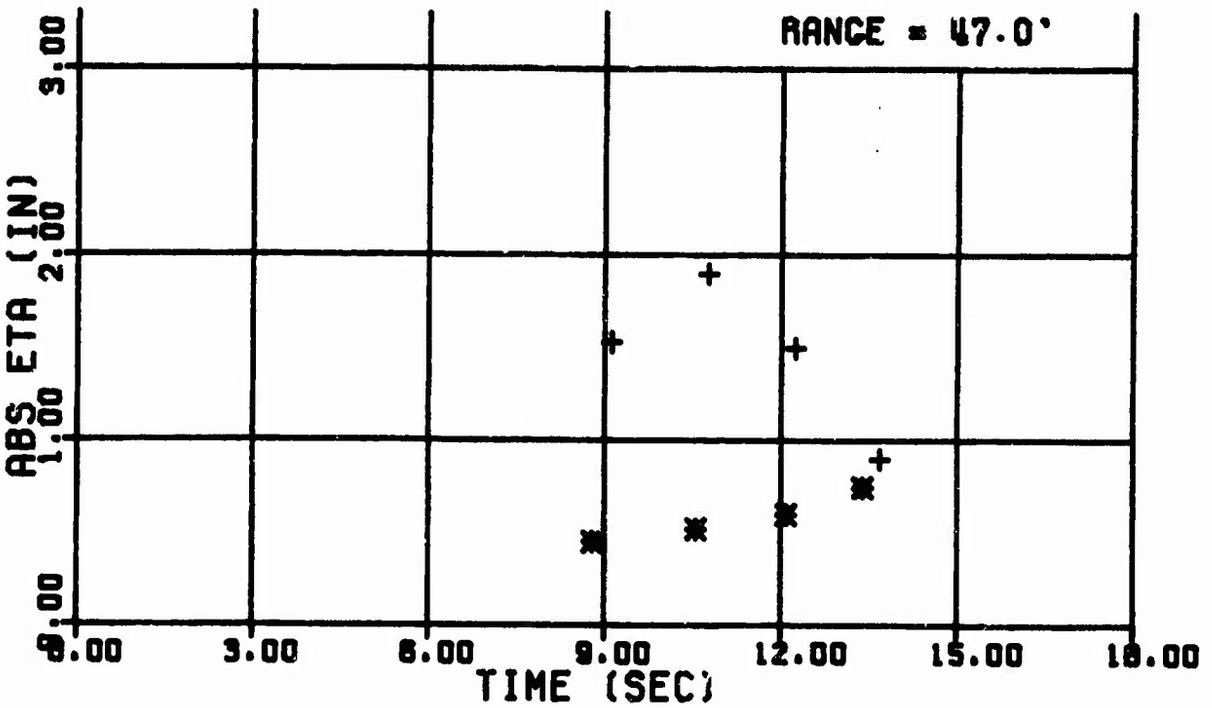

Fig. 47 Wave Trains - Shot 47

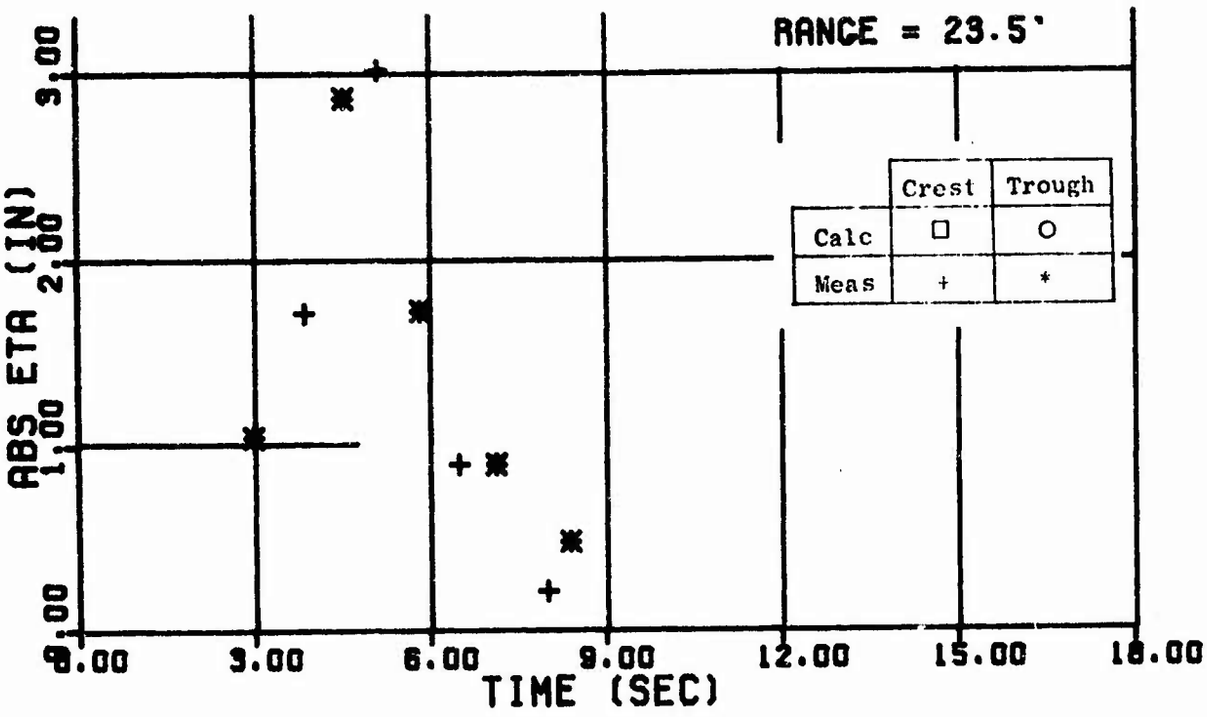

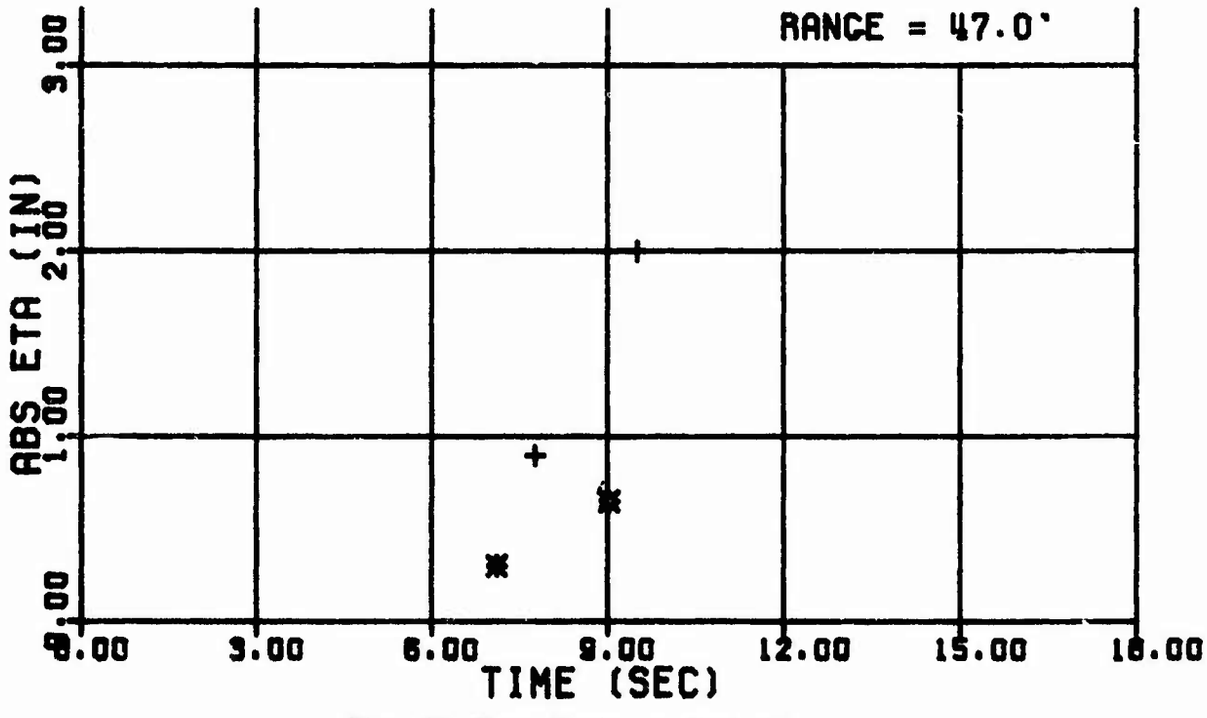

Fig. 48 Wave Trains - Shot 48

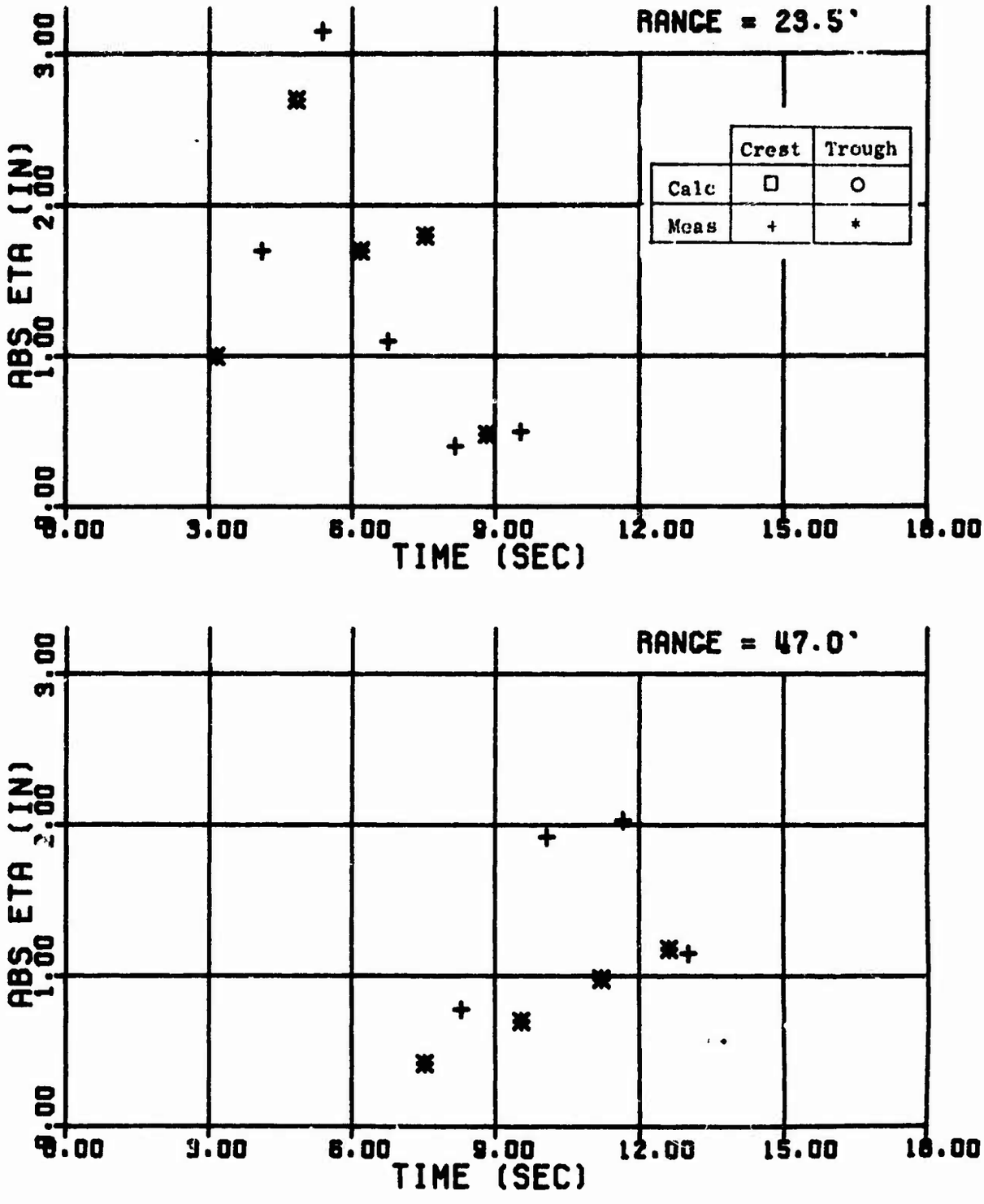

Fig. 49 Wave Trains - Shot 49

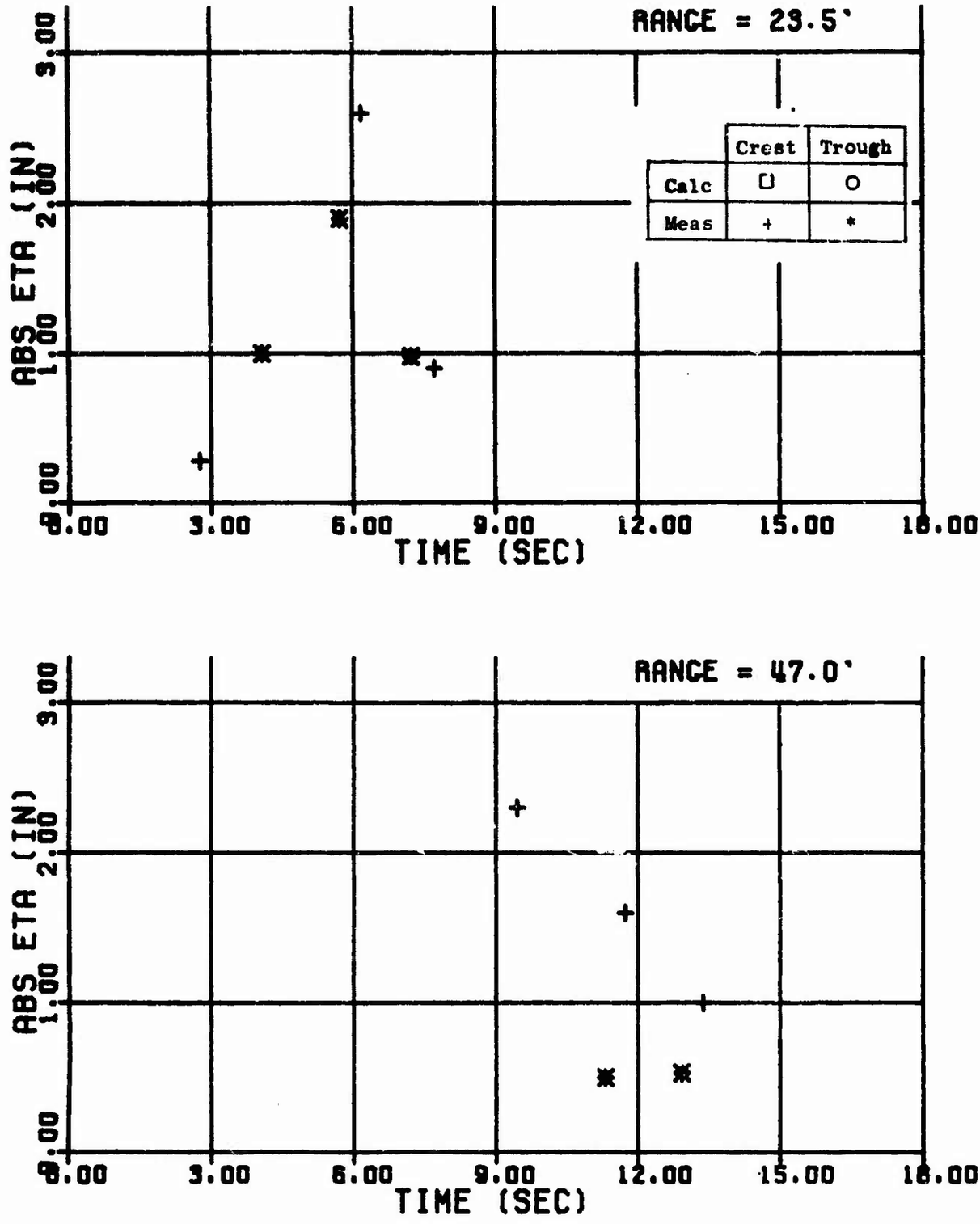

Fig. 50 Wave Trains - Shot 50

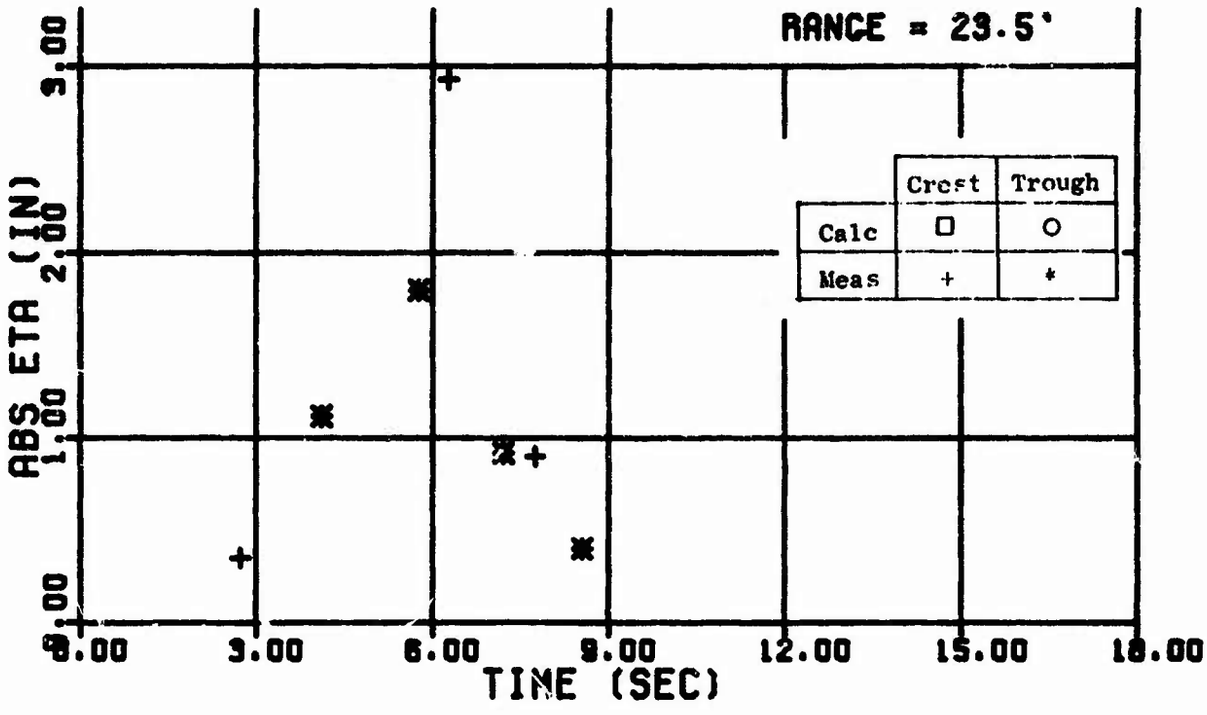

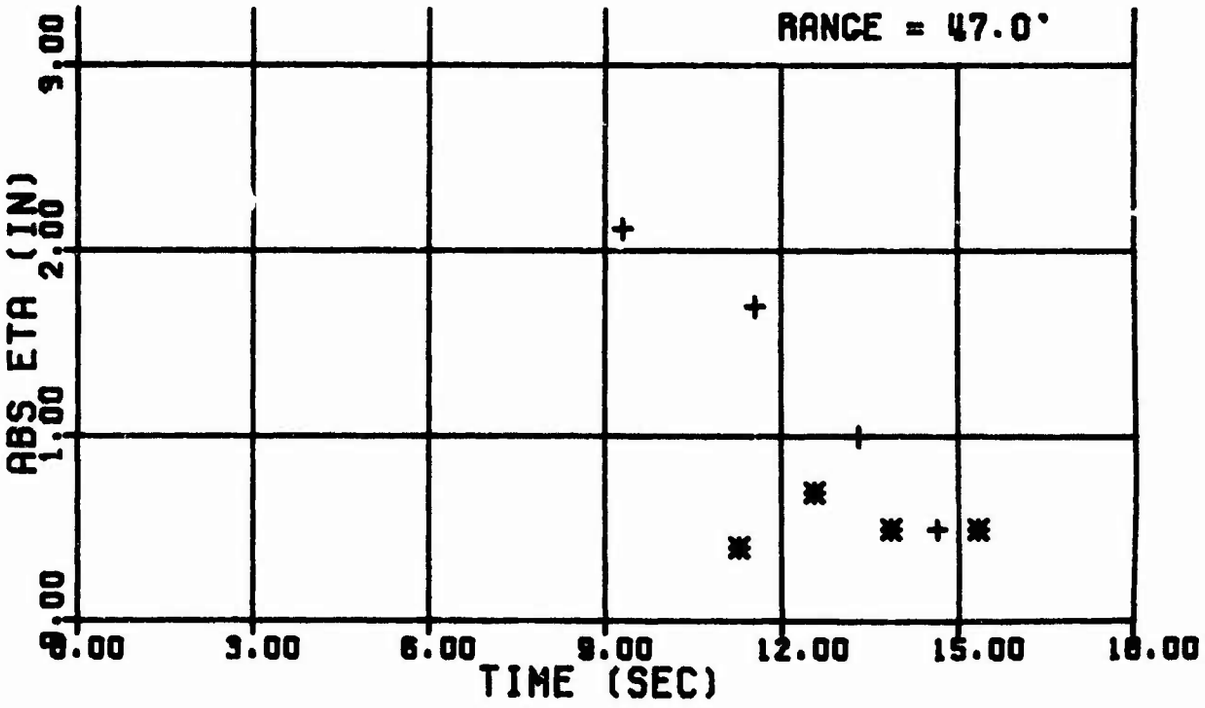

Fig. 51 Wave Trains - Shot 51

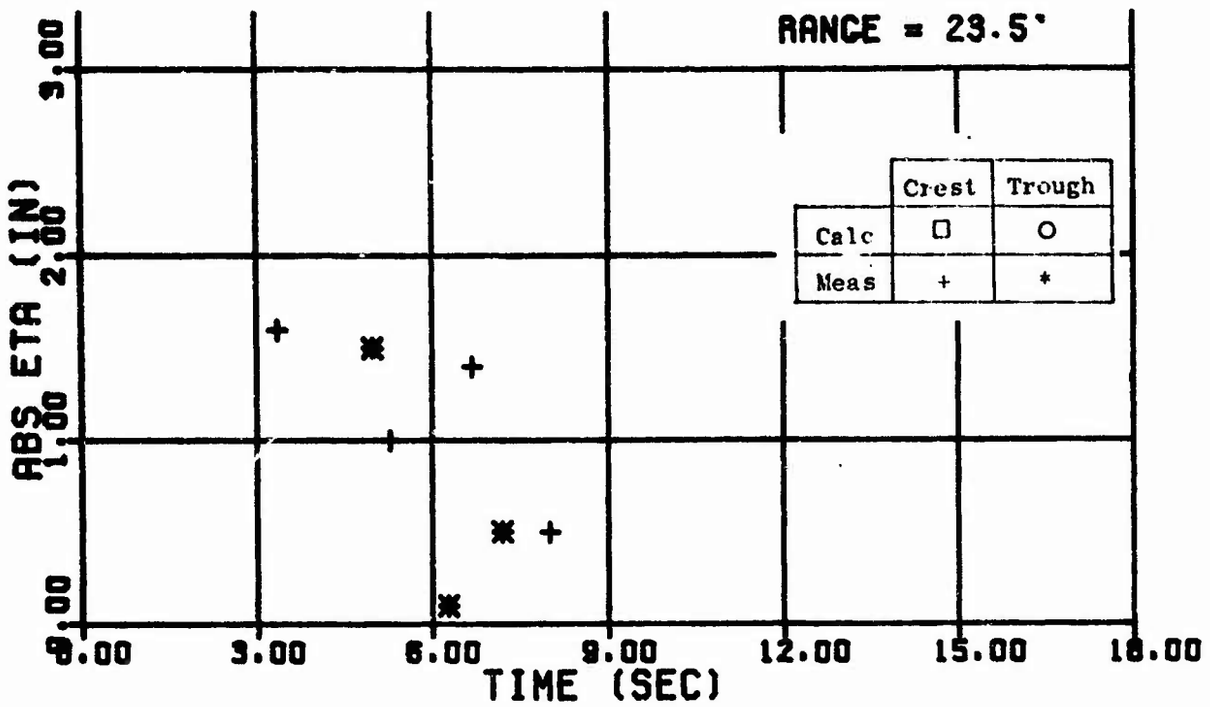

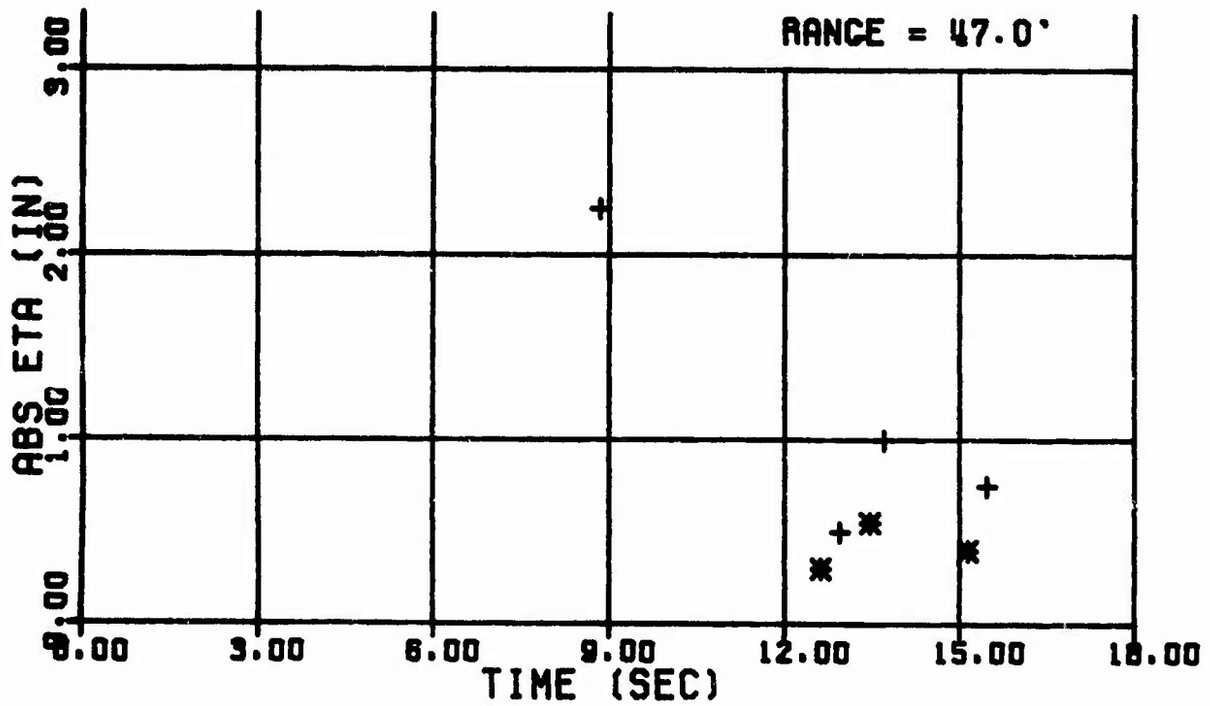

Fig. 52 Wave Trains - Shot 52

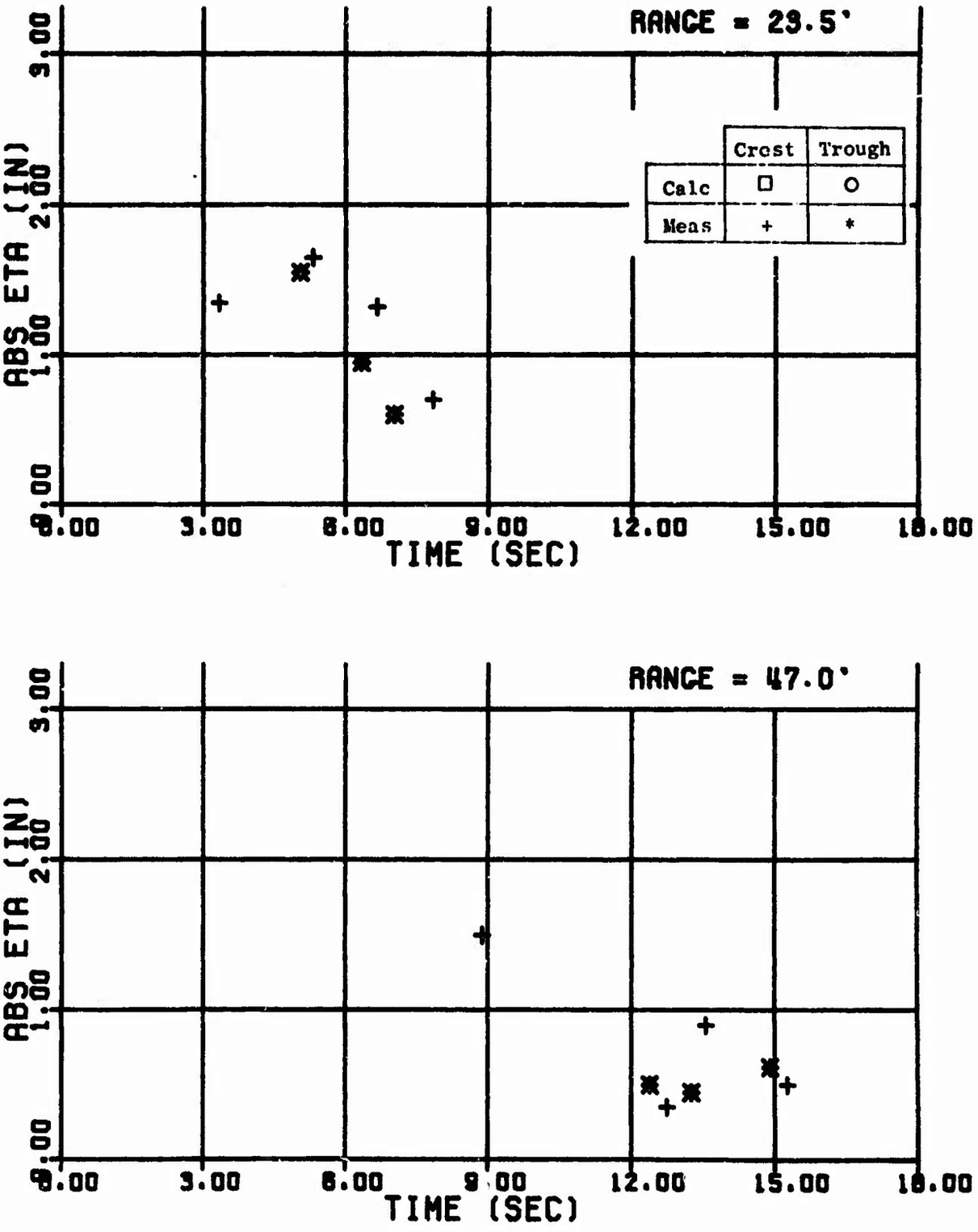

Fig. 53 Wave Trains - Shot 53

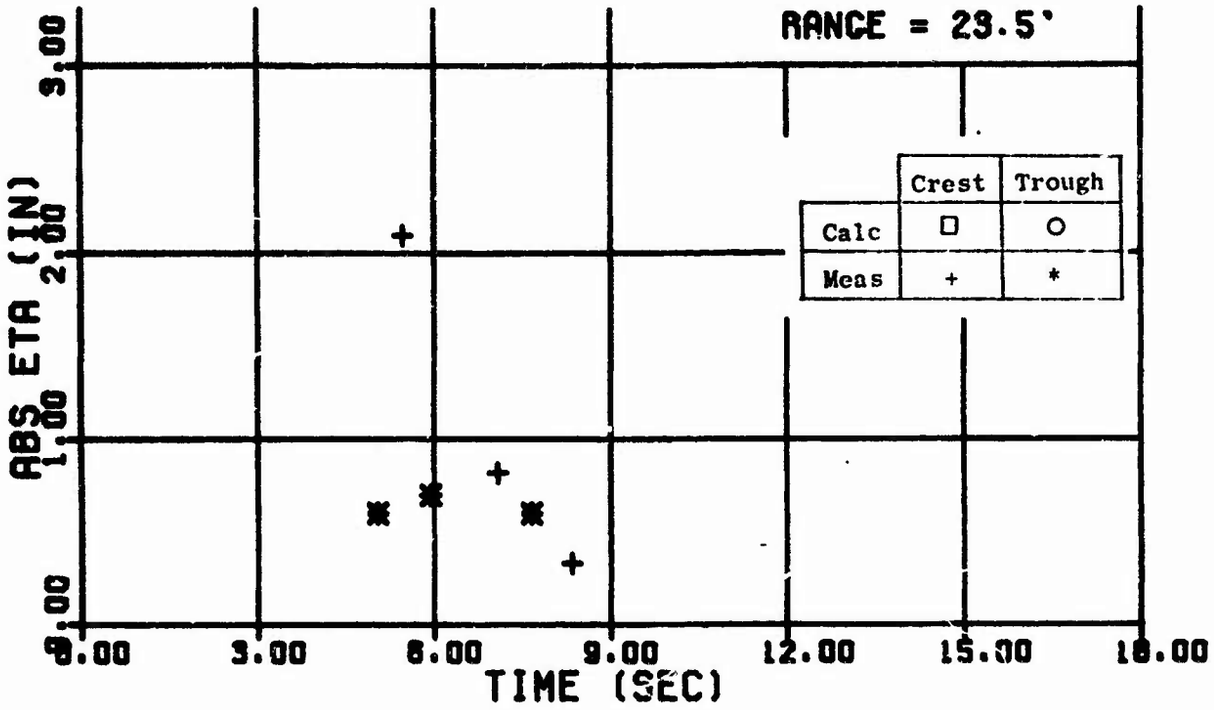

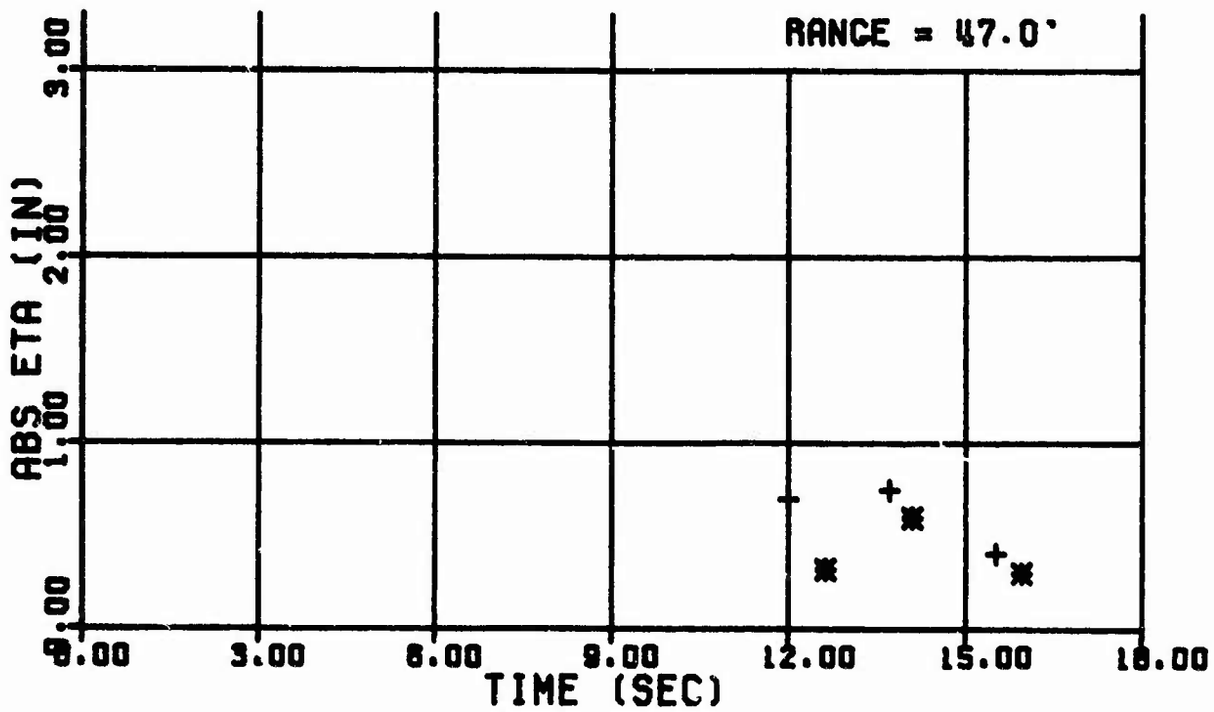

Fig. 54 Wave Trains - Shot 54

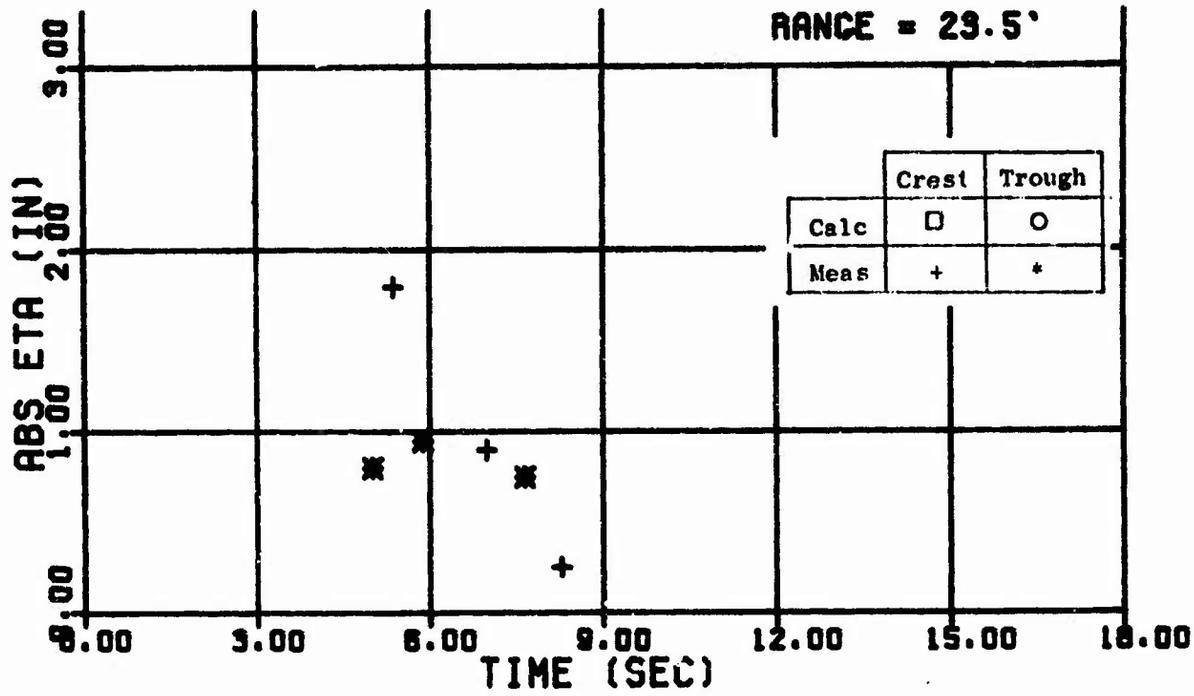

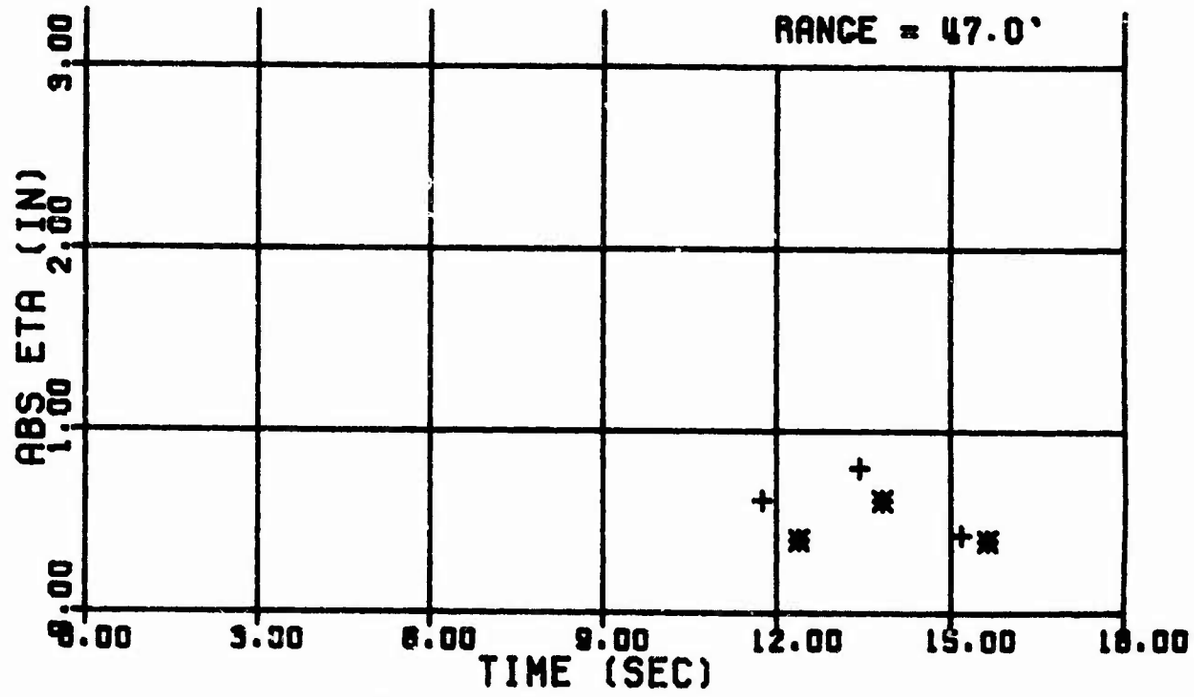

Fig. 55. Wave Trains - Shot 54

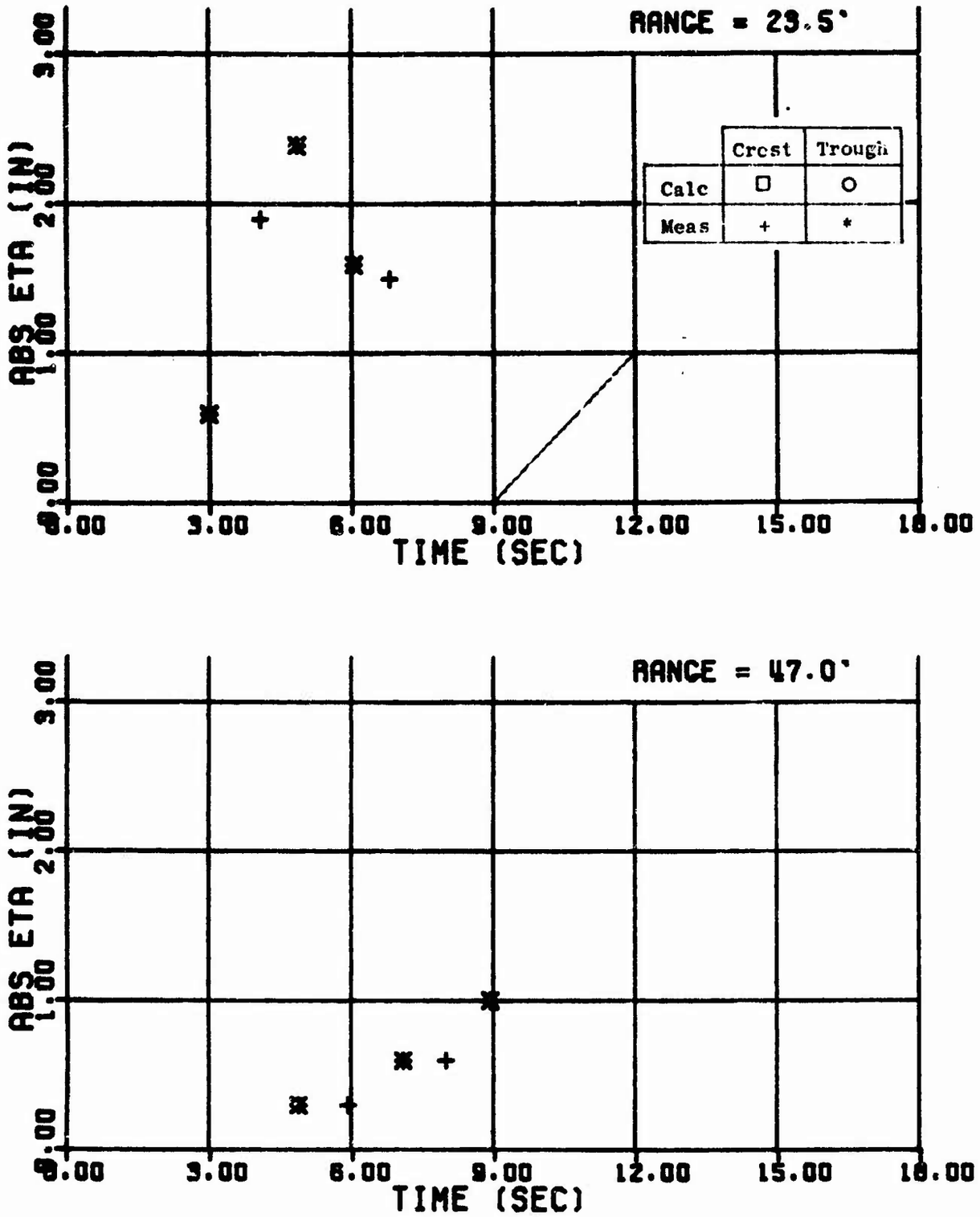

Fig. 56. Wave Trains - Shot 56

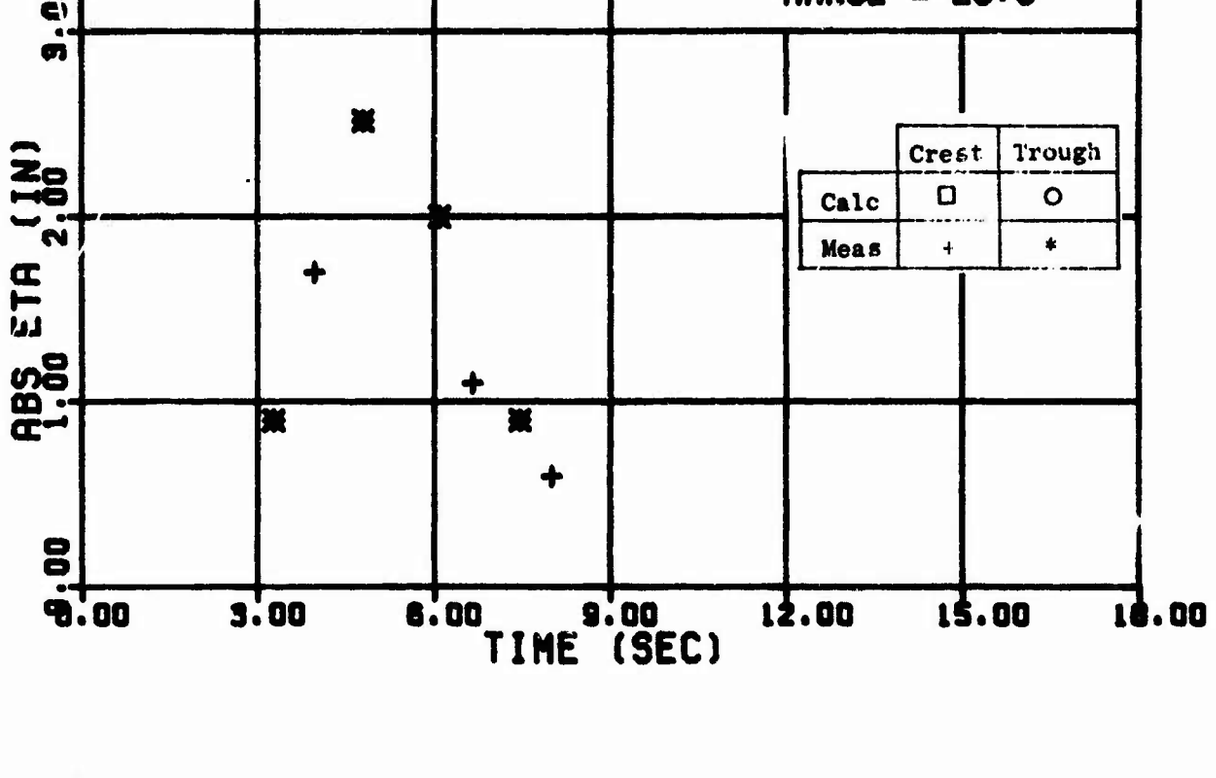

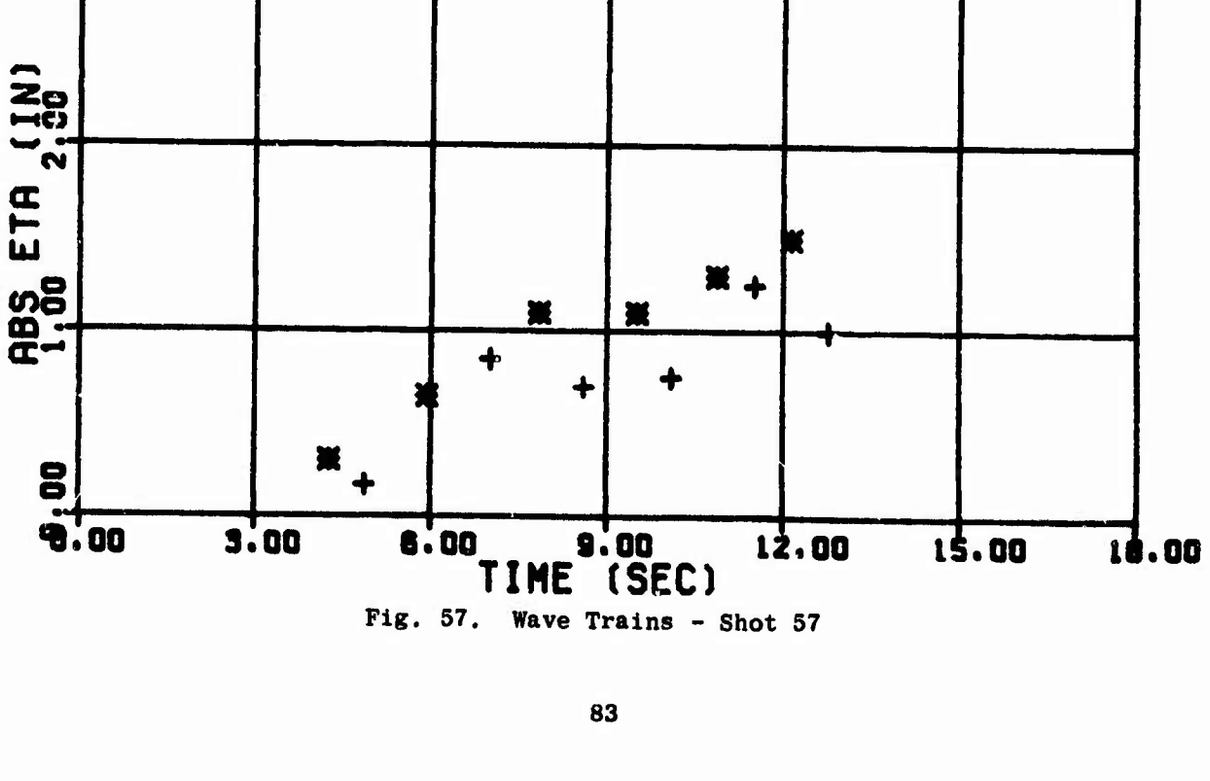

Fig. 57. Wave Trains - Shot 57

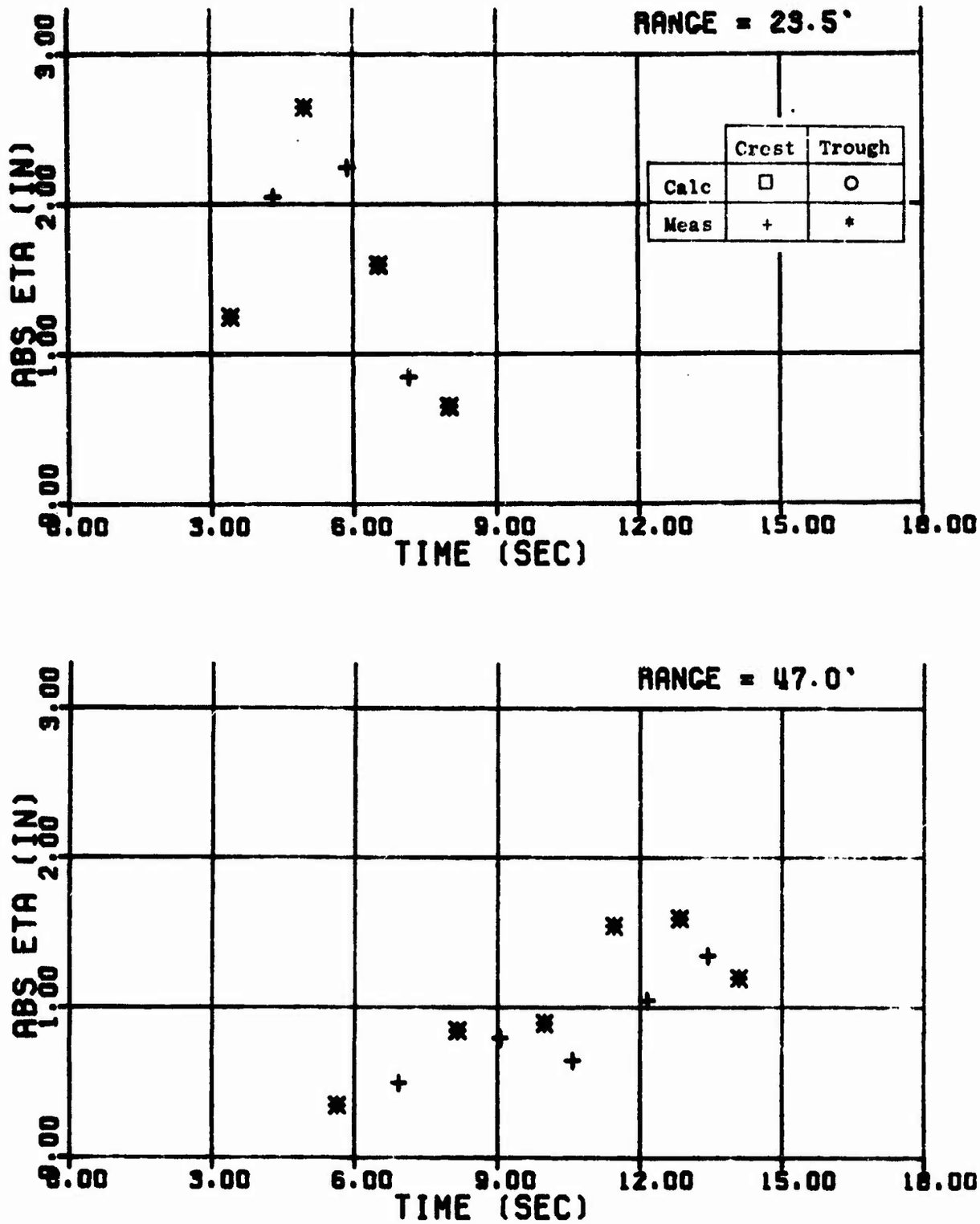

Fig. 58. Wave Trains - Shot 58

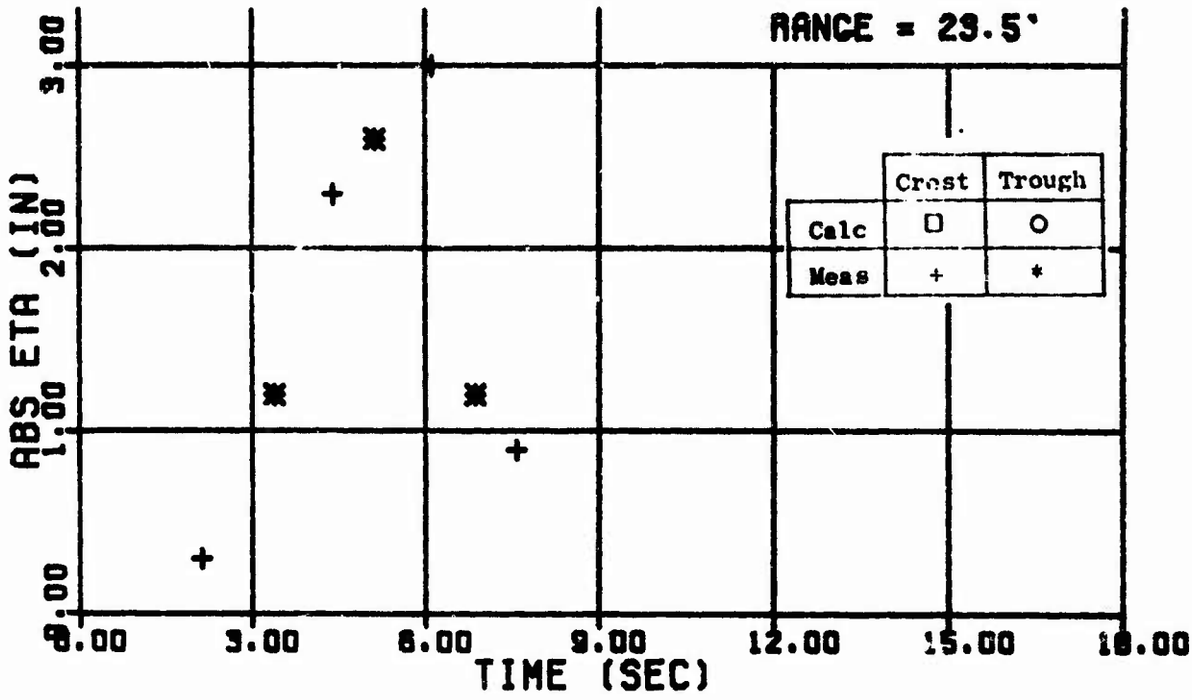

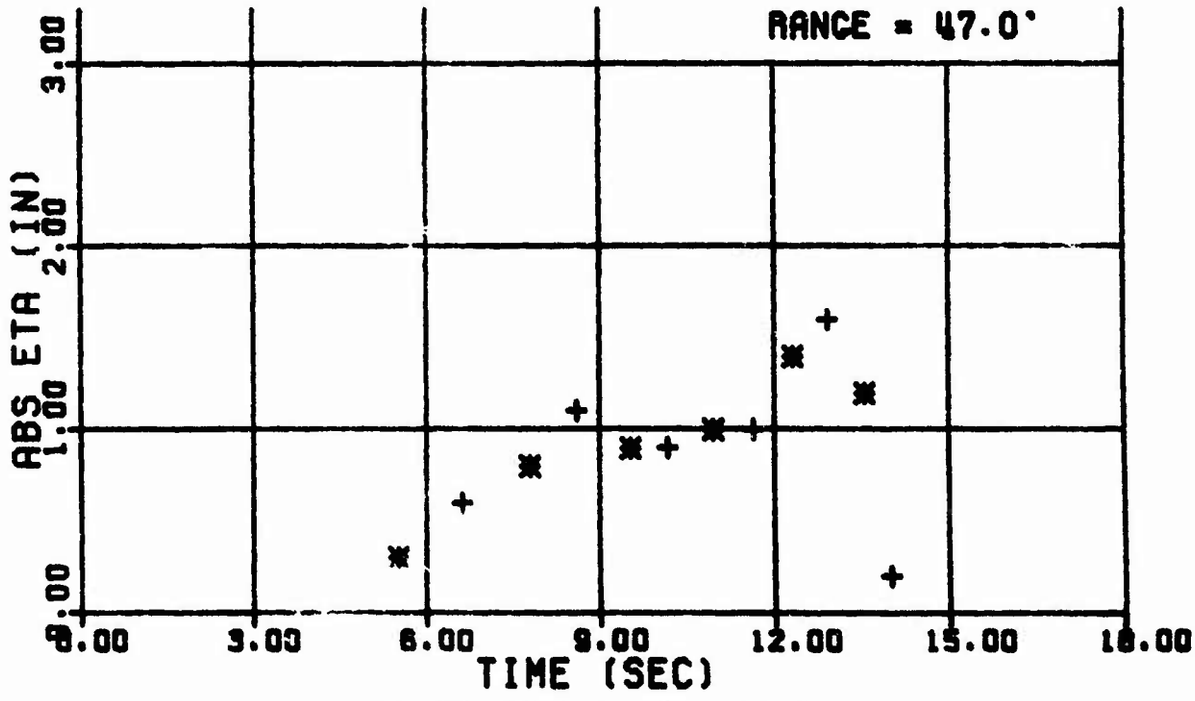

Fig. 59. Wave Trains - Shot 59

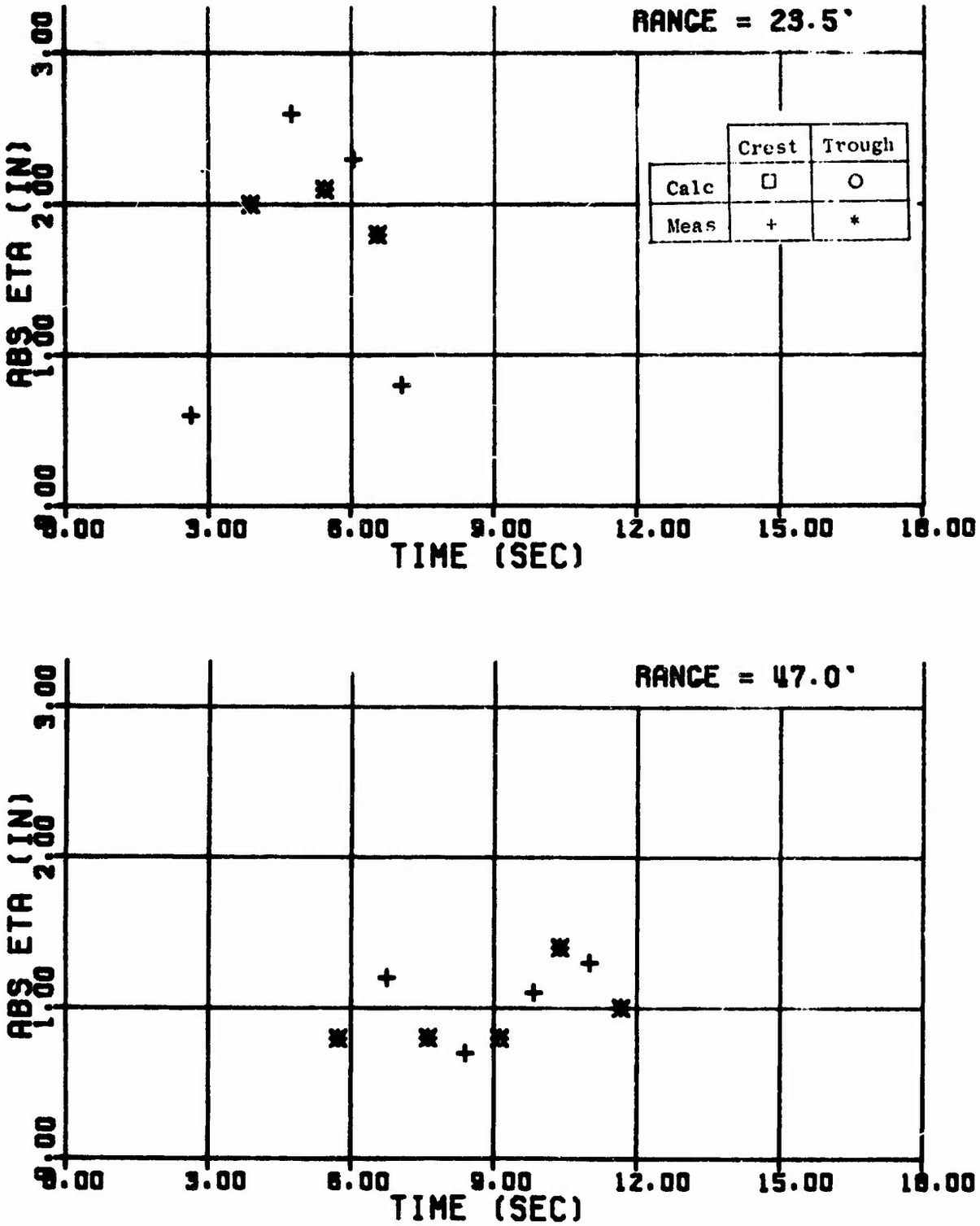

Fig. 60. Wave Trains - Shot 60

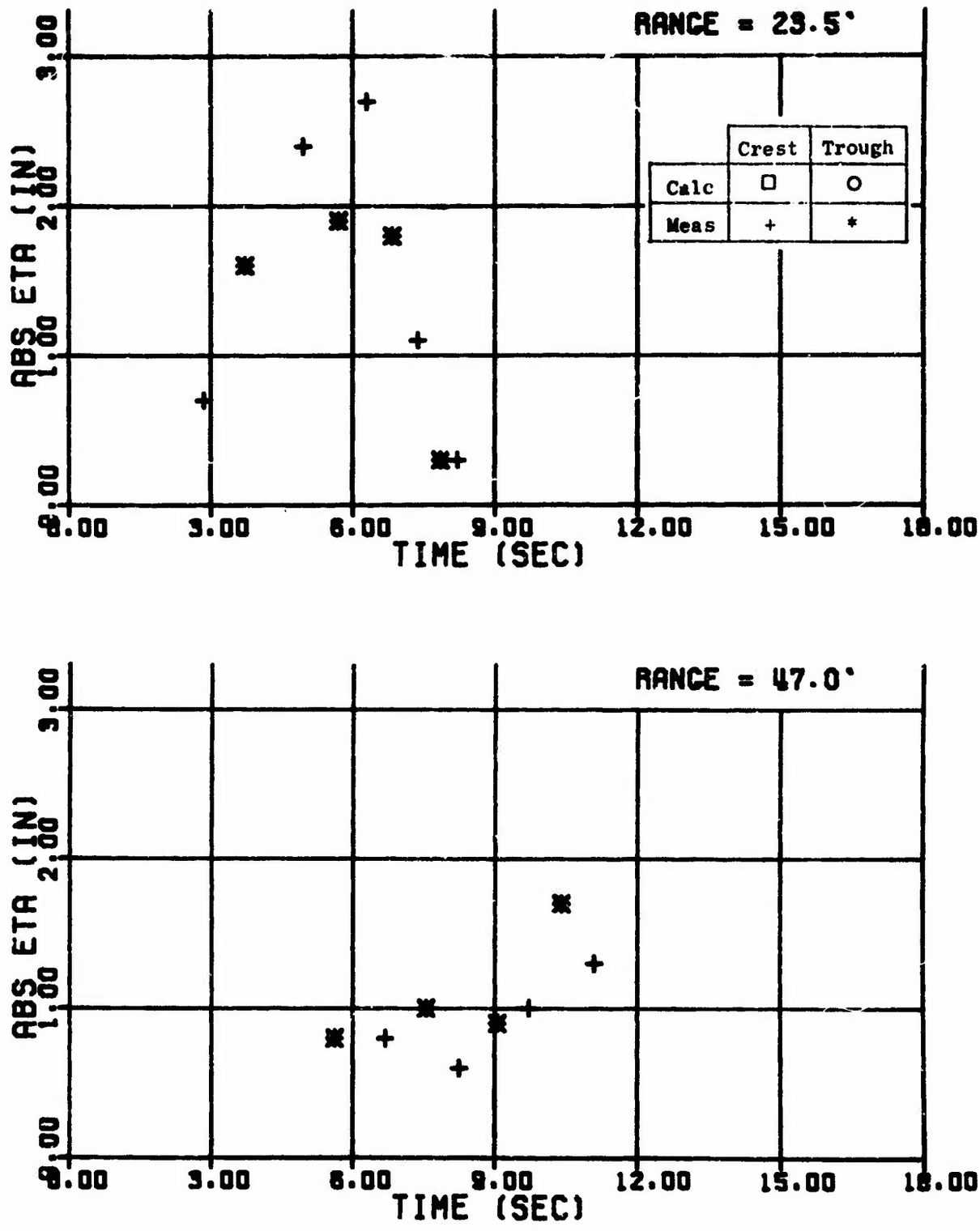

Fig. 61. Wave Trains - Shot 61

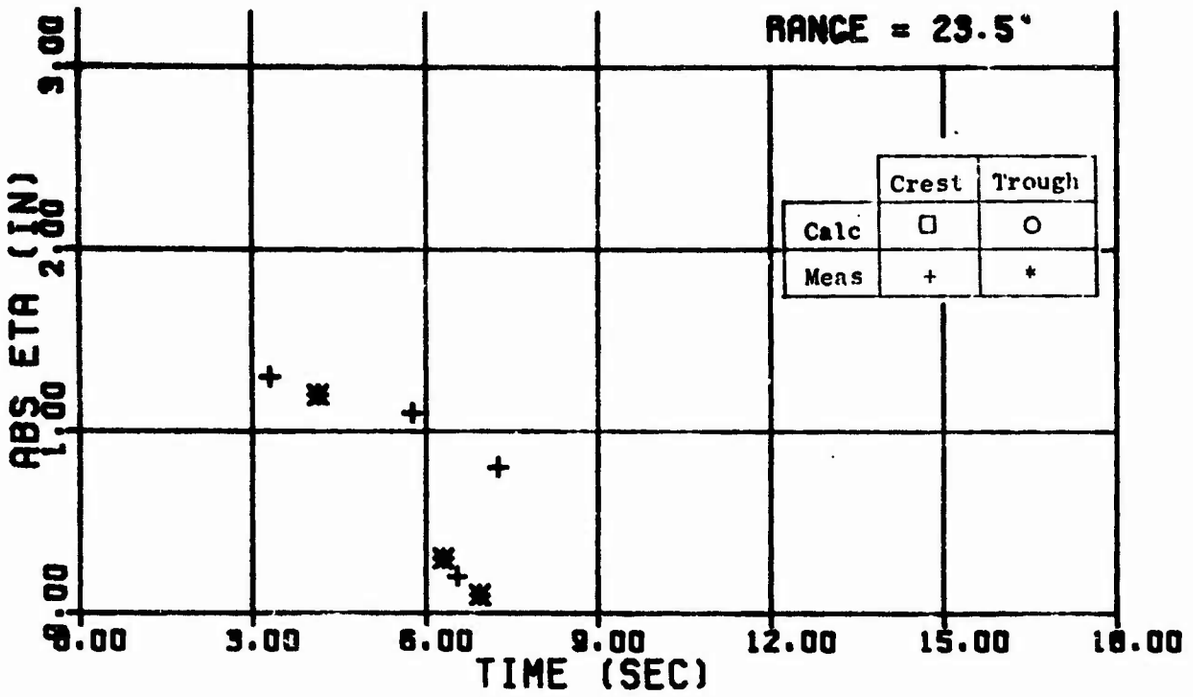

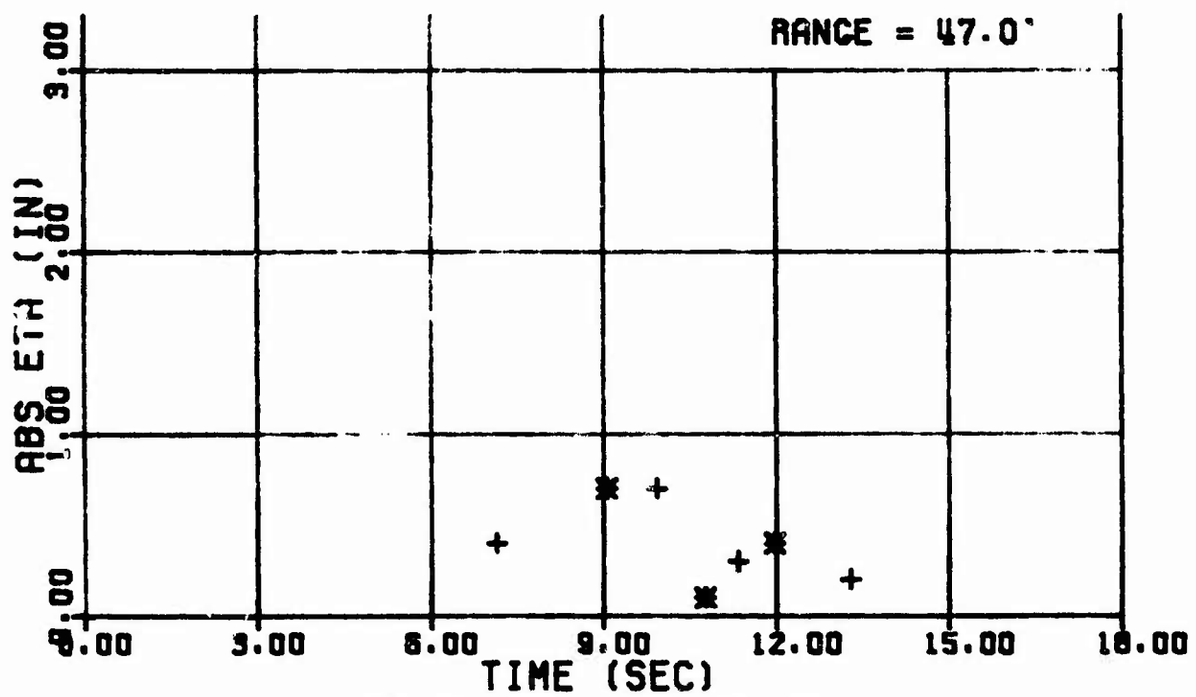

Fig. 62. Wave Trains - Shot 62

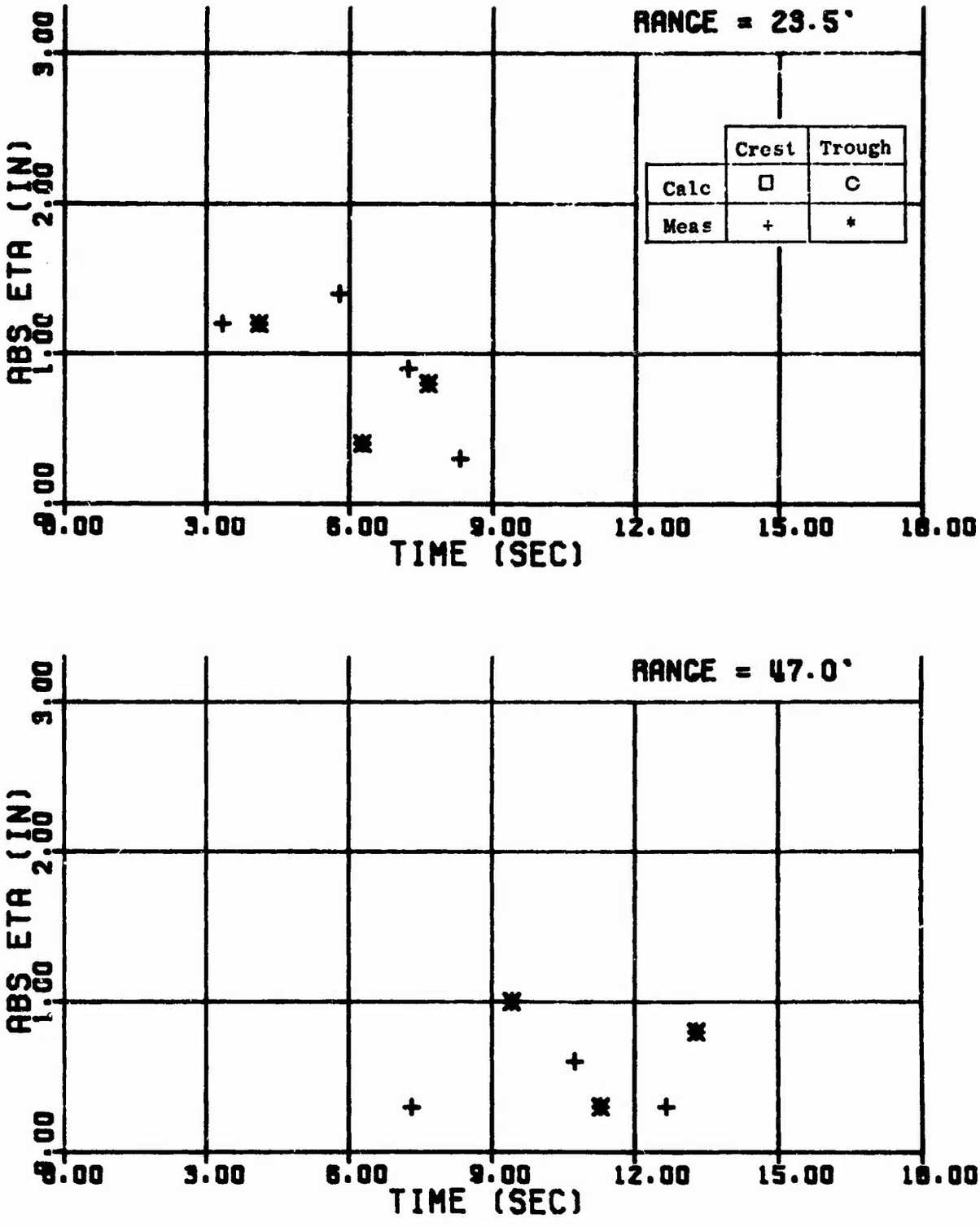

Fig. 63. Wave Trains - Shot 63

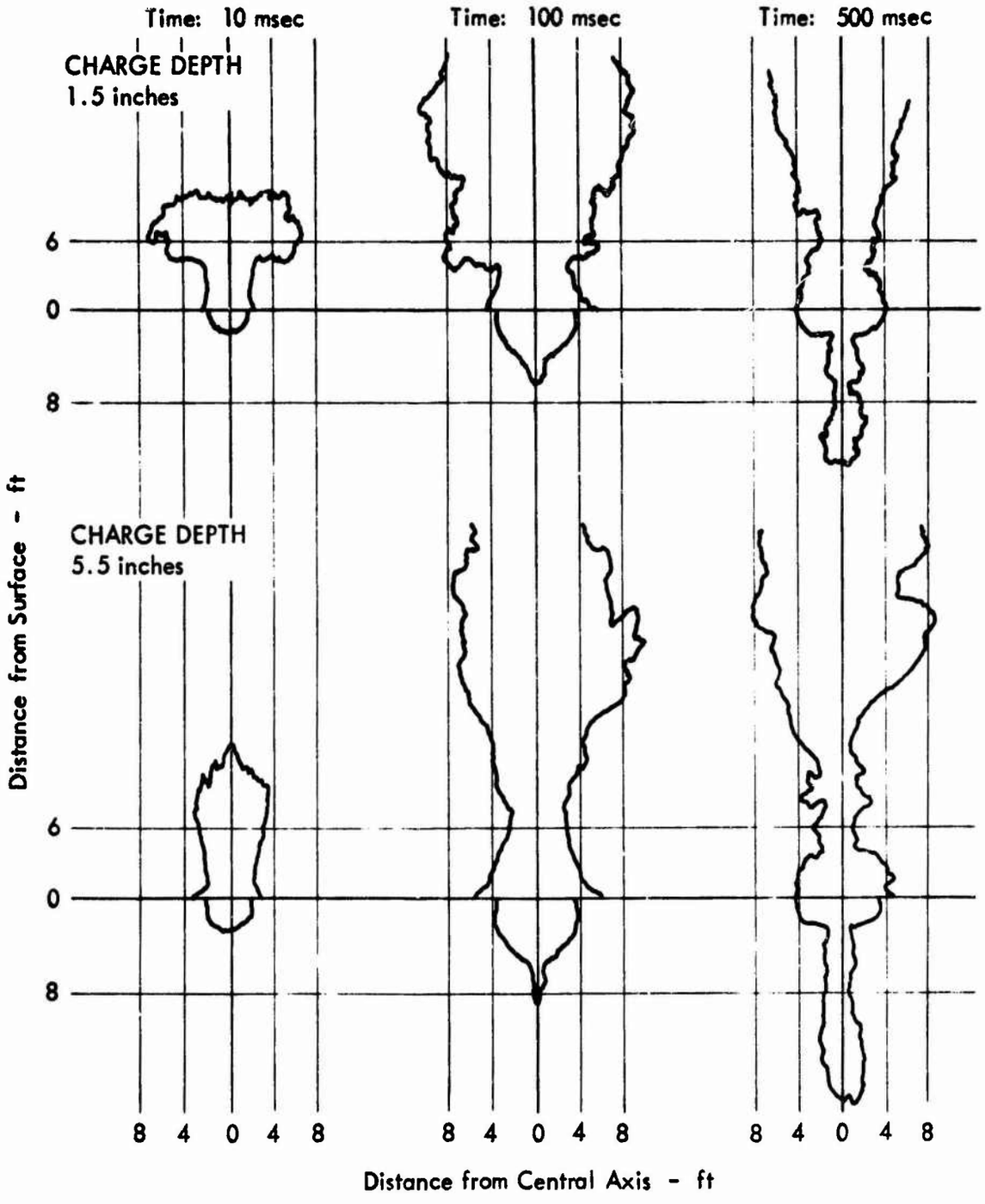

Fig. 64. Cavity and Plume Shapes For 1-lb Charges (Ref. 5)

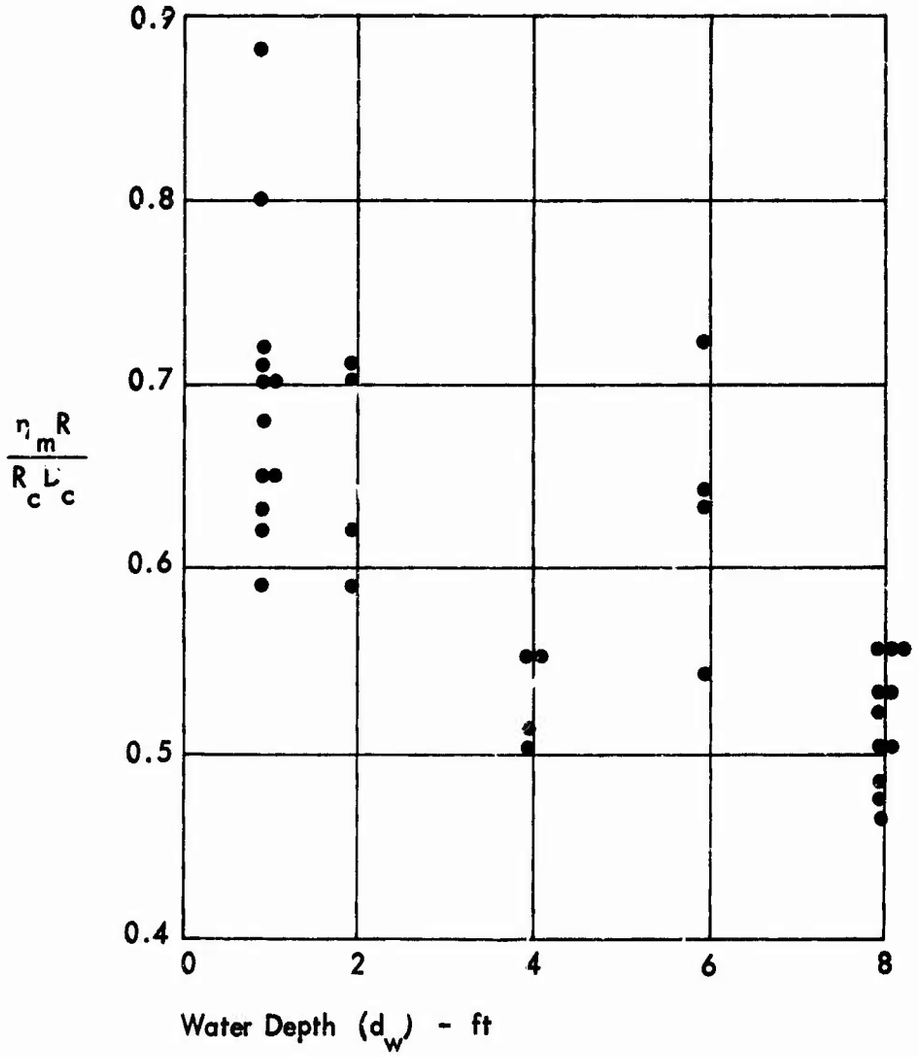

Fig. 65. Dimensionless Peak Wave Height vs Water Depth from Table 3

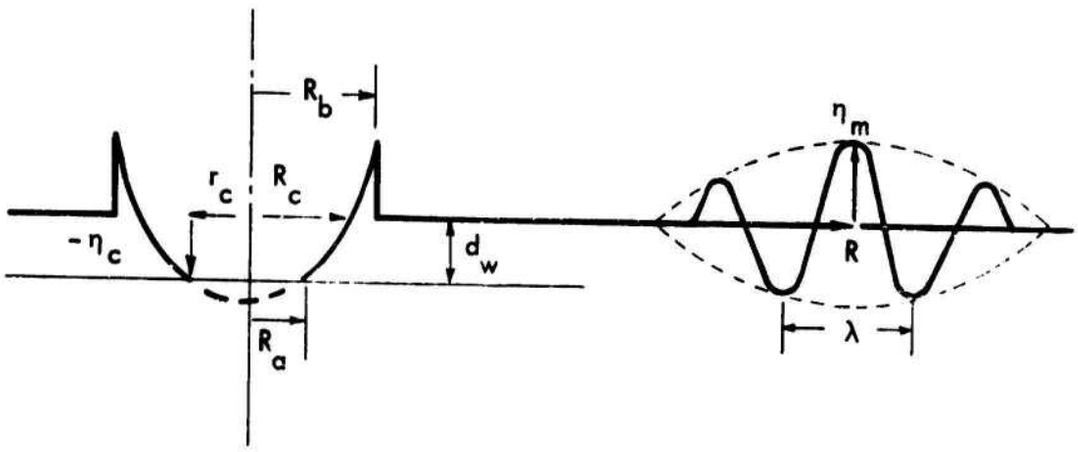

Fig. 66. Theoretical Cavity Shape and Nomenclature

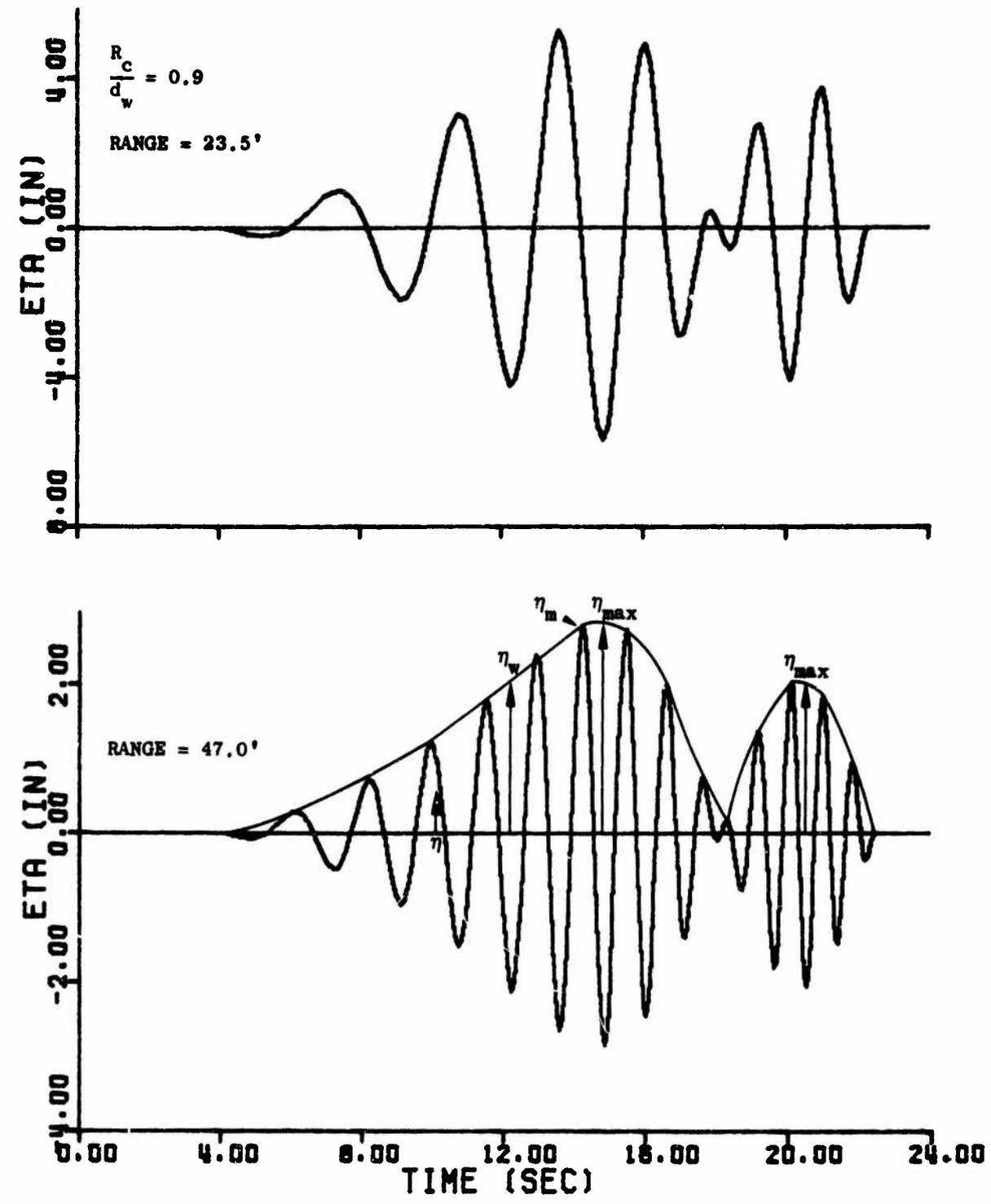

Fig. 67. Calculated Wave Trains

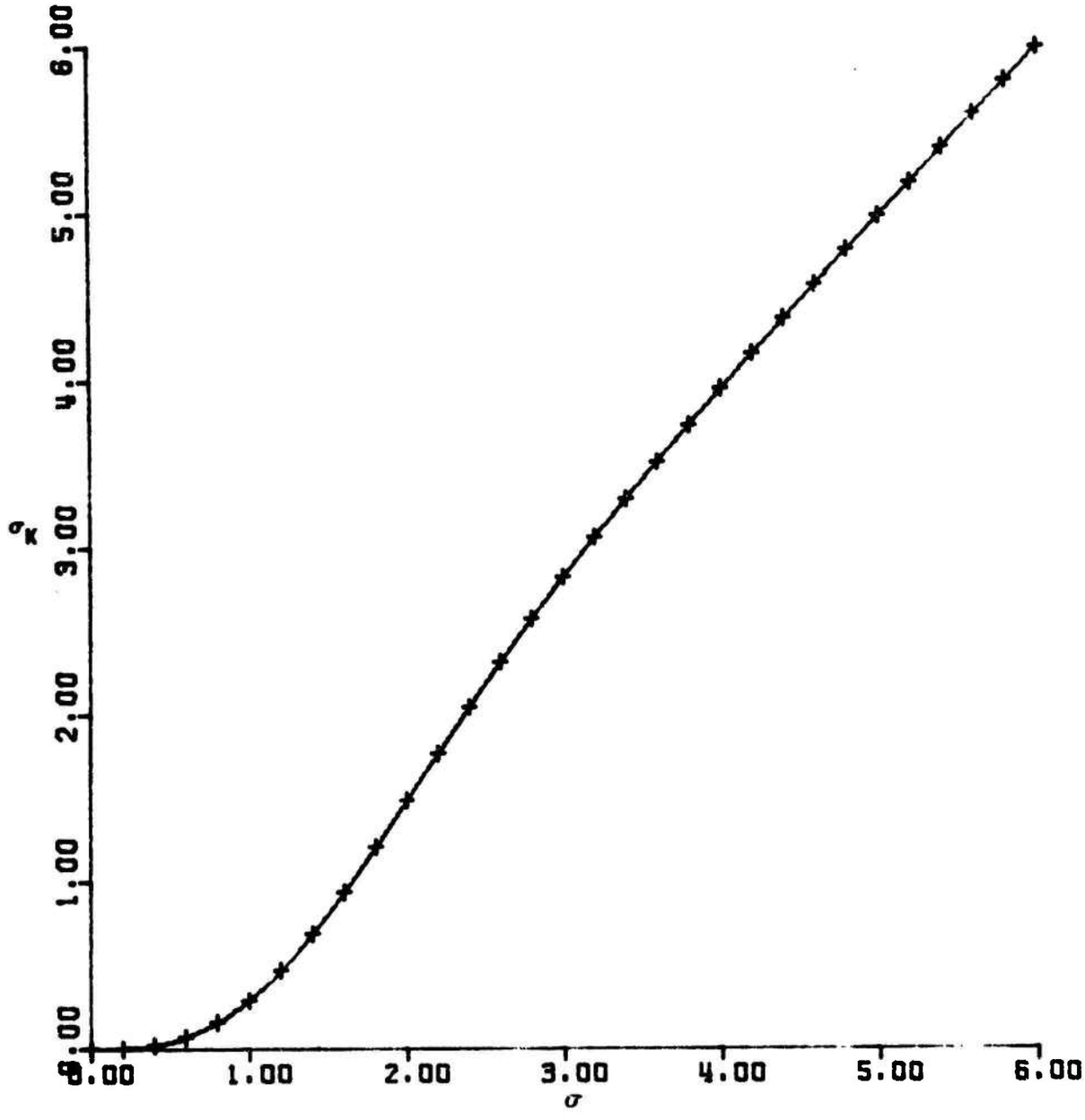

Fig. 68. Plot of Eq. (22), σ_K vs σ

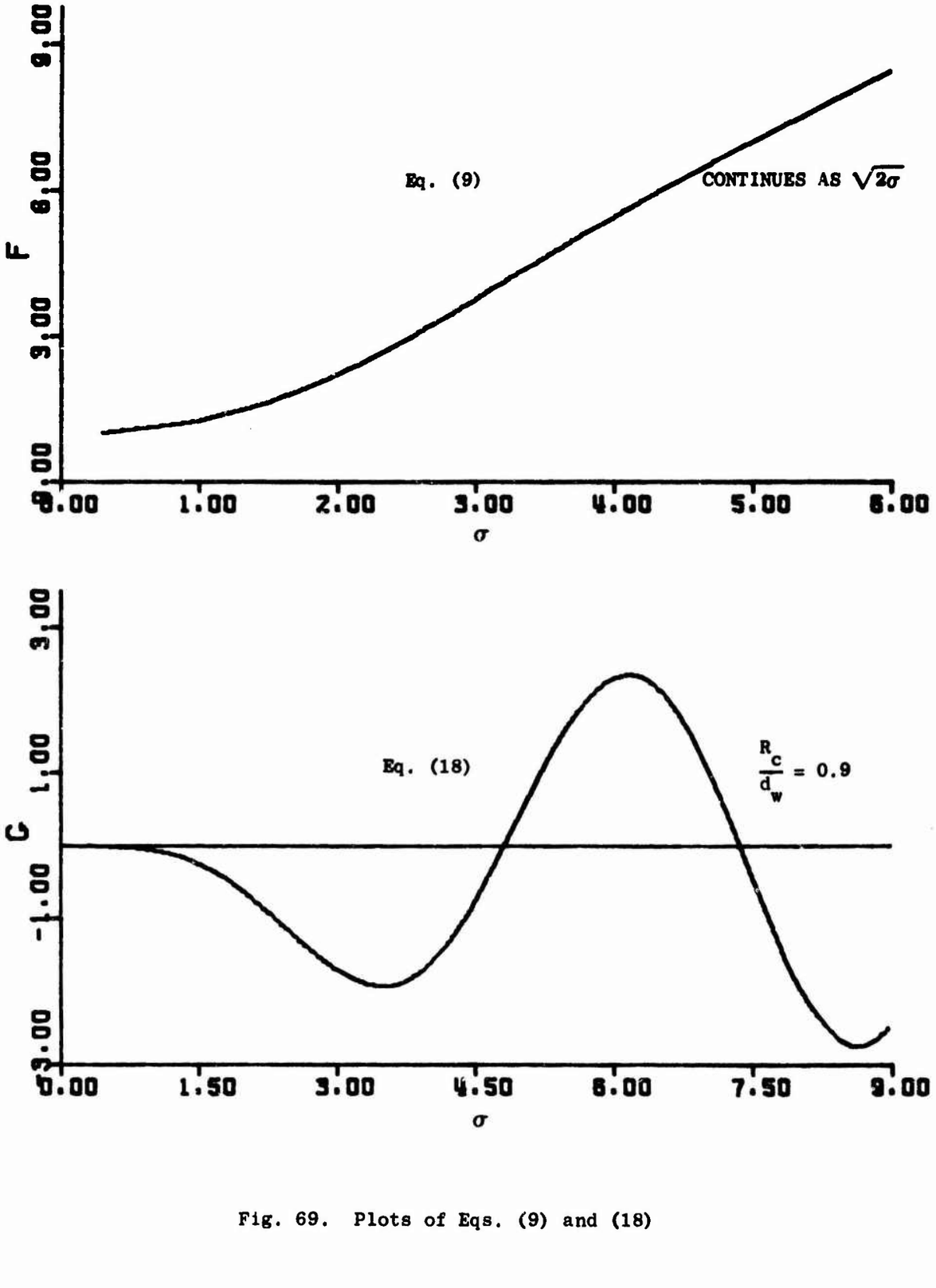

Fig. 69. Plots of Eqs. (9) and (18)

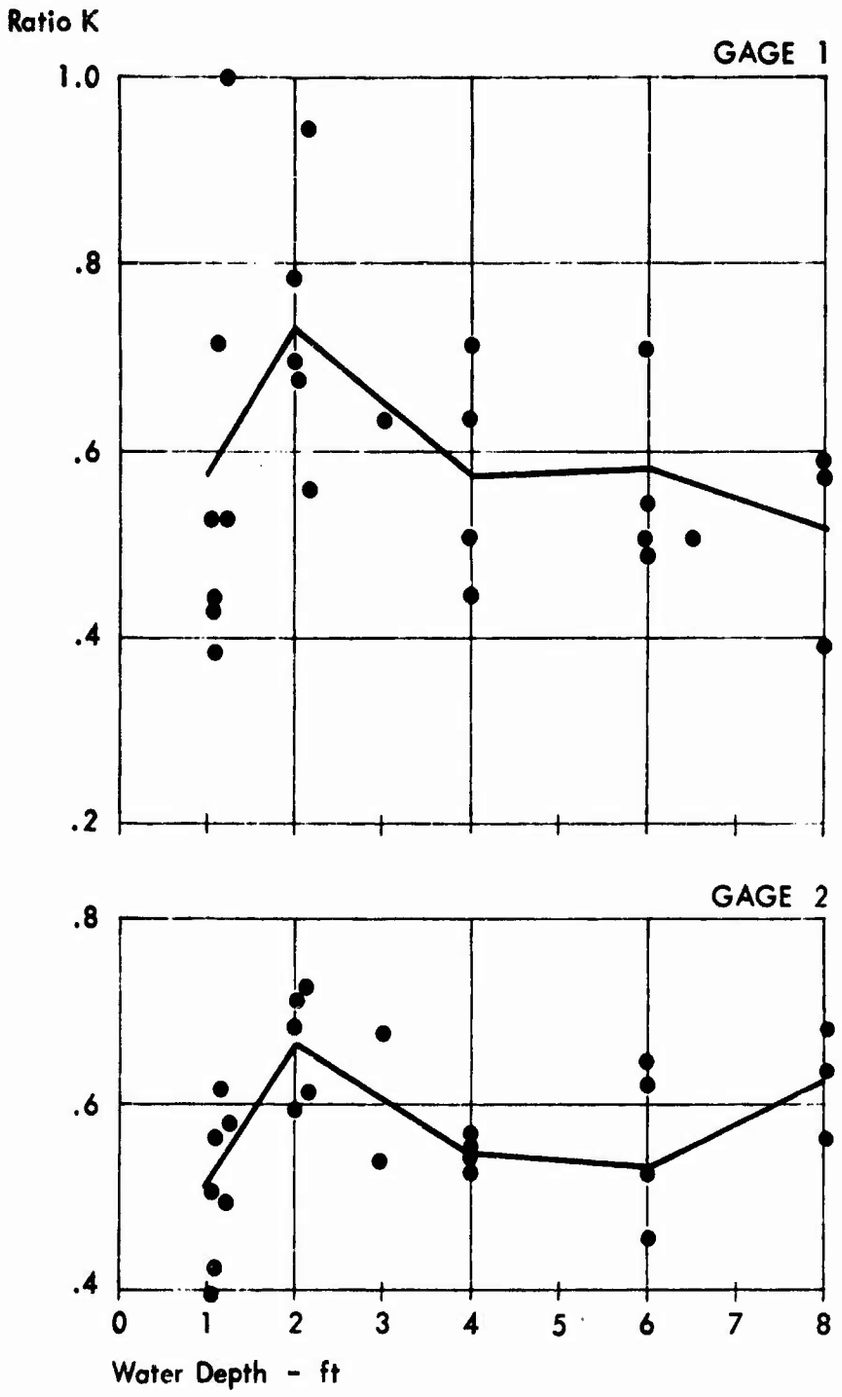

Fig. 70. Ratio of Measured to Calculated Peak Wave Heights K Versus Water Depth

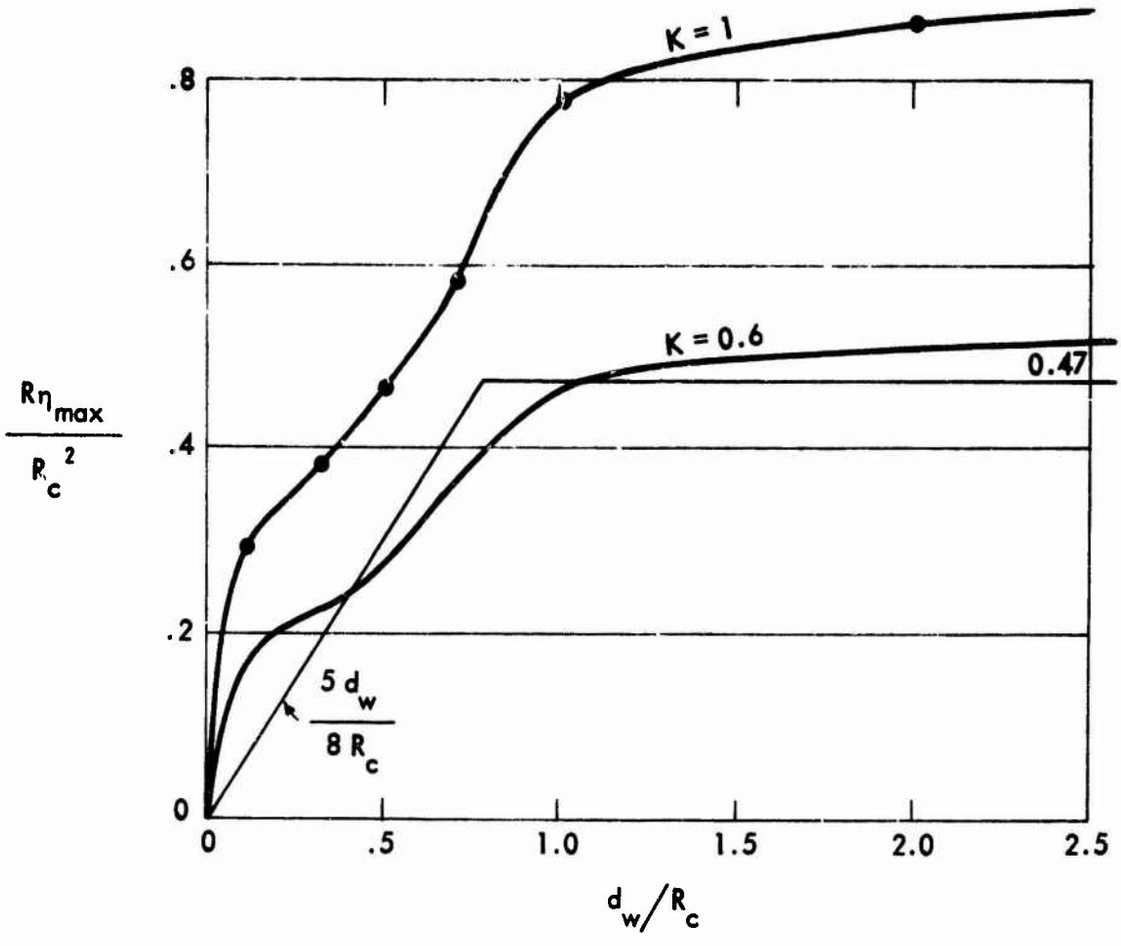

Fig. 71. Calculated Peak Wave Height Versus Water Depth

Table 1

MEASURED CAVITY AND PEAK WAVE DATA FOR
CHARGES EQUIVALENT TO 1 LB OF TNT

Test	Water Depth d_w (ft)	Charge Depth d/R_o	CAVITY Radius R_c (ft)	CAVITY Depth D_c (ft)	CAVITY Time t_c (sec)	PEAK WAVE Gage 1 R_1 = 20 ft η_{m_1} (in.)	PEAK WAVE Gage 1 R_1 = 20 ft t_{m_1} (sec)	PEAK WAVE Gage 2 R_2 = 40 ft η_{m_2} (in.)	PEAK WAVE Gage 2 R_2 = 40 ft t_{m_2} (sec)
FLAT HARD BOTTOM									
1	8	0	3.8	3.3	.23	3.0	4.4	1.7	6.3
2	8	0	3.5	3.6	.23	-	-	1.8	7.0
3	8	1/2	3.8	3.3	.05	3.0	4.5	2.0	6.4
4	8	1/2	3.8	3.4	.23	3.6	4.0	2.0	2.0
5	8	1	4.0	3.5	.23	3.5	4.3	2.0	5.8
6	8	0	3.3	3.0	.23	3.5	4.7	1.6	5.2
7	8	1/2	3.4	3.2	.22	3.2	4.7	1.7	5.4
8	8	1/2	3.4	3.4	.25	3.0	4.7	1.7	7.2
9	8	3/4	3.6	3.2	.27	3.1	4.6	1.7	7.8
10	8	4	3.8	3.5	.23	3.8	3.4	2.2	7.7
11	8	4	3.8	3.6	.23	3.7	3.4	2.2	7.2
12	6*	0	3.2	2.3	.25	2.6	4.6	1.2	10.6
13	6	1/2	3.2	2.3	.25	3.4	4.5	1.4	9.9
14	6	1	3.3	2.6	.22	3.1	4.4	1.8	9.4
15	6	4	3.7	3.0	.22	3.6	3.8	2.1	9.4
16	4	0	3.3	3.0	.25	3.0	4.5	1.6	9.3
17	4	1/2	3.6	3.2	.22	3.1	4.8	1.7	9.8
18	4	1	3.7	3.2	.23	3.0	3.3	1.8	9.0
19	4	4	3.8	3.5	.23	4.3	3.2	2.2	10 1
20	2.17	4	3.8	2.17	.25	4.6	3.5	1.7	9.5
21	2.13	1	3.6	2.13	.27	3.7	3.7	1.6	9.8
22	2.06	1/2	3.4	2.06	.25	2.5	4.0	1.3	9.9
23	2.1	0	3.4	2.0	.27	2.4	4.3	1.2	9.9
24	1.25	4	3.3	1.25	.30	2 2	3.3	1.1	6.7
25	1.21	1	3.8	1.21	.25	1.8	3.7	0.80	9.4
26	1.15	1/2	3.5	1.15	.25	1.7	3.7	0.85	8.9

*Charge weight reduced by half for Shots 12 through 15.

Table 1 (Cont.)

MEASURED CAVITY AND PEAK WAVE DATA FOR
CHARGES EQUIVALENT TO 1 LB OF TNT

Test	Water Depth d_w (ft)	Charge Depth d/R_o	CAVITY Radius R_c (ft)	CAVITY Depth D_c (ft)	CAVITY Time t_c (sec)	PEAK WAVE Gage 1 R_1 = 20 ft η_{m_1} (in.)	PEAK WAVE Gage 1 R_1 = 20 ft t_{m_1} (sec)	PEAK WAVE Gage 2 R_2 = 40 ft η_{m_2} (in.)	PEAK WAVE Gage 2 R_2 = 40 ft t_{m_2} (sec)
27	1.10	0	3.5	1.10	.27	1.4	3.6	0.75	7.0
28	Con-tour	4	3.9	2	.27	3.3	3.7	1.4	10.6
29	↓	1	3.6	2	.25	2.0	3.7	1.4	10.9
30	↓	0	3.5	2	.25	2.2	4.0	1.8	10.5
31	1.08	↓	3.9	1.06	.370	1.60	4.60	.60	9.27
32	1.08	↓	3.9	1.08	.350	1.50	5.51	.55	10.12
33	2.	↓	3.6	2.0	.252	2.65	5.13	1.30	12.54
34	3.	↓	3.75	3.0	.277	-	-	-	-
35	3.	↓	3.75	3.0	.277	3.05	6.13	1.50	13.00
36	4.	↓	3.8	2.75	.260	3.60	6.08	1.55	14.04
37	4.	↓	3.75	2.70	.260	3.60	6.12	1.50	13.08
38	3.	↓	2.40	2.00	.220	-	-	-	-
39	3.	↓	3.40	2.70	.245	-	-	1.40	12.62
40	1.	↓	3.80	1.0	.361	1.55	3.79	.55	6.26
SLOPED OR CONTOURED HARD BOTTOM									
41	-	↓	-	-	-	-	-	-	-
42	1.08	↓	3.75	1.06	.27	1.95	3.26	0.65	10.20
43	1.08	↓	3.60	1.06	.32	1.95	3.47	0.37	10.40
44	2.	↓	3.50	2.0	.25	3.16	5.22	1.30	9.79
45	2.	↓	3.40	2.0	.24	2.50	5.35	1.40	9.98
46	3.	↓	3.50	2.7	.25	2.33	5.22	1.15	6.67
47	3.	↓	3.65	2.7	.25	2.50	5.25	1.90	10.77
48	4.	↓	3.55	2.7	.26	3.02	5.12	2.00	9.50
49	4.	↓	3.55	2.7	.26	3.15	5.38	2.03	11.66
50	4.	↓	3.60	2.6	.24	3.30	4.59	2.30	9.44
51	4.	↓	3.55	2.8	.24	3.60	4.66	2.12	9.30
52	2.	↓	3.75	2.0	.26	1.60	3.35	2.25	6.64
53	2.	↓	3.80	2.0	-	1.65	5.30	1.50	8.67
54	2.	↓	-	-	-	2.10	5.45	0.75	13.72
55	2.	↓	-	-	-	1.60	5.37	0.80	13.43

TABLE 1 (Cont.)

MEASURED CAVITY AND PEAK WAVE DATA FOR
CHARGES EQUIVALENT TO 1 LB OF TNT

Test	Water Depth d_w (ft)	Charge Depth d/R_o	CAVITY Radius R_c (ft)	CAVITY Depth D_c (ft)	CAVITY Time t_c (sec)	PEAK WAVE Gage 1 R_1 = 20 ft η_{m_1} (in.)	PEAK WAVE Gage 1 R_1 = 20 ft t_{m_1} (sec)	PEAK WAVE Gage 2 R_2 = 40 ft η_{m_2} (in.)	PEAK WAVE Gage 2 R_2 = 40 ft t_{m_2} (sec)
FLAT SAND BOTTOM									
56	4.1	0	3.7	3.4	.32	3.7	5.40	1.0	8.91
57	4.1	↓	3.8	3.3	.34	3.5	5.40	1.5	12.16
58	3.1		4.0	3.1	.34	2.7	4.99	1.6	12.84
59	3.1		3.7	3.1	-	3.0	6.12	1.6	12.93
60	2.1		4.2	2.3	.41	2.6	4.77	1.4	10.38
61	2.1		3.8	2.3	.34	2.7	6.31	1.7	10.42
62	1.1		4.0	1.3	.32	1.3	3.29	0.7	9.92
63	1.1		4.3	1.3	.37	1.4	5.86	1.0	9.42

Table 2

WATER DEPTHS OVER SLOPED AND CONTOURED BOTTOMS

Shot	Bottom Shape	WATER DEPTH, d_w (in.) Apex R = 0	Hinge 1 R = 9 ft	Hinge 2 R = 23 ft	Hinge 3 R = 46 ft	End R = 53 ft
28	Contour	25	9.7	8.0	4.0	4.0
29	↓	↓	↓	↓	↓	↓
30	↓	↓	↓	↓	↓	↓
42	Slope	13	9.6	7.3	1.5	0
43	↓	↓	↓	↓	↓	↓
44	↓	25	19.6	14.0	3.4	↓
45	↓	↓	↓	↓	↓	↓
46	↓	37	30.6	20.6	4.3	↓
47	↓	↓	↓	↓	↓	↓
48	↓	49	40.5	27.4	5.7	↓
49	↓	↓	↓	↓	↓	↓
50	Contour	↓	33.0	7.8	3.9	↓
51	↓	↓	↓	↓	↓	↓
52	↓	25	18.1	5.9	2.9	↓
53	↓	↓	↓	↓	↓	↓
54	↓	↓	13.6	6.3	2.6	↓
55	↓	↓	↓	↓	↓	↓

Table 3

CALCULATED VALUES FROM MEASURED DATA FOR CHARGES EQUIVALENT TO 1 LB OF TNT

Shot	d_w (ft)	$\eta_m R$ $(ft)^2$ (Gage 1)	$\eta_m R$ $(ft)^2$ (Gage 2)	$R_c D_c$ $(ft)^2$	$\frac{\eta_m R}{R_c D_c}$ (Gage 2)
1	8	5.0	5.8	12.5	.46
2		-	5.9	12.6	.47
3		5.0	6.7	12.5	.53
4		6.0	6.7	12.9	.52
5		5.8	6.7	14.0	.48
6		5.7	5.4	9.9	.55
7		5.3	5.8	10.9	.53
8		5.1	5.7	11.5	.50
9		5.2	5.8	11.5	.50
10		6.4	7.3	13.3	.55
11		6.2	7.5	13.7	.55
12	6*	4.3	4.0	7.4	.54
13		5.6	4.7	7.4	.63
14		5.2	6.2	8.6	.72
15		6.1	7.1	11.1	.64
16	4	5.0	5.4	9.9	.55
17		5.2	5.8	11.5	.50
18		5.0	6.0	11.8	.51
19		7.2	7.3	13.3	.55
20	2	7.7	5.8	8.2	.70
21		6.2	5.4	7.6	.71
22		4.2	4.3	7.0	.62
23		4.1	4.0	6.8	.59
24	1	3.7	3.7	5.2	.71
25		3.0	2.7	4.6	.59
26		2.9	2.8	4.0	.70
27		2.4	2.5	3.9	.65
28	Contour	5.6	4.8		
29	↓	3.3	4.7		
30		3.8	6.0		
31	1	3.1	3.7	4.2	.88
32	1	2.9	2.6	4.2	.62
33	2	5.2	6.1	7.6	.80
34	3	-	-	11.2	-
35	3	6.0	7.1	11.2	.63
36	4	7.4	7.2	11.0	.65
37	4	7.4	7.1	10.1	.70
38	3	-	-	4.8	-
39	3	-	6.6	9.2	.72
40	1	3.0	2.6	3.8	.68

*Charge weight reduced by half for Shots 12-15

Table 4

COMPARABLE MEASURED CAVITY DIMENSIONS AND PEAK WAVE HEIGHTS WITH CHARGE DEPTH = 0

	BOTTOM SHAPE	WATER DEPTH AT APEX d_o (ft)			
		4	3	2	1.1
Shot number	Flat	36,37	34,35	33	31,32,40
	Sloped	48,49	46,47	44,45	42,43
	Contoured	50,51		52,53,30	
Cavity Radius R_c (ft)	Flat	3.8,3.7	3.7,3.7	3.8	3.9,3.9,3.8
	Sloped	3.6,3.6	3.5,3.6	3.5,3.4	3.8,3.6
	Contoured	3.6,3.6		3.8,3.8,3.5	
Cavity Depth D_c (ft)	Flat	2.7,2.7	3.0,3.0	2.0	1.1,1.1,1.0
	Sloped	2.7,2.7	2.7,2.7	2.0,2.0	1.1,1.1
	Contoured	2.8,2.8		2.0,2.0,2.0	
Peak Wave Height/Water Depth at gage 1 $\frac{\eta_{m_1}(\text{in.})}{d_{w_1}(\text{in.})}$ R_1 = 23.5 ft	Flat	$\frac{3.8}{48}, \frac{3.8}{48}$	$\frac{3.1}{36}$	$\frac{2.6}{24}$	$\frac{1.6}{13}, \frac{1.5}{13}, \frac{1.5}{13}$
	Sloped	$\frac{3.0}{27}, \frac{3.2}{27}$	$\frac{2.3}{21}, \frac{2.5}{21}$	$\frac{3.2}{14}, \frac{2.5}{14}$	$\frac{1.9}{73}, \frac{1.9}{73}$
	Contoured	$\frac{3.3}{7.8}, \frac{3.8}{7.8}$		$\frac{1.6}{2.9}, \frac{1.6}{2.9}, \frac{2.2}{5.0}$	
Peak Wave Height/Water Depth at gage 2 $\frac{\eta_{m_2}(\text{in.})}{d_{w_2}(\text{in.})}$ R_2 = 47 ft	Flat	$\frac{1.6}{48}, \frac{1.5}{48}$	$\frac{1.5}{36}$	$\frac{1.3}{24}$	$\frac{.80}{13}, \frac{.55}{13}, \frac{.55}{13}$
	Sloped	$\frac{2.0}{5.7}, \frac{2.0}{5.7}$	$\frac{1.2}{4.3}, \frac{1.9}{4.3}$	$\frac{1.3}{3.4}, \frac{1.4}{3.4}$	$\frac{.85}{1.5}, \frac{.37}{1.5}$
	Contoured	$\frac{2.3}{3.9}, \frac{2.1}{3.9}$		$\frac{2.2}{5.9}, \frac{1.5}{5.9}, \frac{1.8}{10.1}$	

Table 5

VALUES OF K AND ΔT REQUIRED TO MATCH CALCULATED AND MEASURED WAVE TRAINS

Test	Water Depth d_w (ft)	Cavity Radius R_c (ft)	$\frac{d}{R_o}$	Gage 1		Gage 2	
				K	T (sec)	K	T (sec)
7	8	3.2	1/2	.572	-2.62	.637	-6.06
8	8	3.3	0	.392	-2.52	.567	-7.89
11	8	3.1	3/4	.590	-2.65	.680	-5.45
12	6	3.2	0	.542	-1.61	.452	-3.08
13	6	3.2	1/2	.708	-1.76	.526	-3.81
14	6	3.2	1	.489	-2.91	.620	-3.64
15	6	3.7	4	.508	-1.88	.646	-2.42
17	4	3.6	1/2	.443	-1.80	.565	-2.67
18	4	3.7	1	.505	-1.85	.550	-3.49
19	4	3.8	4	.635	-3.01	.539	-2.42
20	2.17	3.8	4	.557	-1.71	.728	-1.99
21	2.13	3.6	1	.948	-1.49	.616	-1.68
22	2.06	3.4	1/2	.674	-1.61	.598	-1.75
23	2.1	3.3	0	.696	-1.50	.682	-1.77
24	1.25	4.2	4	1.	-1.70	.577	-1.86
25	1.21	3.8	1	.523	+0.02	.493	-1.47
26	1.15	3.5	1/2	.717	-1.37	.615	+0.01
27	1.10	3.4	0	.528	+0.05	.568	-2.00
31	1.08	4.5	0	.440	-1.58	.503	-1.05
32	1.08	3.9	0	.432	-0.75	.396	-1.38
33	2	3.8	0	.784	-1.31	.710	+0.16
35	3	3.75	0	.635	-0.73	.539	-0.65
37	4	3.75	0	.716	-0.68	.526	-1.79
39	3	3.4	0	-	-	.673	-1.58
40	1	3.8	0	.386	-2.35	.423	-2.33

Table 6

CALCULATED PEAK HEIGHTS OF WAVE ENVELOPE

$\frac{d_w}{R_c}$	$\frac{R_c}{d_w}$	$\left(\frac{FG}{\sigma^2}\right)_{max} = \left(\frac{R\eta}{R_c d_w}\right)_{max}$		$\frac{K\eta_{max}}{R_c^2}$
		First Peak	Second Peak	First Peak
∞	$\ll 1$	$\simeq .89\ R_c/d_w$	–	.89
2	1/2	.43	.29	.86
1	1	.78	.58	.78
2/3	1.5	.86	.89	.57
1/2	2	.93	1.01	.47
1/3	3	1.14	1.06	.38
1/10	10	2.98	1.69	.17

REFERENCES

1. Kriebel, A. R., Analysis of Water Waves Generated Explosively at the Upper Critical Depth, Interim Report, URS 679-1, Contract N0014-67-0451, URS Research Company for the Office of Naval Research, Washington, D. C. January 1968

2. Kriebel, A. R., Shallow Water Generation, Interim Report, URS 679-2, Contract N0014-67-0451, URS Research Company for the Office of Naval Research, Washington, D. C. (Secret)

3. Kriebel, A. R. and C. Wilton, Upper Critical Depth, Interim Report, URS 679-3, Contract N0014-67-0451, URS Research Company for the Office of Naval Research, Washington, D. C.

4. Kriebel, A. R., Explosively Generated Water Waves, Interim Report, URS 679-4 Contract N0014-67-0451, URS Research Company for the Office of Naval Research, Washington, D. C.

5. Hendricks, J. W.and D. L. Smith, Above- and Below-Surface Effects of One-Pound Underwater Explosions, HYDRA I, TR-480, U.S. Naval Radiological Defense Laboratory, October 1960

6. Pace, C. E., R. W. Whalin, and J. N. Strange, Surface Waves Resulting from Explosions in Deep Water, TR 1-647, U.S. Army Engineers Waterways Experiment Station, April 1968

7. Whalin, R. W. and D. J. Divoky, Water Waves Generated by Shallow Water Explosions, Final Report S-359, Contract NBY-66206, Natl. Engr. Sc. Co., September 1966

8. Walter, D., Explosion-Generated Wave Tests, Mono Lake, California, Final Report URS 654-2, Contract Nonr 4959(00), URS Corp, January 1966

9. LeMehaute, B., et al., Explosion-Generated Wave Environment in Shallow Water, Final Report TC-116, Contract DASA 01-67-C-0099. Tetra Tech., Inc., Pasadena, California, August 1967 (Secret)

UNCLASSIFIED
Security Classification

DOCUMENT CONTROL DATA - R & D

(Security classification of title, body of abstract and indexing annotation must be entered when the overall report is classified)

1. ORIGINATING ACTIVITY (Corporate author) URS RESEARCH COMPANY 1811 Trousdale Drive Burlingame, California - 94010	2a. REPORT SECURITY CLASSIFICATION (U) 2b. GROUP

3. REPORT TITLE

CAVITIES AND WAVES FROM EXPLOSIONS IN SHALLOW WATER

4. DESCRIPTIVE NOTES (Type of report and inclusive dates)

Final Report

5. AUTHOR(S) (First name, middle initial, last name)

A. R. Kriebel

6. REPORT DATE	7a. TOTAL NO. OF PAGES	7b. NO. OF REFS
October 1969	109	9

8a. CONTRACT OR GRANT NO.	9a. ORIGINATOR'S REPORT NUMBER(S)
N00014-67-C-0451 (NR 089-053/12/20-66)	679-5
b. PROJECT NO.	
c.	9b. OTHER REPORT NO(S) (Any other numbers that may be assigned this report)
d.	

10. DISTRIBUTION STATEMENT

This document has been approved for public release and sale; its distribution is unlimited.

11. SUPPLEMENTARY NOTES	12. SPONSORING MILITARY ACTIVITY
	DEFENSE ATOMIC SUPPORT AGENCY AND OFFICE OF NAVAL RESEARCH

13. ABSTRACT

Photographic data for the cavities and surface waves generated by explosions in shallow water are described. The data were obtained in a slender wedge-shaped tank of water having one transparent sidewall. Ideally the tests would be equivalent to those for a 1-lb sphere of TNT exploded in a shallow test pond with a vertical axis of symmetry. The cavities and waves generated in the wedge tank did correspond roughly with such data, but there were differences in detail caused by the sidewalls of the wedge tank and the ceiling over it.

The wedge tank data indicate that the horizontal radius of the expanded cavity is nearly independent of the water depth, even when the water depth is less than one-third the cavity radius. The wave trains are nearly independent of the water depth until the depth is less than three-fourths the cavity radius, after which the wave heights begin to decrease in proportion to the water depth.

The cavities and waves were hardly affected when the hard bottom of the tank was replaced by sand, even when the water was shallow. A surf zone was created in the wedge-tank when the bottom was contoured, so that the waves shoaled. The measured wave trains corresponded reasonably well with those predicted by the theory of Kranzer and Keller for an initially motionless cavity. The calculated wave trains were based on the procedure developed by Whalin, on the measured cavity dimensions, and on two empirical factors.

DD FORM 1 NOV 68 1473 REPLACES DD FORM 1473, 1 JAN 64, WHICH IS OBSOLETE FOR ARMY USE.

UNCLASSIFIED
Security Classification

14. KEY WORDS	LINK A		LINK B		LINK C	
	ROLE	WT	ROLE	WT	ROLE	WT
Water waves						
Underwater explosions						
Blast simulation						
Shoaling						
Wave prediction methods						
Experimental water wave tank						